Republic of Iraq
Ministry of Higher Education
and Scientific Research

EXPERIMENTAL AND NUMERICAL STUDY OF FIN HEAT SINKS SYSTEMS

A THESIS

SUBMITTED TO THE COLLEGE OF ENGINEERING OF THE UNIVERSITY OF BABYLON IN PARTIAL FULFILMENT OF THE REQUIREMENTS FOR THE DEGREE OF MASTER OF SCIENCE IN MECHANICAL ENGINEERING

BY

Farouq Hassan Ali

Al-Innawi

(B.Sc., ٢٠٠١)

(February ٢٠٠٥)

١٤٢٦ A.

٢٠٠٥ A. M

H

جمهورية العراق

وزارة التعليم العالي والبحث العلمي

دراسة تجريبية و عددية لأنظمة مغاطس حرارية مزعنفة

رسالة
قدمت إلى كليه الهندسة في جامعه بابل وهي جزء
من متطلبات نيل درجه ماجستير علوم في
الهندسة الميكانيكية

مقدمة من قبل

فاروق حسن علي

العناوي

(شباط ٢٠٠٥)

١٤٢٦ هـ ٢٠٠٥ م

بسم الله الرحمن الرحيم

﴿ وما توفيقي إلا بالله عليه توكلت وإليه أنيب ﴾

صدق الله العلي العظيم

سورة هود الآية (٨٨)

DEDICATION

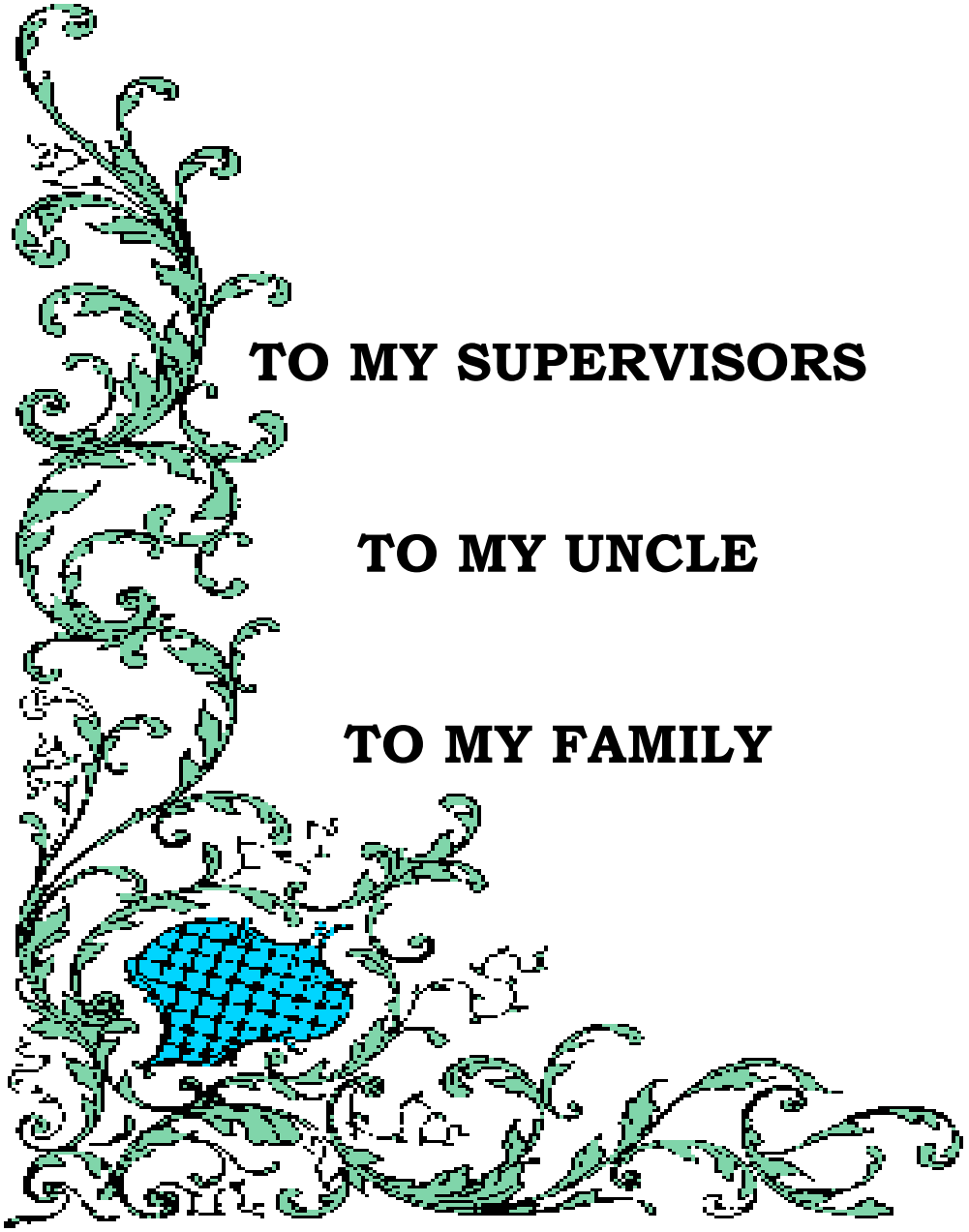

TO MY SUPERVISORS

TO MY UNCLE

TO MY FAMILY

خلاصـــــــــــــة

لقد جرت مقارنة أداء انتقال الحرارة لمغاطس حرارية (Heat Sinks) مزعنفة شائعة الاستخدام وذلك بدراسة توزيع درجات الحرارة و السرع خلال المغطس الحراري.

لقد جرت المقارنة لمغاطس حرارية مصنوعة من مادة الألمنيوم وهي مغطس حراري ذو زعانف طولية, مغطس حراري ذو زعانف مسمارية مربعة المقطع موزعة بشكل متعاقب, مغطس حراري ذو زعانف مسمارية دائرية المقطع موزعة بشكل متعاقب أيضا, في ظروف حمل حراري قسري وباستخدام الهواء كمائع تبريد. لقد استخدمت الزعانف الطولية لتقليل خسارة الضغط خلال المغطس الحراري وذلك بتقليل الدوامات وكذلك لتعزيز الأداء الحراري بواسطة الحصول على اكبر مساحة سطحية لانتقال الحرارة.

ان معظم الاجهزة الالكترونية تعمل في مدى درجات حرارة تتراوح مابين (٤٠) إلى (٦٠) درجة مئوية لذلك قمنا بتغيير سرعة الهواء من (٢) م\ثا إلى (٦) م\ثا وكذلك قمنا بتغيير الفيض الحراري من (٢٠) واط إلى (٤٠) واط للحصول على مدى درجات الحرارة المطلوبة.

قيست درجات الحرارة خلال المغطس الحراري باستخدام (١٥) متحسس حراري لكل مغطس حراري موزعة عليه بشكل متساو. و قيست سرعة الهواء خلال المغطس الحراري باستخدام مقياس متحرك لقياس درجات الحرارة والسرعة في نفس المكان.

استخدم برنامج (ANSYS Software Package) للقيام بالدراسة النظرية باستخدام ظروف االجريان ثابت الحرارة. هذا البرنامج ذو أمكانية عالية لحساب السرع و الضغوط و فحص الدوامات التي تحدث نتيجة الاصطدامات بالزعانف الطولية و المسمارية أثناء الجريان عبر المغطس الحراري.

بمساعدة برنامج أل (ANSYS) قمنا بدراسة نماذج ثلاثية الأبعاد في حالة الوضع الأفقي فقط, حيث سهولة وضع وتغيير الظروف الحدودية خلال البرنامج و التي تتضمن جميع مديات السرع المستخدمة في الدراسة العملية.لقد كان الجريان غير انظغاطي و لزج. هذا البرنامج قام بحل معادلة الاستمرارية و معادلة العزم باستخدام موديل اضطرابي (K-ε model).

جرت مقارنة المقاومة الحرارية، المقاومة الحرارية النسبية، معامل انتقال الحرارة، توزيع السرع و درجات الحرارة لثلاثة انواع من المغاطس الحرارية.

المغطس الحراري ذو الزعانف الطولية اظهر اقل كمية هواء غير متأثر و اقل مقاومة حرارية من باقي الشكلين الآخرين في حالة وجود الفيض الحراري عند قاعدة المغطس الحراري، وذلك لان الزعانف الطولية تمتلك اكبر مساحة حمل حراري.

المغطس الحراري ذو الزعانف الاسطوانية يمتلك أعلى مقاومة حرارية نسبية من باقي التصميمين الاخرين. وذلك لحسن توزيع السرع حول الزعانف الدائرية.

النتائج أظهرت انه عندما تمتلك المغاطس الحرارية نفس مساحة الحمل الحراري تكون الزعانف الاسطوانية الاختيار الأفضل, اما في حالة امتلاك المغاطس الحرارية نفس مساحة التوصيل الحراري فأن الزعانف الطولية هي الافضل وذلك لانها تعطي اكبر مساحة حمل حراري.

ACKNOWLEDGMENTS

(In The Name of Allah, The Gracious, The Merciful)

First of all, I would like to express my deep thanks and gratitude to my supervisors, ***Dr. Tahseen A. Al-Hattab & Dr. Haroun S. AL-Janabi,*** *and especially for* ***Dr. Ala'a M. Hussien & Dr. Abdul-Kareem A. Wahab*** *for their great support, guidance, advice and assistance throughout the various stages of the present work.*

I would like also to thank all the staff of Mechanical Engineering Department, advance computer laboratory and ***Mr. Nabil AL-Saffar*** *for the facilities during my work.*

I record my sincere gratitude to my family and to my friends for their encouragement and support during the period of preparing this work.

Finally, I am grateful to those who have helped me to carry out this research.

٢٠٠٥

ABSTRACT

In this study has been compared the heat transfer performance of various commnly fin geometries by studying the temprature and velocity distribution.

Comparitive thermal tests have been carried out using aluminum heat sinks with extruded fins, staggered square pins, and staggered cylinderical pins in forced convection air flow environments. The extruded fin heat sink was designed to minimize the pressure losses across the heat sink by reducing the vortex effects to enhance the thermal performance by maintaining large exposed surfaces area available for heat transfer. Experimental and theoretical investigation were carried out.

The most electronic components operates in the range of temprature between (٤٠)^{o}c and (٦٠)^{o}c therfore in the experimental tests, air velocity was varied from (٢) m/s to (٦) m/s and the heat flux from (٢٠) Watt to (٤٠) Watt are used to obtain the range of temprature.

The temprature of the solid structure was measured experimentally by using (١٥) thermocouple. They are distributed on the heat sinks uniformly.The velocity and temprature of the flow field in the test section was measured experimentally using portable anemometer.

A software packages (ANSYS ٥.٤) was used to carry out the theoretical study using adiabatic flow condition. This gives a good ability to calculate the velocity and pressure distributon and sketching the eddies wake behind the pins and fins in the core of the heat sink.

By the aid of this software package a three-dimemsional model was built by putting horizontal orintation only. The model boundary condition can be easily varied through (ANSYS ٥.٤), including all ranges used in the present study. The flow was analyzed for three-dimensional steady, adiabatic,

incompressible and viscous. Navir-stocks equations and continuity equation were solved. A two-equation K-ε model (turbulence model) was also solved by this program.

A comparision of thermal resistance, relatave thermal resistance, heat transfer coefficient, velocity and temprature distribution for three types of heat sincks are presented.

The straight fin experienced the lowest amount of flow by-pass over the heat sink. For this particular application, where the heat source is localized at the bottom of the heat sink base plate, the overall thermal resistance of the straight fin was lower than the other two designs mainly due to fins have large area of convection.

The relative thermal resistance for cylinderical pin-fin heat sink was higher than the other tow designs. This is due to the improve distribution of air flow around the circular pin.

The result show that when the heat sinks have the same area of convection, the cylinderical pin-fin heat sink was the best choice while when the heat sinks have the same area of conduction the straight fin was the best choice because it give large exposed surface (large area of convection).

Contents

CHAPTER ONE-INTRODUCTION		
١.١	General	١
١.٢	Objectives	٦
١.٣	Model Description	٧
CHAPTER TWO-LITERATURE REVIEW		
٢.١	Introduction	٩
٢.٢	Experimental Work	٩
٢.٣	Theoretical Work	٢١
٢.٤	Experimental and Theoretical Work	٢٧
٢.٥	Literature Review Conclusion	٣٥
CHAPTER THREE-THEORETICAL WORK		
٣.١	Introduction	٣٩
٣.٢	Governing Equations	٤٠
٣.٣	Fins Geometries	٤٣
٣.٤	The Boundary Conditions	٤٥
٣.٥	Numerical Solution	٤٥
٣.٥.١	ANSYS Program	٤٦
٣.٥.٢	ANSYS GUI	٤٧
٣.٥.٣	Performing a Typical ANSYS Analysis	٤٧
٣.٥.٣.١	Model and Mesh Performing	٤٨
٣.٥.٣.٢	Solid Model Mesh	٤٩
٣.٥.٣.٤	Solving the Problem	٥١
٣.٥.٣.٥	Examining the Results	٥٣
٣.٥.٣.٦	Checking Results of Computer Model	٥٣

CHAPTER FOUR-EXPERIMENTAL WORK		
٤.١	Introduction	٥٥
٤.٢	Experimental Apparatus	٥٦
٤.٢.١	Interface Card and Software Driver	٥٧
٤.٣	Measurement Procedure	٥٨
٤.٣.١.	Velocity Measurement	٥٨
٤.٣.٢	Temperature Measurement	٥٩
٤.٣.٣	Thermal Conductivity Measurement	٦١
٤.٤	Errors	٦٢
CHAPTER FIVE-RESULTS AND DISCUSSION		
٥.١	Experimental Results	٧٣
٥.١.١	Thermal Resistance	٧٣
٥.١.٢	Local Heat Transfer Coefficients	٧٦
٥.١.٣	Velocity Distribution	٧٨
٥.١.٤	Temperature Distribution	٨١
٥.٢	Theoretical Results	٨٣
٥.٢.١	Velocity Distribution	٨٣
٥.٢.٢	Resultant Velocity Distribution	٨٥
٥.٢.٣	Vector Velocity Distribution	٨٥
٥.٢.٤	Experimental	٨٥

CHAPTER SIX-CONCLUTIONS AND SUGGESTIONS		
٦.١	Conclusions	١١٦
٦.٢	Suggestions for Future Work.	١١٧
References		١١٩

Nomenclature

The following symbols are used generally throughout the text.

Others are defined when used.

Symbol	*Description*	*Unit*
A	Conduction Area	m^2
$A_{conv.}$	Convection Area	m^2
c	Specific Heat	$KJ/kg.^oc$
D	Cylinder Pin Diameter	mm
H	Pin-Fin Height	mm.
H_b	Sink Base Thickness	mm
h	Heat Transfer Coefficient	$W/m^2.^oc$
k	Thermal Conductivity	$W/m.^oc$
L	Heat Sink Length	mm
L	Square Pin Side Length	mm
M	Heat Sink Width	mm
N	Total Number of Finite Element Nodes	-
n	Current Global Iteration	-
P	Pitch Distance	mm
P_r	Perimeter	m
Q_v	Volumetric Heat Source	Watt
$q_{Conv.}$	Heat Convected	Watt
$q_{Tot.}$	Total Power Supplies	Watt

q_{loss}	Heat Losses	Watt
R_{th}	Thermal Resistance	^{o}c/Watt
Re	Reynolds Number	-
T	Temperature	^{o}c
T_B	Base Temperature of Heat Sink	^{o}c
T_b	Base Temperature of Pin-Fin	^{o}c
T_∞	Ambient Temperature	^{o}c
t	FinThickness	mm.
t	Time	sec
u	Velocity in x-Direction	m/s
V	Velocity	m/s
v	Velocity in y-Direction	m/s
pa	Pascal	N/m^{۲}
w	Velocity in z-Direction	m/s
x	Horizontal Coordinate	mm.
y	Vertical Coordinate	mm.

Abbreviations

AHTC	Adiabatic Heat Transfer Coefficient	-
BFC	Body Fitted Coordinate	
CFD	Computational Fluid Dynamics	-
Coef.	Coefficient	-
Eq.	Equation	-
Fig.	Figure	-
FEA	Finite Element Analysis	-
PGA	Pin Grid Array	-
SKF	Super Position Kernal Function	-

Ref.	Reference	-
Temp.	Temperature	^{o}c
Tran.	Transfer	-
Vol.	Volume	cm^{3}

Greek Symbols

α	Thermal Diffusivity	cm^{2}/s
ρ	Density	kg/cm^{3}
t	Time	s
∇	Gradient	-
Φ	Degree of Freedom	
μ	Laminar Viscosity	Kg/m.s
μ_e	Effective viscosity	Kg/m.s
μ_t	Turbulent Viscosity	Kg/m.s
υ	Kinematics Viscosity	cm^{2}/s

CERTIFICATION

We certify that this thesis titled "***EXPERIMENTAL AND NUMERICAL STUDY OF FIN HEAT SINKS SYSTEMS"*** was prepared by ***Mr. Farouq Hassan*** **Ali** under our supervision at the ***University of Babylon*** in partial fulfillment of the requirements for the degree of ***Master of Science in Mechanical Engineering (Power Mechanics).***

Signature:
Name: Dr. Haroun A-K. Shahad
(Supervisor)

Date: / /٢٠٠٥

Signature:
Name: Dr. Tahseen A. AL-Hattab
(Supervisor)

Date: / /٢٠٠٥

Chapter 1

Introduction

١.١ General

Electronic equipment has made its way practically through every aspect of modern life, from toys and appliances to high power computers.

The reliability of electronics of a system is a major factor in the overall reliability of the system. Electronic components depend on the passage of electric current to perform their duties, and they become potential sets for excessive heating, since the current flow through a resistance is accompanied by heat generation. Continued miniaturization of electronic system has resulted in a dramatic increase in the amount of heat generated per unit volume, comparable in magnitude to these encountered at nuclear reactors and the surface of the sun. unless properly designed and controlled, high rate of heat generation results in high operating temperatures for electronic equipment, which jeopardizes its safety and reliability.

The failure rate of electronic equipments increases exponentially with temperature. Also, the high thermal stress in the solder joints of electronic components mounted on circuit boards resulting from temperature variation are major causes of failure. Therefore, thermal controls have become increasingly important in the design and operation of electronic equipments[١].

Due to advances in packaging design and increased chip power densities, improvements in integrating the box and board level thermal design are required

in order to continue using air as a coolant of choice for desktop computers. Air flow is not ducted within present desktop computers and as a results, the thermal performance of compact heat sink is not fully realized due to by-pass flow. Until recently, electronic package designs yielded chip junction-to-case thermal resistance greater than (٠.٥) ^{o}C/W.

During the past few years, the electronics industry has been demanding more and more efficient heat exchanger designs. In particular, the speed of electronic chips is seriously bounded by the thermal power that the chips produce. As a consequence, electronics chips have to be intensively cooled using specially designed heat exchangers submerged into air or water flow as in printed circuit board, central processor unit, sparsely populated card, uninterruptible power supplies, telecommunications systems, airplanes, satellite, space vehicles, ships, submarines and missiles.

In today's electronic equipments, total system dissipated power levels are increasing with every new design. Increase in power levels combined with the market expectation of reduced package sizes lead to heat problem. This problem if uncontrolled can significantly shorten the life of the electronic components.

Although this "increased power- decreased size" scenario has been prevalent for many decades, the industry's ability to make smaller electronic components reduces size cooling components.

Market demands have shifted attention to decreasing the volume and increasing thermal efficiency. For some electronics (typically uninterruptible power supplies and telecommunications systems) the market also demands reduced floor space and places sever limitations on acoustic noise. These limitations force designs toward more expensive heat removal techniques.

Total power level is not the only problem. Heat density, or Watts per square centimeter, at the semiconductor is a growing problem, too. This is the result of denser electronics and increased clock frequencies. High heat flux densities

combined with high overall power levels are the main problems for thermal management. These thermal challenges can cause failure even if the heat sink surface area and air flow are sized correctly.

The constant demand for speed and performance in electronics is unfortunately accompanied by ever increasing thermal dissipation. Air heat exchanger or " heat sink " continues to be the most viable thermal solution for the electronic industry primarily because of low cost and high reliability.

Heat sink for electronics depends on conduction from the electronic package to the heat sink base, followed by conduction into the extended surfaces and convection to the cooling fluid.

A unique aspect of heat exchanger used in electronics is the possibility that the flow can bypass the heat exchanger core entirely, and leak from the core to the bypass duct.

As the power density in electronic systems continues to increase, there is a growing interest in the cooling design of electronic package. In particular, since the use of geometrically complex heat sinks is prevalent in the cooling of all computers (from laptops to mainframes), the need for effective modeling tools which are preferably well integrated with a mechanical design tool is very important. These models, if used appropriately, will significantly reduce the time required for new products.

In contrast to the previous, where the heat exchanging structures are isothermal, the heat exchangers in the electronics industry consist mostly of highly conducting materials. This further complicates numerical calculations as well as experimental work due to the conjugate nature of heat transfer.

In view of the proliferation of office environment computing, air-cooling has gained considerable attention. Due to the poor thermal properties of air compared with water, it become necessary to resort to using extended surfaces,

commonly termed as heat sinks. Even in the high-end servers or supercomputer products, air-cooling is gaining grounds due to the lower hardware cost and higher reliability.

The use of heat sinks to improve the heat transfer rate from a module has to be implemented with great care. The increased surface area usually requires an increase in the air pressure drop in that region, and if there are other paths for the air to flow through at a lower pressure drop, the resulting air starvation in "enhanced" region may actually result in a lower heat transfer rate. Careful analysis or testing is therefore necessary under the actual system condition to ensure effectiveness of the design.

Flow through heat sinks refers to heat sinks wherein the flow inters the heat sinks from one end and travels more or less in a straight line to exit from the other end. One of the simplest, and most cost-effective heat sink designs used is the linearly extruded aluminum heat sink. Aluminum has many characteristics that make it an excellent heat sink material. It is easily in fine detail with inexpensive tooling. These heat sinks can be extruded to a maximum fin density ratio (the height to width spacing between fins) of approximately (٥) to (١). This limit is a result of manufacturing costs and tolerance control, as described by **Kiley and Soule (١٩٩٠)**[٢]. Such heat sinks are commonly used for many applications, but are limited to relatively low-power dissipation due to the limitation of total surface area per volume. Higher aspect ratios of up to (٢٥) or more can be attained by using epoxy-bonded fin heat sinks as described an Fig. (١-١).

Fig. (١-١) Epoxy-bonded fin heat sinks.

These heat sinks consist of an extruded or machined base, which is flat on the module-facing side and grooved on the fin side. The fins are then epoxies into the grooves. The epoxy interface does, however, add a thermal resistance to the system. This difficulty can be overcome by brazing or soldering the fins to the base, resulting in reduced overall resistance at a higher cost, **Kiley and Soule (١٩٩٠)**[٢] and **Soule (١٩٩٣)**[٣]. Both aluminum and copper can be used to construct this type of heat sink, depending on the system requirements and allowable overall weight.

Pin-fin heat sinks are also commonly used and have the add advantage of not requiring specific positioning relative to flow direction. Pin-fin heat sinks can be manufactured either by starting with a linearly extruded parallel plate heat sink and then cutting the plates to form the pins, or by building them using more costly specialized techniques such as epoxy bonding, brazing and soldering. Round pins or other cross-section shapes can also be manufactured using casting as shown in Fig. (١-٢).

Fig. (١-٢) Pin-Fin heat sinks.

Other less commonly used heat sinks included folded-fin heat sinks where sheet metal (٠.٠٠٥) to (٠.٠٨) cm is corrugated to form fins as in Fig. (١-٣).

Fig. (١-٣) Folded fin heat sinks.

For parallel plate heat sinks it is important to design the heat sink accounting for all air flow paths, since the air can be by-pass the heat sink if other low-resistance paths exists.

١.٢ The Objective of the Present Work

The objective of the present thesis is to study temperature and velocity distribution of three types of heat sinks at different inlet velocity and heat flux by using experimental and numerical techniques. The inlet velocity of air varies from (٢,٣,٤ to ٦) m/s and heat flux from (٢٠,٣٠ to ٤٠) Watt.

An experimental study has been carried out in the heat transfer Lab in Babylon University by using Free and Forced Convection Heat Transfer Units which are made by P.A.Hilton LTD (England). Changes in some of its parts are made to suit our study. These changes will be described in Chapter Four.

A numerical study has been obtained by using Computational Fluid Dynamic techniques. A three-dimensional solid model was constructed using Ansys package. Its dimensions are equal to the actual dimensions.

In the theoretical calculation we can calculate velocity values in three dimensions, resultant velocity, velocity vector, are predicted.

١.٣ Model Description

In the present work, three types of heat sinks which are commonly used to cooling electronic components were made, Square pin-fin, Cylindrical pin-fin and longitudinal fins (extruded fin). All the heat sinks are made of aluminum with thermal conductivity (١٥٧) W/m.^{o}C and the base dimension of the heat sink are (١١٠) mm Length, (١٠٠) mm Width, and (١٥) mm Thickness. The height of the fins are kept at (٦٨) mm. The three types of heat sink have the same area of conduction. Fig. (١-٤) describes three types of heat sink configurations.

1

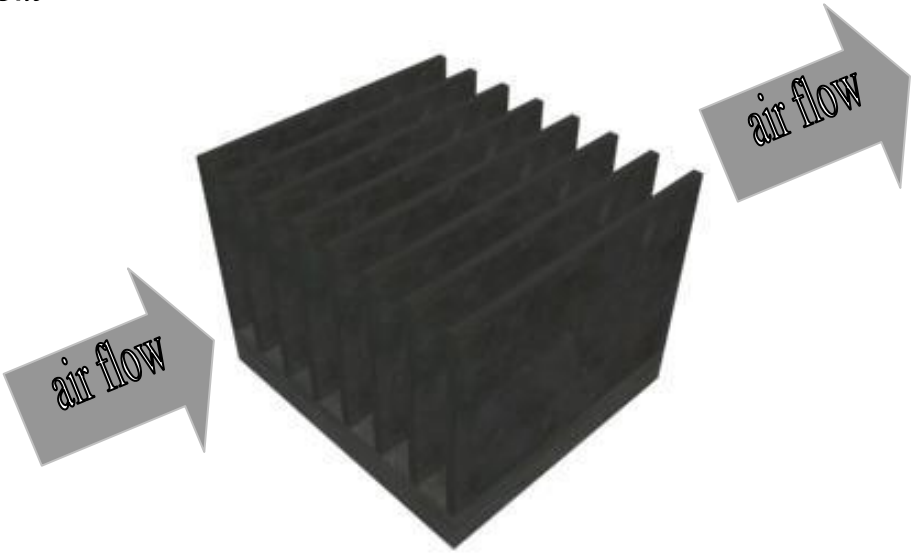

Longitudinal fin heat sink.

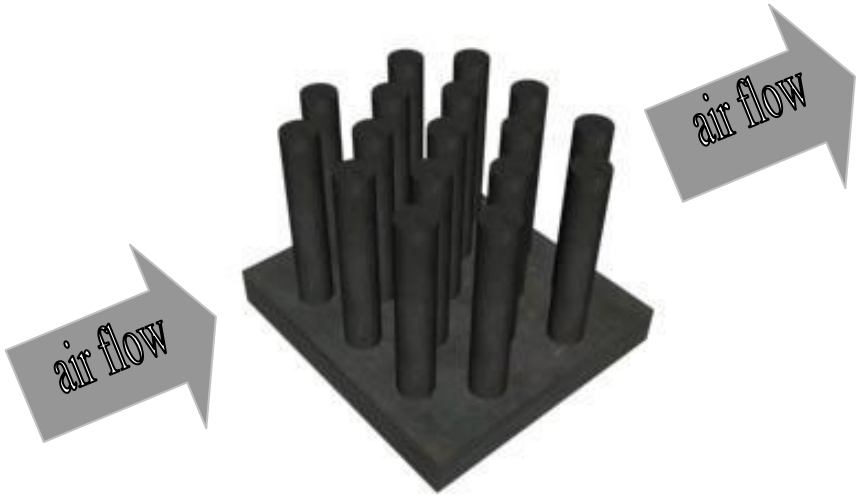

Cylindrical pin-fin heat sink.

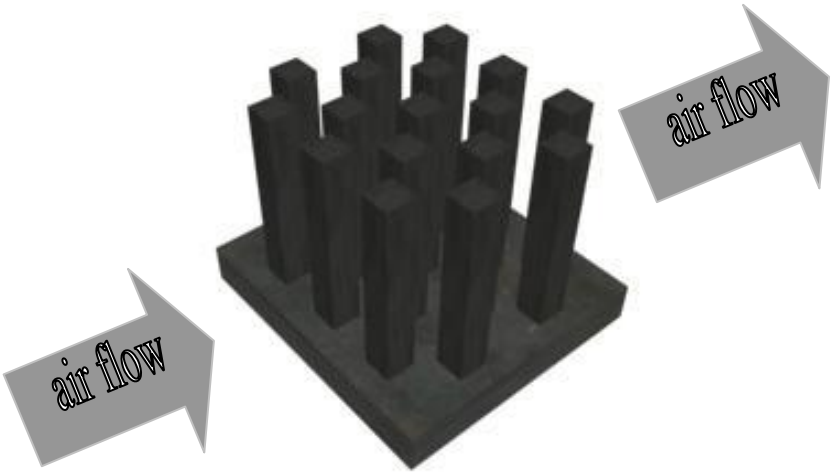

Square pin-fin heat sink.

Fig. (١-٤) Description of geometries of the present study.

Chapter 2

Literature Review

٢.١ Introduction

Enhancement techniques are frequently called for assist in the dissipation of a given heat load and in attainment of thermal control. The attachment of fins (i.e. extended surface) to primary heat transfer surface is a common approach to enhancement. A wide variety of fining arrangements is now in use and, among these, particular attention will be given here extruded fin and pin-fin. A longitudinal fin, cylindrical and square pin-fin attached perpendicular to a primary heat transfer surface and, in most applications, it is customary to use an array of fins and pin-fins to attain the desired enhancement. In conventional practice, an air stream moves parallel to the primary heat transfer surfaces and passes in cross flow through the fins and pin-fins.

A numerical and experimental investigation was conducted in order to demonstrate potential thermal performance that can be achieved by utilizing ducted air, compact heat sink design and by utilizing a chip carrier package which minimizes junction-to-case thermal resistance.

This chapter deals with recent developments in advanced air cooled heat sinks.

٢.٢ Experimental Works

The earliest experimental study for the flow and heat transfer between the fin array was performed by **Sparrow and Ramsey (١٩٧٨)**[٤], and **Sparrow** *et*

al **(١٩٨٠)**[٥] had conducted experimental studies on in-line and staggered pin-fin arrays, with various pin-tip clearance.

The pressure drop was measured across the arrays, and the heat transfer was measured by applying the analogy between heat and mass transfer to mass transfer coefficients measured via the Naphthalene sublimation technique.

The description of the apparatuses is facilitated by references to the diagram shown in Fig. (٢-١).

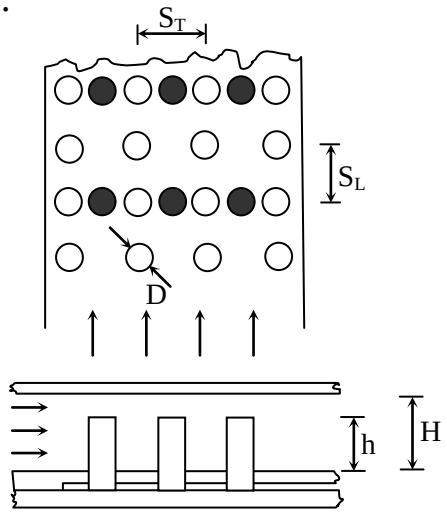

Fig. (٢-١) Diagram description of the pin-fin.

The open circles depict the deployment of the cylinders that comprise the in-line arrays studied here while the black circles depict the deployment of staggered array. The quantities (S_T, S_L and D) are identical for the two arrays, with (S_T/D=٣) ,($S_L/D=\sqrt{3/2}$) ($S_T/D\approx$ ٢.٦), (D=٠.٥٥٦) cm. The experiments encompassed h/H ratio of (٠.٢٩), and (٠.٨٧٥) with (H=١.٩١) cm. For most of the cases studied, the row-by-row heat transfer coefficient was found to vary only in the initial rows, and attained a fully developed heat transfer coefficients were also found to be insensitive to the pin height, that is to tip clearance. The coefficients increased moderately as the fin height increased (and thus the clearance decreased).

The pressure drop was very sensitive to the fin height; it was also found that in-line arrays had a lower heat transfer coefficient, but also had a lower

associated pressure drop across the heat sink, probably due to the increase of air by-pass.

Sparrow an Hajiloo (١٩٨٠)[٦] had studied experimentally the heat transfer and pressure drop characteristics of an array of staggered plates.
During the course of the experiments, the plate thickness and Reynolds number were varied parametrically. Fig. (٢-٢) describes the apparatuses under study.

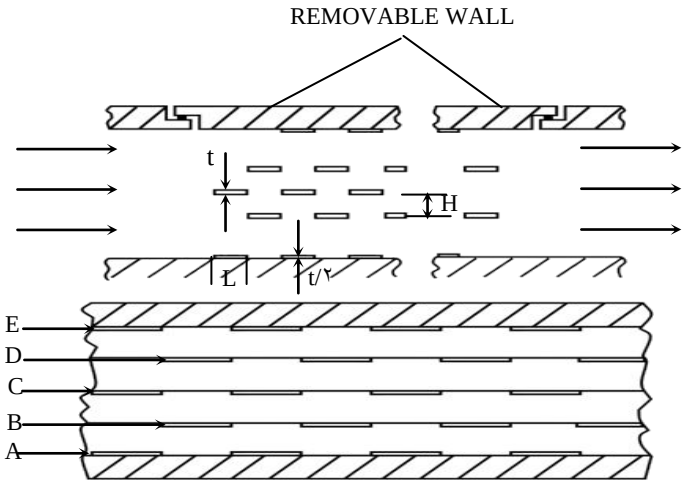

Fig.(٢-٢) Test section. upper diagram: placement of the staggered plates; lower diagram: built-up side wall showing recesses for positioning of plates.

The length (L=٢.٥) cm and the ratio of thickness to the length (t/L) are (٠.٠٤), (٠.٠٨) and (٠.١٢), (H=٠.٦٦٧) cm, the Reynolds number ranges between (١٠٠٠) and (٩٠٠٠) for each of the three plate thicknesses investigated.

Mass transfer measurements employing the Naphthalene sublimation technique were made to obtain the heat transfer results via the heat-mass transfer analogy. For a given operating condition, the per-plate heat transfer coefficients were found to be the same for the second and all subsequent rows. The fully developed heat transfer coefficients increase with Reynolds number for all the plate thickness investigated, but in different manner for all the different thicknesses. In general, thicker plates give rise to higher heat transfer coefficients, especially at the large layer Reynolds number.

The measured friction factors also increase with plate thickness. For the thickest plates the friction factor was found to be independent of the Reynolds number, signaling the dominance of inertial losses.

Tuckerman and Pease (١٩٨١)[٧] had designed a silicon micro heat sink based upon this principle and were able to dissipate very high heat flux levels, (٧٩٠) Watt/cm^{٢} with associated water temperature rise of (٧٠) ˚C based upon the same principle (micro channels).

Sparrow and Larson (١٩٨٢)[٨] had performed an experimental study to determine per fin heat transfer coefficient for pin-fin arrays exposed to a novel air flow arrangement. The flow enters the array longitudinally but, owing to blocking action of the fin base surface, is forced to turn and exit the array with a predominantly cross flow orientation. The effect of two dimensionless geometric parameters on the heat transfer and pressure drop characteristics was studied.

These parameters are the ratio (H/D) of the pin-fin height to diameter and the ratio (S/D) of the pin-fin center-to-center spacing to the diameter.

Three values of (H/D) were employed in the experiments, namely, (٤),(٨) and (١٢), while the selected nominal values of the (S/D) ratio were (٢) and (٤).

The larger of the fin diameter was (٠.٦٣٥) cm. for this diameter and with the side dimension (L) of the base plate equal to (٧.٦٨٤) cm, It is readily calculated that for a (٣٦) fin array of the type shown in the diagram of Fig.(٢-٣), the center-to-center spacing (S) is (١.٤١٠) cm.

This yields an (S/D) ratio of (٢.٢٢), which is an adequate approximation of the desired nominal value S/D = (٢). The fins were first fabricated with the height (H=١٢D) (H is the fin height that is exposed to the air flow).

Once the experiments for the (H/D) ratio were completed, the height was reduced to correspond to (H/D=٨). When the data runs for (H/D=٨) had been

carried out, a further reduction in height was made so that runs for (H/D=٤) could be made.

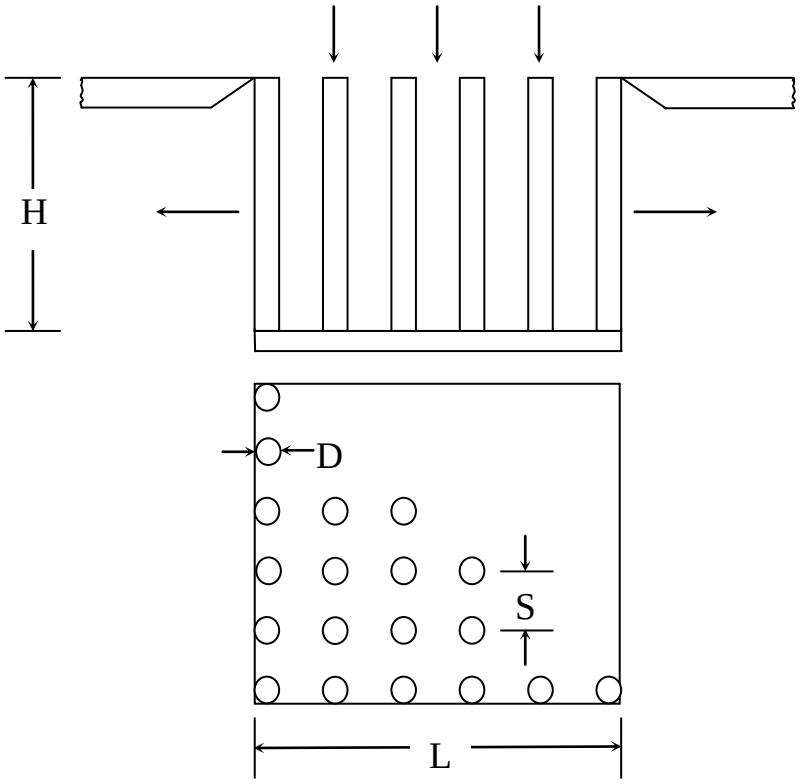

Fig.(٢-٣) Schematic of pin-fin array and air flow arrangements.

The smaller of the fin diameter was (٠.٣٥٧) cm, and the corresponding center-to-center distance was (١.٤٦٥) cm, which yields an S/D ratio equal to (٤.١٠) (approximating the nominal (S/D) value of (٤.٠)). Again the fins were initially fabricated with a height (H=١٢D), and the height was successively reduced to (H/D=٨) and to (H/D=٤) as the experiments proceeded.

For each geometric configuration, the Reynolds number was varied over an order of magnitude. In general, the results show that the fins situated adjacent to the edges of the array have higher heat transfer coefficients than those situated in the interior of the array. The Nusselt numbers for the edge- adjacent fins are virtually independent of (H/D) and (S/D) when they are correlated with Reynolds number based on a cross flow velocity.

The result show that the equation (٣-١) is remarkably close to the least square fit of the data for the corner fin (١).

$Sh = 0.385\,\mathrm{Re}_C^{\,0.625}$	...(٢.١)

The Sherwood number data for location (٤) and (٥) are interleaved, they have been fit with a common least squares power law

$Sh = 0.357\,\mathrm{Re}_L^{\,0.582}$	...(٢.٢)

The data for location (٦) (nearest the center of the array) are the lowest of all, and they have been fit to a separate least square line, The deviation between equation (٣-٢) and (٣-٣) is about (٣٠٪).

$Sh = 0.190\,\mathrm{Re}_L^{\,0.626}$	...(٢.٣)

For the interior fin, Reynolds number based on a longitudinal flow velocity was used to achieve a correlation which was insensitive to (H/D) and (S/D).

The pressure drop across the array was measured and presented in dimensionless form relative to a specially defined velocity head which gave a universal pressure drop resulting for all operating conditions.

Sparrow *et al.* **(١٩٨٢)**[٩] had studied the experimental investigation of heat transfer and pressure drop for air flow in arrays of heat generating rectangular modules deployed on one wall of a flat rectangular duct. Experiments were performed with fully populated arrays, arrays in which there are missing modules, arrays where barriers are implanted to obtain heat transfer enhancement, and arrays in which there are both a missing module and barrier.

Fig. (٢-٤) shows the array of rectangular modules along one wall of a flat rectangular duct. The dimension ratios defining the array and its related flow passage are;

(t/L=٣/٨), (S/L=١/٤), (H+t/L=١)

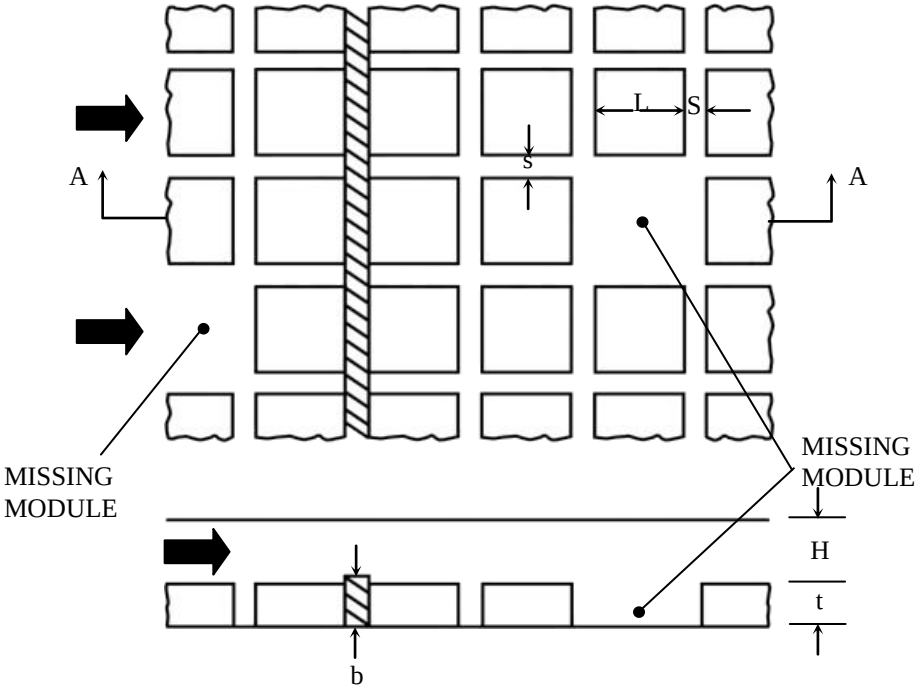

Fig.(٢-٤) Array of rectangular deployed along one wall of a flat rectangular duct.

Two barrier heights (b) were employed in the heat (mass) transfer experiments with the heights specified by;

b/(t+H)=(١/٢) and (٥/٨)

For the fully populated array without barriers, row-independent (fully developed) heat transfer coefficients were encountered for the ٥th and all subsequent rows can be represented as

$Nu = 0.0935\,\mathrm{Re}^{0.72}$	...(٢.٤)

When there is a missing module in the array, the heat transfer coefficients at neighboring modules are increased, with greatest enhancement about (٤٠ %) occurring when the missing module is just upstream of the module of interest.

The enhancement due to side-by-side pairs of missing modules differs very little from that which induces a single missing module. The implantation of a barrier in the array is shown to be an effective enhancement device, with the greatest effect about a factor of (٢) being felt in the second row downstream of the barrier but with residual enhancement persisting considerably further downstream. Under some conditions, the enhancing effects of a missing module and a barrier were found to be mutually reinforcing. Pressure distribution were measured in arrays with and without barriers, and the barrier induced pressure losses were identified.

Metzger *et al.* **(١٩٨٣)**[١٠] and **Steuber and Metzger (١٩٨٦)**[١١] had conducted a similar extensive experimental investigation of the heat transfer and pressure losses from partial length pin-fins in high aspect ratio rectangular ducts. Twenty-five pin-fin array configurations were studied. They found that the heat transfer coefficients were higher for fin extending the entire height of the channel. However, the associated pressure drop was also higher.

Goldberg (١٩٨٤)[١٢] had proposed a laminar flow copper heat sink for air cooling capable of delivering heat flux in excess of (٢٥) W/cm^{٢} at the chip level with an associated air temperature of (٦٠) ˚C.

Sparrow and Kadle (١٩٨٦)[١٣] had studied the effect of tip to shroud clearance on the resulting heat transfer.

In this experimental study the flow was turbulent, and the clearance above the fins was parametrically varied. It was determined that the heat transfer dropped significantly for increased clearance above the fins.

For clearance of (١٠),(٢٠) and (٣٠) percent of the fin height it was determined that the heat transfer rate was (٨٥),(٧٤) and (٦٤) percent of the no clearance case.

Mahalingham and Andrews (١٩٨٨)[١٤] had conducted an extensive experimental study of micro channel silicon heat sinks with air as the cooling medium. Two channel widths were studied, (٠.٠٢٥) and (٠.٠١٢٧) cm with corresponding fin height of (٠.١٧) and (٠.١١٤) cm.

The resulting aspect ratios where therefore (٦.٨) and (٩). The heat sinks were built by machining the silicon and then housing it to prevent air leakage.

The resulting heat sinks resembled a miniature extruded straight finned heat sink. Temperature and pressure drop measurements were taken at the inlet and exit section of the heat sinks. The pressure drop was found to increase linearly with the air flow rate for the range investigated.

A simplified non-compressible flow analysis (Mach number<٠.٣) was introduced, and the results of the analysis were in good agreement with the measurements.

Minakami *et al.* **(١٩٩٢)**[١٥] had reported a flow through cooled heat sink using miniature pins, the side length of the copper pins had only (٠.١٩) mm manufactured by etching. It was found that the pin spacing in the flow direction, for optimal thermal performance had about (٤.٥) pin diameters. The heat transfer increased monotonically as the transverse fin pitch decreased, with an associated penalty in pressure drop increase.

Hollworth and Durbin (١٩٩٢)[١٦] had conducted an experimental study to determine the performance of a system of low velocity air jets used to cool a simulated electronic package. The test model consisted of a uniform array of rectangular elements to a circuit board.

Each element was cooled by a cluster of four jets, and the spent fluid was vented at one end of the channel formed between the circuit board and the plate from which the jets were discharged. Results indicate that (for the geometry tested) the largest portion of the total pressure drop occurs across the jet orifices. Further, the cross flow of spent air appears to enhance heat transfer for those elements near the exit end of the channel.

Writz *et al.* (١٩٩٤)[١٧] had investigated experimentally the effect of fin density on the flow by-pass and hence on the thermal performance of the heat sink for straight fin heat sink. The heat sinks were made of aluminum with fixed fin thickness of (٢.٣) mm. The results for the fin height were varied from approximately (٨) mm to (٣٢) mm and the number of fins were changed from (٦) to (٩) to (١٢) fins to obtain flow by-pass.

The results showed flow by-pass values according to their definition up to (٦٠ %) and showed that the effective influence of flow by-pass was to reduce the overall heat transfer rate.

Azar and Mandrone (١٩٩٤)[١٨] had studied experimentally circular pin heat sinks with base dimension (٣.١٧٥ × ٣.١٧٥) cm and (١.٢٧) cm pin height. Since the air was allowed to by-pass the heat sink it was found that increasing the pin density at first increased the heat transfer but a further increase in pin density reduced the heat transfer due to greater air by pass. Thus reaching an optimal density. Results were reported mostly for a pin diameter of (٢.٢٩) mm for different upstream air speed.

Pressure drops were not reported; however, it is expected that when sufficient by-pass space exists, more or less similar air-speed upstream of the heat sink will produce similar pressure drop if the velocity measurements are made sufficiently upstream of the heat sink.

Tahat *et al.* **(١٩٩٤)**[١٩] had performed an experimental optimization of a ducted flow-through heat sink.

The circular pin material was aluminum, with a fixed diameter and pin height of (٦.٣٥) mm and (٦٠) mm, respectively, in both in-line and staggered configurations on a (٣٠٠ × ١٧٠) mm base. The number of pins was varied. It was found that the optimal pin spacing in the transverse direction was between (١) mm and (٣) mm and the longitudinal spacing was about (٧.٨) mm for both staggered and in-line arrays to obtain the maximum heat transfer rate. Pressure drop data were reported but was not considered in the optimization.

Marline (١٩٩٤)[٢٠] had studied many experimental procedure were used to compare thermal performance characterization for similar shaped air-cooled heat sinks manufactured from metallic and non metallic materials as shown in Fig. (٢-٥).

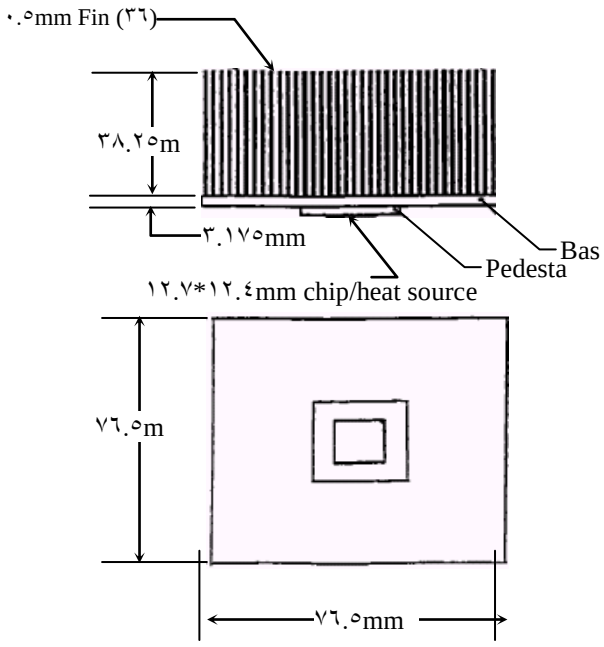

Fig.(٢-٥) Schematic diagram of fin heat sink.

The heat sink geometry was designed and optimized with the intent of cooling a single die which is dissipating (١٠٠) Watts in desktop, work station environment. One of the heat sinks was fabricated by bonding a copper base to a machined. Graphite fin structure which has a unidirectional thermal

conductivity of (٨٠٠) W/m ^{o}C. at the air velocity of (١٥٠ linear feet per minute) (١fm) and an estimated pressure loss of less than (٠.٠٣٩) inches of water, the measured sink-to-air thermal resistance was (٠.٥٣) ^{o}C /W for this copper/graphite hybrid design.

Measured junction-to-sink thermal resistance were less than (٠.٢) ^{o}C /W. when a commercially available land grid array package was used to direct attach a copper heat sink to a (٠.٥" × ٠.٥" × ٠.٠١٥") thermal test chip. Measured heat sink thermal resistance were in relatively good agreement with predicted heat sink resistance values for sea level atmospheric conditions. A modelling simplification technique is presented which allows the numerical computational time to be reduced by at least (٥٠) percent for heat optimization studies.

Shaukatullah *et al.* **(١٩٩٦)**[٢١] had reported an experimental optimization study of pin-fin arrays in cross flow with low velocities. Pin-fin arrays from (٤×٤) to (٨×٨), heights from(٥ to ٢٥) mm and width from (١.٥ to ٢.٥) mm. Results showed that a different optimal heat sink design existed from every flow velocity. All results are for a (٢٥) mm base.

Wirtz *et al.* **(١٩٩٧)**[٢٢] had reported an experimental results on the thermal performance of model fan-sink assemblies consisting of small axial flow fan which impinges air on a square array of pin-fins. Cylinder, square, and diamond shape cross-section pin-fin shapes were considered. The overall heat sink thermal resistances, R were evaluated at fixed applied pressure rise and fixed fan power.

It was concluded that cylindrical pin-fins gives the best overall fan-sink performance. In addition, only impinging flow drawn through the fin arrays was considered.

Mario *et al.* **(٢٠٠٢)**[٢٣] had conducted experimental results on the heat transfer characteristics of in line square pin fin heat sinks with and without top

by pass. A self consistent set of aluminum heat sinks were utilized, were the pin height was varied from (١٢.٥) mm to (٢٢.٥) mm; the pin pitch was varied from (٣.٤) mm to (٥.٨) mm, and the base dimensions were kept fixed at (٢٥ × ٢٥) mm. The overall base to ambient thermal resistance was measured as a function of Reynolds number and by-pass height. It was determined that the overall thermal resistance for the tallest pins increase by no more than (٢٥ %) from its zero clearance value to its value at a clearance ratio of (٣.٠).

٢.٣ Theoretical Works

The earliest analysis work for the flow and heat transfer between the fins arrays was performed by **Sparrow** *et al.* **(١٩٧٨)**[٢٤] They made an analysis of the laminar heat transfer characteristics of an array of longitudinal fins with an adiabatic shroud situated adjacent to the fin tips. The analysis involves the solution of the velocity field in the inter-fin space and in the shroud clearance gap beyond the tips, after which the governing energy equations for the fluid and the fins are solved simultaneously. Solutions are obtained for representative values of dimensionless parameters which describes the system geometry and the fin conductance. It is shown in Fig. (٢-٦), where the fin spacing parameter (S=s/H=٠.١ and ٠.٥), clearance parameter (C=c/H=٠.٠, ٠.٠٢٥, ٠.٥ and ١.٠).

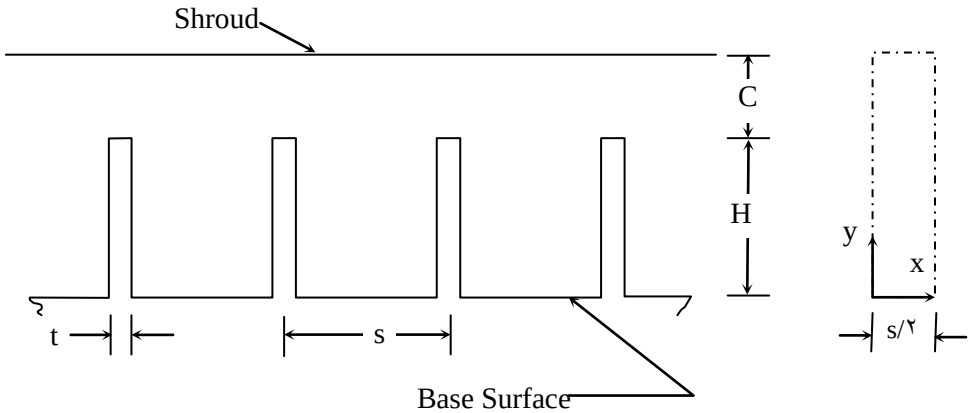

Fig. (٢-٦) Schematic cross sectional view of the shrouded fin array.

In the analysis, the following dimensionless coordinates and geometrical grouping will be employed.

$$X = \frac{x}{H}, Y = \frac{y}{H}, Z = \frac{\left(\frac{z}{H}\right)}{\left(\frac{\overline{w}H}{\alpha}\right)}, C = \frac{c}{H}, S = \frac{s}{H} \qquad \ldots(٢.٥)$$

For hydrodynamically developed flow, the momentum equation reduced to balance between the viscous and pressure forces. In dimensionless terms, the reduced momentum equation can be written as

$$\frac{\partial^2 W}{\partial X^2} + \frac{\partial^2 W}{\partial Y^2} + 1 = 0 \qquad \ldots(٢.٦)$$

Where W is a dimensionless velocity

$$W = \frac{w}{\left(\frac{H^2}{\mu}\right)\left(\frac{-dp}{dz}\right)} \qquad \ldots(٢.٧)$$

The results show that the heat loss is a minimum adjacent to the base and increases along the fin in the direction of the tip.

The maximum fin heat loss occurs either at the tip or intermediate between the base and the tip, depending on whether or not there is clearance between the fin tips and the shroud. The calculated heat transfer coefficients vary along the fin and, in some cases, take on negative values. Heat loss variations are also encountered along the base surface, the extent of which depends on the fin conductance, the inter-fin spacing, and the extent of the clearance gap. With regard to the overall heat loss, the fin is, on a unit area basis, a more efficient transfer surface than is the base. The results demonstrate

that the conventional uniform heat transfer coefficient model is inapplicable to shrouded fin arrays.

Webb and Ramadhyani (١٩٨٥)[٢٥] had analyzed fluid flow and heat transfer characteristics for a constant property fluid flowing laminarly through a parallel plate channel with staggered transverse ribs and a constant heat flux along both walls as shown in Fig.(٢-٧).

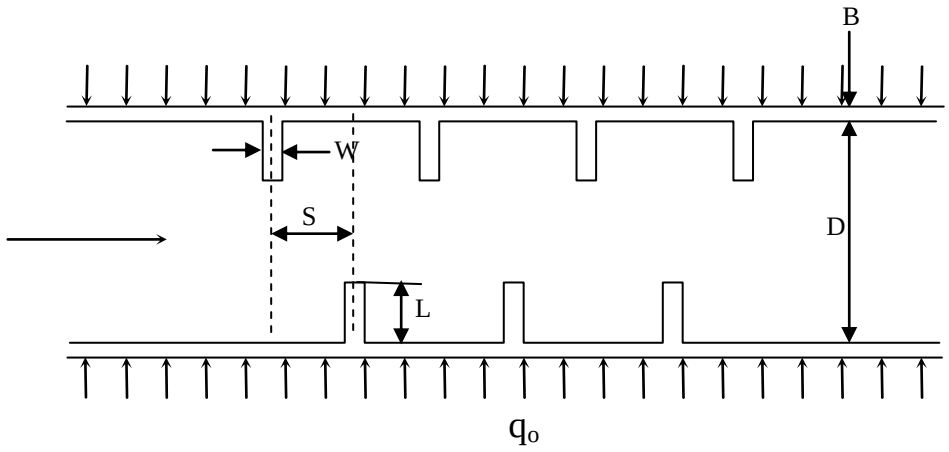

Fig. (٢-٧) Schematic of staggered fin array.

The flow is governed by the continuity and momentum equation

$\frac{\partial u}{\partial x}+\frac{\partial v}{\partial y}=0$	...(٢.٨)
$\rho\left(u\frac{\partial u}{\partial x}+v\frac{\partial u}{\partial y}\right)=\beta-\frac{\partial p}{\partial x}+\mu\left(\frac{\partial^2 u}{\partial x^2}+\frac{\partial^2 u}{\partial y^2}\right)$	...(٢.٩)
$\rho\left(u\frac{\partial v}{\partial x}+v\frac{\partial v}{\partial y}\right)=-\frac{\partial p}{\partial y}+\mu\left(\frac{\partial^2 v}{\partial x^2}+\frac{\partial^2 v}{\partial y^2}\right)$	...(٢.١٠)

The governing equation for the temperature field is

$\rho C_p\left(u\frac{\partial T}{\partial x}+v\frac{\partial T}{\partial y}\right)=k\left(\frac{\partial^2 T}{\partial x^2}+\frac{\partial^2 T}{\partial y^2}\right)$	...(٢.١١)

After a finite entry length the flow becomes periodically fully developed. Computations were carried out in the fully developed regime for different Reynolds numbers, Prandtl number and geometric arrangements. The effect of the Reynolds number on the flow and heat transfer was studied by varying Reynolds from (٣٤٠) to (٢٠٠٠) for (S/D=١) and two values of (L/D=٠.١٢٥) and (٠.٢٥). The rib height effect was analyzed by varying (L/D) from (٠.٠٦٢٥) to (٠.٣٧٥) for (Reynolds=٣٤٠) and (S/D=١). Rib spacing was studied in the range of (S/D) from (٠.٥) to (٢.٠) for (Re=٣٤٠) and (L/D=٠.٢٥). The influence of the conducting top and bottom walls on the heat transfer was investigated for all of the above cases by obtaining thermal solution for both (B/D=٠) and (B/D=٠.٠٥). The Prandtle number dependence was analyzed by solving the energy equation for (Pr=٠.٧) and (Pr=٧.٠) for all the velocity fields computed.

The influence of conjugate heat transfer in the top and bottom walls was also investigated. The protruding ribs result in the formation of separated zones in the flow field yielding substantially higher friction factors. The presence of conducting channel walls yields significantly higher overall Nusselt numbers due to the lateral redistribution of energy flow.

The geometrical configuration of approximation (L/D=٠.٢٥) and (S/D=١.٥) yields a combination of increased overall Nusselt number and comparatively low resulting friction factor. However, The augmentation of heat transfer under these conditions is probably only justifiable for high Prandtle number fluids such as water or fluorocarbons. The increase in heat transfer for gases (Pr=٠.٧) is not substantial enough to offset the added friction factor penalty.

Constans *et al.* **(١٩٩٤)**[٢٦] had developed a design tool to study pin-fin heat sink optimization. A conduction model was developed for the heat transfer

within the pins and boundary conditions were applied using empirical relations for the heat transfer coefficient.

The ellipsoid of algorithm was used to predict the minimized temperature, with the outputs as fin height, width, and spacing. The pressure drop was not considered in the optimization and was not estimated for the optimized heat sink.

Dereje and Arnold (١٩٩٥)[٢٧] had presented the application of an integrated design tool in thermal modeling of electronic packages.

The heat sink considered is pinned-finned with a rectangular and circular cross section. Two flow cases were considered; impinging and parallel flow as shown in Fig. (٢-٨) with dimensions.

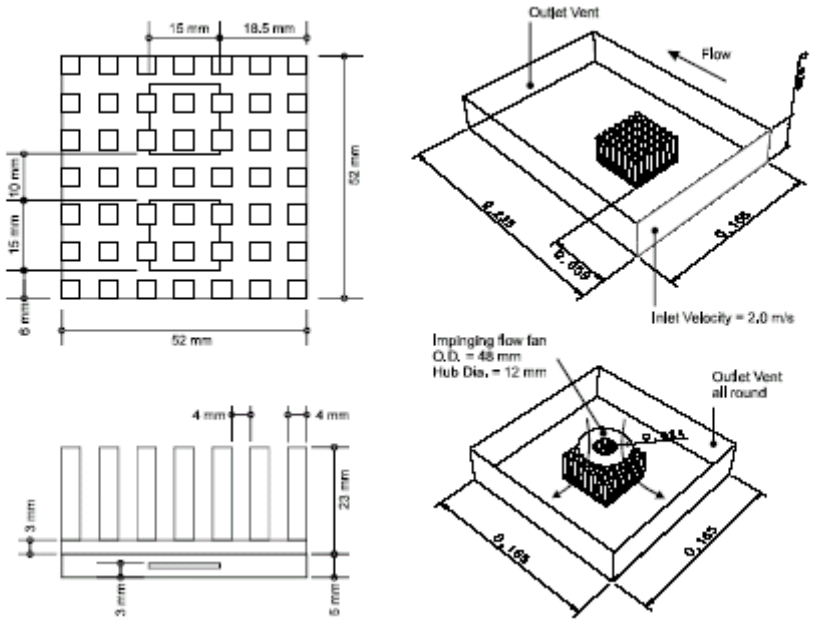

Fig. (٢-٨) Parallel and impingement air flow.

The time averaged Navir-stocks equation for conservation of mass, momentum and energy as below

$\frac{\partial v_x}{\partial x} + \frac{\partial v_y}{\partial y} + \frac{\partial v_z}{\partial z} = 0$	...(٢.١٢)

$\rho\left(u\frac{\partial u}{\partial x}+v\frac{\partial u}{\partial y}+w\frac{\partial u}{\partial z}\right)=-\frac{\partial p}{\partial x}+\mu_e\left(\frac{\partial^2 u}{\partial x^2}+\frac{\partial^2 u}{\partial y^2}+\frac{\partial^2 u}{\partial z^2}\right)$	...(٢. ١ ٣)
$\rho\left(u\frac{\partial v}{\partial x}+v\frac{\partial v}{\partial y}+w\frac{\partial v}{\partial z}\right)=-\frac{\partial p}{\partial y}+\mu_e\left(\frac{\partial^2 v}{\partial x^2}+\frac{\partial^2 v}{\partial y^2}+\frac{\partial^2 v}{\partial z^2}\right)$	...(٢. ١ ٤)
$\rho\left(u\frac{\partial w}{\partial x}+v\frac{\partial w}{\partial y}+w\frac{\partial w}{\partial z}\right)=-\frac{\partial p}{\partial z}+\mu_e\left(\frac{\partial^2 w}{\partial x^2}+\frac{\partial^2 w}{\partial y^2}+\frac{\partial^2 w}{\partial z^2}\right)$	...(٢. ١ ٥)
$u\frac{\partial \mathrm{T}}{\partial x}+v\frac{\partial \mathrm{T}}{\partial y}+w\frac{\partial \mathrm{T}}{\partial z}=\alpha\left(\frac{\partial^2 \mathrm{T}}{\partial x^2}+\frac{\partial^2 \mathrm{T}}{\partial y^2}+\frac{\partial^2 \mathrm{T}}{\partial z^2}\right)$	...(٢. ١ ٦)

For the turbulent case

$\mu_e=\mu+\mu_t$	...(٢. ١ ٧)

The fluid are incompressible, Newtonian fluid and solved for ٣D flow conditions. The eddy viscosity assumption is used to model the Reynolds stresses. For the fixed viscosity model, the turbulent viscosity is modeled as

$\mu_t=0.01\rho V_m L_t$	...(٢. ١ ٨)

Where V_m is a mean flow velocity scale and L_t a turbulent eddy length scale.

A novel approach is utilized for solving the simultaneous conductions, convection (conjugate) problem. The conduction/convection problem is solved using an element based on finite volume technique.

The results for parallel flow show that the chip junction temperature for the circular pin heat sink is (٤.٨) ^{o}C cooler than the square pin under the same flow conditions. For impinging flow condition, the chip junction temperature for

circular pin is (٢.٠) ^{o}C cooler than the square pin under the same conditions. In addition, the chip junction temperature for circular pin heat sink for impinging flow is less than for parallel flow conditions.

The circular pins, with equivalent surface area, are more effective. This is due to the improved distribution of air flow around the circular pin. The square pins promote dead zone behind each pin. The pressure loss across the circular pin heat sink is (٢.١) Pa higher than the square pin heat sink. This is likely due to the larger pin diameter for the circular pins which results in less space available for the flow between the pins. The larger pin diameter was used in order to match the surface area of the circular and square pins.

Paul (٢٠٠١)[٢٨] had performed a set of computational analysis for a system level model to test the validity of the concept of the Adiabatic Heat Transfer Coefficient (AHTC) and Superposition Kernel Function (SKF) using (FLOTHERM) software, a commercial (CFD) tool. The (AHTC) is a special sub-set of the general definition of the heat transfer coefficient and is in fact the correct heat transfer coefficient for the immediate ambient temperature that a surface will see.

This makes the (AHTC) compatible with the principle of superposition and therefore, a useful tool in the design process.

Because (CFD) solves the physics of flow and heat transfer implicitly for a model, the concept of the (AHTC) can be used directly without addition analysis method except for a quick matrix multiplication process. The method in (CFD) requires that each heat source is activated as a unit value in turn and the results are stored for any number of probed points in the system. These points are then tabulated and post processed with the actual system heat load to determine the system temperature. For forced convection system where radiation and natural convection effects are minimal the results of this study have shown excellent correlation.

٢.٤ *Experimental and* Theoretical Works

Kadle and Sparrow (١٩٨٦)[٢٩] had measured and analyzed the heat transfer rates from shrouded parallel plate heat sinks to a turbulent air stream. Average Nusselt numbers were determined by complimentary use of the experimental and analytical results and were found to compare with the widely used Petukhov–Popov correlation. Fig.(٢-٩) shows the Nusselt number as a function of the Reynolds number.

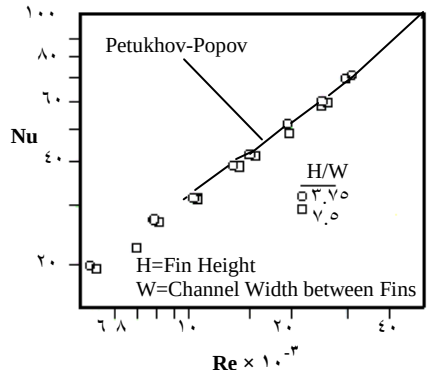

Fig. (٢-٩) Average Nusselt number versus Reynolds number.

For channels with very high aspect ratio, H >>W, the hydraulic diameter (D) approximately equal (٢W). The heat transfer coefficient can then be maximized by minimizing W. These results in very narrow channels with a very high aspect ratio, a large pressure drop across the heat sink and laminar flow, (Re < ٢١٠٠).

The limitation on narrowing the channel is basically the high pressure drop required to drive the flow.

You (١٩٨٩)[٣٠] had determined the heat transfer coefficient between a complex micro structure and flowing fluid by experimental apparatus to demonstrate the usefulness of the proposed method for the determination of the

heat transfer coefficient between the complex microstructure and the flowing fluid.

A test model of microchannel was used in which study. The pressure drop was measured and found to be compatible with the results for the case of the circular tube. The measurements of wall temperatures together with the air temprature at entarance and exit sections were used to analytically determine the heat transfer coefficient of the microchannel within an air flow. The functional relation between the Nusselt number and the Reynolds number which was also compatible with analytical solutions for the circular tube reveals that the use of the proposed method is satisfactory.

Vivek and Karl (١٩٩١)[٣١] had studied thermal analysis of Pin Grid Array chip package and heat sink using a commercial (CFD) code. Experimental measurements have been performed on similar (PGA) and heat sink in a wind tunnel. It was shown that modeling accuracy is good if it was performed with reasonable initial assumptions and boundary conditions. The computed junction temperatures and thermal resistance results were within (١٠ %) of the measured results.

Once the numerical models were calibrated against the experimental results, the model was used to optimize the thermal performance of a (PGA) package. It was shown, that by optimizing a (PGA), thermal resistance of the package can be significantly decreased.

A methodology has been presented, showing the way numerical (CAD) design tools can be used for optimization and improvement of a package design for better thermal performance.

Knight *et al.* **(١٩٩١)**[٣٢] had studied analytically the optimization for straight fin heat sinks under fully ducted conditions. The constraints on the optimization of heat transfer rates were the pressure drop, pumping work, heat

sink width, length and height. The output of the scheme was the fin and channel gaps for which the thermal resistance was computed and a minimum value was obtained by changing the number of fins and the pin to channel thickness ratio. The results were experimentally verified by changing the number of fins from (٦) to (١٢) fins for a fixed fin thickness of (٣.١٧٥) mm.

Mohaney and Vader (١٩٩٣)[٣٣] had performed an experimental and numerical study of a multichip high aspect ratio heat sink with laminar flow.

A good agreement was found between the experimental measurements and heat transfer rates from the heat sinks. The effect of power variation from chip to chip was investigated numerically. Different heat sink materials were also evaluated.

Christopher and Seri (١٩٩٤)[٣٤] had developed a numerical and experimental study using aluminium heat sinks made with extruded fin, cross-cut rectangular pin, and elliptical shaped pins in low air flow environments. Fig.(٢-١٠) describes the geometry of the heat sinks.

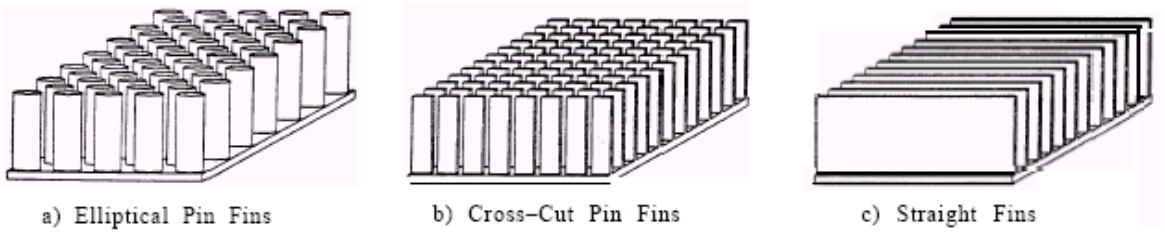

Fig. (٢-١٠) Schematic diagram of heat sinks.

The heat sinks were made of cast aluminium alloy with thermal conductivity equal to (١٦٨) W/m.^{o}C., the elliptical pin-fin heat sink was made by an extrusion alloy. The specific pin detail can only be made economically by this process. Each pin cross section is in the shape of an ellipse with a major axis of (٥.٥٤) mm and minor axis of (١.٢٧) mm. However, the leading and trailing ends of the ellipse came to a sharp edge, simulating the air foil feature. The

(١٠٥) pins were staggered with an outer grid being (١٠×٦) and an inner grid of (٩×٥).

In order to determine the applicability of this shape in heat sink design similar test samples with conversional rectangular longitudinal extruded fins were made. The heat sink extrusion chosen for this test has ten (١.٥٢) mm thick fins equally spaced across (٥٨.٤٢) mm. The overall height of the profile was (٢٩.٢١) mm with a base thickness of (٢.٥٤) mm. Two extruded heat sinks were made and one had an additional manufacturing process called cross-cutting. This material removal enables air to pass through pins in a manner similar to the elliptical pin-fin design. There were nine cuts along the (٥٨.٤٢) mm length, and each cut removed (١.٥٢) mm of material with (٤.٣٢) mm long pins.

A commercial package is available which incorporates the above expressions. Sauna'M from thermal solutions, Inc. is a conjugate thermal modelling tool which incorporates computer aided design and heat transfer required with (CFD) and (FEA) analysis. This software allows for accurate modelling of the heat sink base plate with fin by accounting for conduction heat transfer from the exposed surfaces. The thermal gradients are predicted along the entire heat sink plate.

The elliptical pin heat sink was designed to minimize the pressure losses across the heat sink by reducing the vortex effects and to enhance the thermal performance by maintaining large exposed surface area available for heat transfer. The performance of the elliptical pin heat sink was compared with those of extruded straight and cross-cut fin heat sinks. The results of the straight fin were also compared with this obtained by using Sauna^{TM}, a commercially available heat sink modelling program developed based on empirical expression. In addition to the thermal measurements, the effect of air flow by-bass characteristics in open duct configuration was investigated. As expected, the straight fin experienced the lowest amount of flow by-bass over the heat sink.

For this particular application, where the heat source is localized at the centre of the heat sink base plate, the overall thermal resistance of the straight fin was lower than other two designs mainly due to the combined effect of enhanced lateral conduction along the fins and the lower flow by-bass characteristics.

Arnold *et al.* **(١٩٩٥)**[٣٥] had been developed a next generation system, based on proven simulation technology, that improves efficiency over currently available solutions. The package combines the intuitive characteristics of thermal network modelling with powerfull Computational Fluid Dynamics technology to model (٣D) fluid flow. Experimental thermal measurements for several cases are compared to values calculated by the system.

A cross-cut pin-fin heat sink was modelled with a uniform heat load applied to the bottom of the sink and air flow across the fins. The sink temperature was measured at the centre of base on the aluminium heat sink. A complete description of the heat sink as well as the experimental test measurement is shown in Fig. (٢-١١).

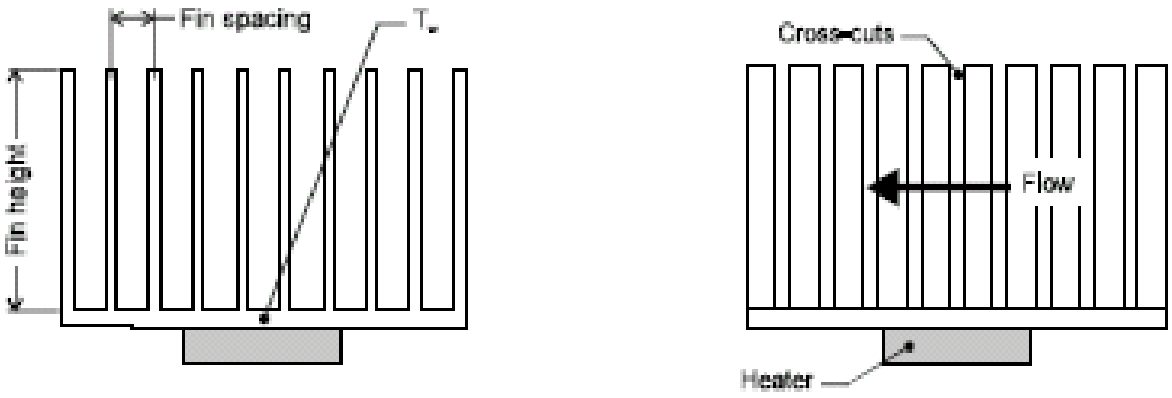

Front View Side View

Fig.(٢-١١) Cross-cut pin-fin heat sink.

The sink consists of (١٠) straight fins; (٢٥.٤) mm fin height, (١.٥٢) mm fin thickness and (٦.٣٢) spacing between fins. The fins were cross-cut at nine equally spaced points of the sink and each cut removed (١.٥٢) mm of material.

A constant velocity field was defined upstream from the sink. A (٤٠) Watt heat loaded was applied to the centre of the sink base over a (٢٥.٤) mm by (٢٥.٤) mm area. Several cases were solved using (٠.٥) m/s, (١.٠) m/s, (٢.٠) m/s and (٤.٠) m/s inlet velocity at the entrance of the heat sink. In all cases the inlet air temperature was (٢٠) ^{o}C.

The result were slightly less accurate at the lower flow of (٠.٥) m/s. This may be partly due to the limitations of predicting precise heat transfer coefficients in low Reynolds number turbulent flows. Good correlation with experimental results is demonstrated for each of the test cases. In addition, the need for flexible modelling tools is demonstrated to facilitate an understanding of heat transfer and fluid flow which are an essential part of the thermal engineering process.

Sath and Sammakia (١٩٩٨)[٣٦] had resulted in the recent emphasis on low-cost high-end servers and desktop workstation and a renewed interest in the development of high –performance air-cooled system.

A new generation of advanced heat sink designs capable of dissipating up to (١٠^{٥}) Watt/m^{٢} have been proposed and developed.

Better manufacturing tolerance, low defects, and an improved understanding of card and enclosure effects have been attained and shown to be critical to achieve the desired thermal performance.

Advanced internal thermal enhancements, encompassing high thermal conductivity adhesives and greases have also been implemented.

Adam and Izundu (٢٠٠٠)[٣٧] had studied the thermal characteristics of straight-channel longitudinal fin heat sinks under forced air cooling Computational Fluid Dynamic code.

The study focused on investigating the viability of employing commercially available (CFD) codes as effective and efficient means of gathering the vast amount of data required to adequately quantify heat sink characteristics in ducted flow. The ducted heat sink assembly is shown in Fig.(٢-١٢).

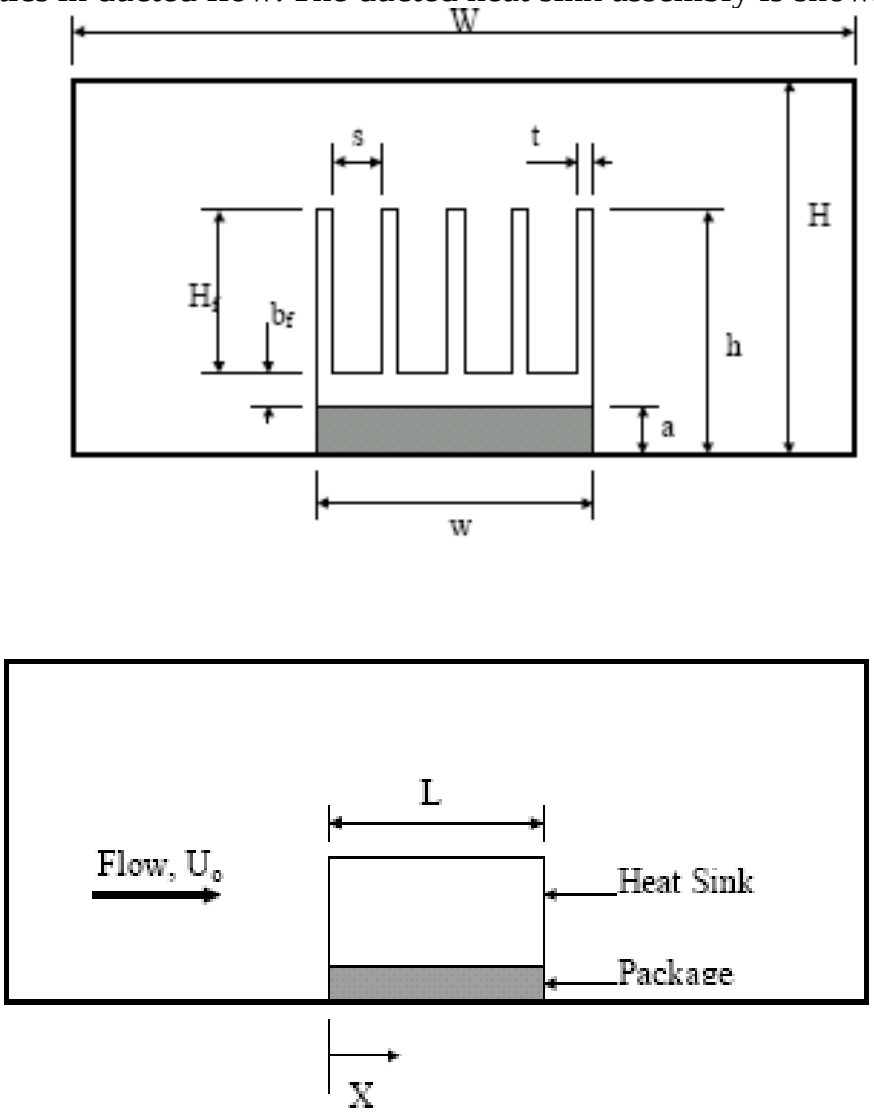

Fig. (٢-١٢) Ducted heat sink geometry.

Definitions of the dimensional parameter nomenclature and dimensional values used in the study are summarized in Table (٢-١).

The thermal boundary condition consists of a constant heat dissipation of (٥٠) Watt at the base of each heat sink. The heat sink material was specified as aluminum with thermal conductivity, *k*, of (٢٠٠) Watt/m.^{o}C.

The parameters studied include the tip clearance and span wise spacing across a range of approach flow rate and fin densities. These parameters were used to examine the influence of flow by-pass phenomena on the thermal resistance and pressure drop across the heat sinks. The numerical results are very good agreement with Wirtz [١٧].

The result had shown that for the same fin density and tip clearance, that the by-bass effect is more pronounced at lower approach flow rates, and decreases, albeit gradually at higher flow rates. This effect was even more pronounced in Wirtz et al[١٧] study presumably because of the zero lateral clearance used in this study.

Flow by-pass arises because the fins are present on obstruction to the air flow. An increase in the fin density increase the flow resistance through the heat sink. Thus the fluid will tend to flow toward the regions of lower flow resistance, which in this case are the lateral and tip gaps around the heat sink. The increased flow resistance with fin density is caused by two factors: Increased frictional losses due to increased fluid surface contact area, and increased acceleration or form losses due to the more pronounced change in flow cross section at the location of the heat sink.

As has been demonstrated by the results obtained in the present study, Computational Fluid Dynamics and Heat Transfer Models offer practical and effective means of gathering the vast amount of data required.

Baris *et al*. **(٢٠٠١)**[٣٨] had presented an experimental and analytical study aimed at obtaining physical insight into the behavior of square, in-line pin-fin heat sinks. In the experimental study, various size aluminum heat sinks were utilized, where the pin heights were (١٢.٥) mm and (٢٢.٥) mm, and the base dimensions were kept fixed at (٢٥×٢٥) mm. A “two-branch by pass model” was developed, in which a one- dimensional differential approach was used to model the fluid flow through the heat sink and its top by pass duct. Central to the

analysis is the introduction of accurate correlations for inlet, exited and core pressure drop within the heat sink.

Pressure drop predictions correlated with the experimental data when pressure drop coefficients measured for the heat sinks were used. Agreement was poorer when classical circular tube bundle pressure drop correlations were utilized, but the accuracy was high enough for design purpose. Inlet and exit pressure losses were as important as the core pressure drop in establishing the overall flow and pressure drop.

٢.٤ Literature Review Conclusion

It can be conclude from the literature review that the governing equations for conjugate problem is very difficult to solve analytically, especially for the complex shape of heat sinks. Hence, some assumptions are used to simplify the solution.

For the case of pin-fin heat sinks configuration, however, work is spars. The obvious reason for this is that within pin-fin heat sinks, the flow is dominated by flow separation and complex three-dimensional flow at the pin-base junction. Hence, simple closed form analytical model of the friction and heat transfer coefficients is not possible.

Pioneers in these efforts typically used general purpose Computational Fluid Dynamics (CFD) programs and Finite Element (FE) or Finite Difference (FD) based thermal analysis programs. The general purpose nature of these products, as well as the state of (CFD) technology, dictated that users are to achieve any reasonable results.

Recent advances in Computational Fluid Dynamics and heat transfer simulation have recently introduced several commercially available software packages. These packages are increasingly utilized by thermal engineers as design tools for thermal engineering.

In the present study had been attempt to compare the heat transfer performance of various commonly used fin geometries. Realistic, manufacturable geometries are optimized for minimizing thermal resistance at moderate turbulent air velocities. The basis of comparison was chosen to be that all of the heat sink fins have the same area of conduction and same area of base plate. CFD simulation were carried out an a Three-dimensional adiabatic flow. The air velocity was in the range (٢) to (٦) m/s.

parameter	Range Modeled
N, number of fins	{٩,١٢}
a, component package height	٦ mm
b_f, sink base thickness	٤ mm
w, sink/package width	٥٦ mm
L, sink/package width	٥٦ mm
t, fin width	٢.٥ mm
s, fin gap width	(w-N*t)/(N-١)
h_f, fin height	h_f = ٢٤ mm
h, total package/sink height	h = h_f + (a+b_f) = ٣٤ mm
H, duct height	H={٣٤mm,٤٤mm,٥٤mm}
W, duct width	W = {٥٦mm,٢٨٨mm)

Table (٢-١) Summarized dimensional values of study by Adam[٣٧].

The Reference	Type of the Work	Tow or Three Dimensions	Parallel or Impingement Flow
Sparrow, [٤]	Experimental	-	Parallel
Sparrow, [٥]	Experimental	-	Parallel
Sparrow, [٦]	Experimental	-	Parallel
Tuckerman,[٧]	Experimental	-	Parallel
Sparrow, [٨]	Experimental	-	Impingement
Sparrow, [٩]	Experimental	-	Parallel
Metzger, [١٠]	Experimental	-	Parallel
Steuber, [١١]	Experimental	-	Parallel
Goldberg, [١٢]	Experimental	-	Parallel
Sparrow, [١٣]	Experimental	-	Parallel
Mahalingam. [١٤]	Experimental	-	Parallel
Minakami, [١٥]	Experimental		Parallel
Holleorth, [١٦]	Experimental	-	Impingement
Wirtz, [١٧]	Experimental	-	Parallel
Azar, [١٨]	Experimental	-	Parallel
Tahat, [١٩]	Experimental	-	Parallel
Marlin [٢٠]	Experimental		Parallel
Shaukatullah, [٢١]	Experimental	-	Parallel
Wirtz, [٢٢]	Experimental	-	Parallel
Mario, [٢٣]	Experimental	-	Parallel
Sparrow, [٢٤]	Experimental	-	Parallel
Webb, [٢٥]	Theoretical	(٢-D)	Parallel
Constans, [٢٦]	Theoretical	(٢-D)	Parallel
Dereje, [٢٧]	Theoretical	(٢-D)	Parallel
Paul, [٢٨]	Theoretical	(٣-D)	Parallel
Kadel, [٢٩]	Theoretical	(٣-D)	Parallel
You, [٣٠]	Exp.and Theo.	(٢-D)	Parallel
Vivek, [٣١]	Exp.and Theo.	(٢-D)	Parallel
Knight, [٣٢]	Exp.and Theo.	(٣-D)	Parallel
Mohaney, [٣٣]	Exp.and Theo.	(٣-D)	Parallel
Chrstopher, [٣٤]	Exp.and Theo.	(٣-D)	Parallel
Arnold, [٣٥]	Exp.and Theo.	(٣-D)	Parallel
Sath, [٣٦]	Exp.and Theo.	(٣-D)	Parallel
Adam, [٣٧]	Exp.and Theo.	(٣-D)	Parallel
Baris, [٣٨]	Exp.and Theo.	(٣-D)	Parallel

Table (٢-٢) Abstract of the Literature Review.

Chapter 3

Theoretical Work

٣. ١ Introduction

A study of heat sink fin technologies has given information for the important design criteria for practical cooling of electronic components.

The design of pin-fin heat sinks challenges existing thermal modeling techniques. It is generally accepted that the most comprehensive modeling for a heat sink system would be Computational Fluid Dynamics (CFD). Either by using a finite volume or finite difference method, the actual phenomena at the fin surface can be quantified. Unfortunately, significant modelling and run time is needed to accurately represent small pins with complex meshing. A second technology, Finite Element Analysis(FEA) can also be useful in determining performance, especially conductivity gradients. The heat transfer coefficient can be determined by using advance (FEA) codes which incorporate fluid mechanics. However, each pin must be individually discredited, increasing the modelling time substantially.

Most of the numerical models in the past have focused on low density rectangular fin array as the modeling for denser fins and resulted in a grid size that surpassed the capacity of the computer system available to a practicing engineer. Also, there has been very little effort in computational modeling of cylindrical and other non-Cartesian fins as most of the available commercial

(CFD) codes did not have Body-Fitted-Coordinates (BFC) or unstructured meshing capability.

Even for those codes that had (BFC), the modeling of a high density fin array was impossible due to the higher number of required control volumes.

It is to be emphasized that if the problem cannot be solved in a reasonable time, the model is not of too much practical value as it would be difficult to perform a parameterized study when each simulation takes a significant amount of time. According, most models have consisted of decoupling the conduction heat transfer from the convective heat transfer. This is accomplished by first coming up with a heat transfer coefficient (using a CFD code, or a correlation), and then using a finite element code (FEA) to solve the conduction problem.

٣.٢ Governing Equations

The governing equations solved for the flow field are the continuity, momentum and energy equations in three dimensions, and these are;

$$\frac{\partial \rho}{\partial t}+\frac{\partial(\rho Vx)}{\partial x}+\frac{\partial(\rho Vy)}{\partial y}+\frac{\partial(\rho Vz)}{\partial z}=0 \qquad \ldots(٣.١)$$

$$\rho\left(\frac{\partial u}{\partial t}+q\nabla u\right)=\rho Xx-\frac{\partial p}{\partial x}+\frac{\partial}{\partial x}\left\{\mu\left[2\frac{\partial u}{\partial x}-\frac{2}{3}(divq)\right]\right\}+\frac{\partial}{\partial y}\left[\mu\left(\frac{\partial u}{\partial y}+\frac{\partial v}{\partial x}\right)\right] + \frac{\partial}{\partial z}\left[\mu\left(\frac{\partial w}{\partial x}+\frac{\partial u}{\partial z}\right)\right] \qquad \ldots(٣.٢)$$

$$\rho\left(\frac{\partial v}{\partial t}+q\nabla V\right)=\rho Xy-\frac{\partial p}{\partial y}+\frac{\partial}{\partial y}\left\{\mu\left[2\frac{\partial v}{\partial y}-\frac{2}{3}(divq)\right]\right\}+\frac{\partial}{\partial z}\left[\mu\left(\frac{\partial v}{\partial z}+\frac{\partial w}{\partial y}\right)\right]+ \frac{\partial}{\partial x}\left[\mu\left(\frac{\partial u}{\partial y}+\frac{\partial v}{\partial x}\right)\right] \qquad \ldots(٣.٣)$$

$$\rho\left(\frac{\partial w}{\partial t}+q\nabla w\right)=\rho Xz-\frac{\partial p}{\partial z}+\frac{\partial}{\partial z}\left\{\mu\left[2\frac{\partial w}{\partial z}-\frac{2}{3}(divq)\right]\right\}+\frac{\partial}{\partial x}\left[\mu\left(\frac{\partial w}{\partial x}+\frac{\partial u}{\partial z}\right)\right]+$$
$$\frac{\partial}{\partial y}\left[\mu\left(\frac{\partial v}{\partial z}+\frac{\partial w}{\partial y}\right)\right] \qquad \ldots(٣.٤)$$

$$\frac{\partial}{\partial t}(\rho C_pT)+\frac{\partial}{\partial x}(\rho V_xC_PT)+\frac{\partial}{\partial y}(\rho V_yC_pT)+\frac{\partial}{\partial z}(\rho V_zC_pT)=\frac{\partial}{\partial x}\left(k\frac{\partial T}{\partial x}\right)+\frac{\partial}{\partial y}\left(k\frac{\partial T}{\partial y}\right)$$
$$+\frac{\partial}{\partial z}\left(\frac{\partial T}{\partial z}\right)+Q_v \qquad \ldots(٣.٥)$$

Where;

V_x, V_y, V_z = components of the velocity vector in x, y and z directions.

ρ = density

μ_e = effective viscosity

Q_v = Volumetric heat source

C_p = specific heat

k= thermal conductivity.

The equations above are the Navir-stocks equation and energy equation [٣٩]. Some terms must be eliminated when solving the problem. For the steady state analysis the time dependent terms must be eliminated. The density enters as a constant value. Therefore, the final form of the continuity and momentum

equations is as follows;

$$\frac{\partial v_x}{\partial x}+\frac{\partial v_y}{\partial y}+\frac{\partial v_z}{\partial z}=0 \qquad \ldots(٣.٦)$$

$$\rho\left(u\frac{\partial u}{\partial x}+v\frac{\partial u}{\partial y}+w\frac{\partial u}{\partial z}\right)=-\frac{\partial p}{\partial x}+\mu_e\left(\frac{\partial^2 u}{\partial x^2}+\frac{\partial^2 u}{\partial y^2}+\frac{\partial^2 u}{\partial z^2}\right) \quad \ldots(٣.٧)$$

$$\rho\left(u\frac{\partial v}{\partial x}+v\frac{\partial v}{\partial y}+w\frac{\partial v}{\partial z}\right)=-\frac{\partial p}{\partial y}+\mu_e\left(\frac{\partial^2 v}{\partial x^2}+\frac{\partial^2 v}{\partial y^2}+\frac{\partial^2 v}{\partial z^2}\right) \quad \ldots(٣.٨)$$

$$\rho\left(u\frac{\partial w}{\partial x}+v\frac{\partial w}{\partial y}+w\frac{\partial w}{\partial z}\right)=-\frac{\partial p}{\partial z}+\mu e\left(\frac{\partial^2 w}{\partial x^2}+\frac{\partial^2 w}{\partial y^2}+\frac{\partial^2 w}{\partial z^2}\right) \quad \ldots(٣.٩)$$

$$u\frac{\partial \mathrm{T}}{\partial x}+v\frac{\partial \mathrm{T}}{\partial y}+w\frac{\partial \mathrm{T}}{\partial z}=\alpha\left(\frac{\partial^2 \mathrm{T}}{\partial x^2}+\frac{\partial^2 \mathrm{T}}{\partial y^2}+\frac{\partial^2 \mathrm{T}}{\partial z^2}\right) \quad \ldots(٣.١٠)$$

For the turbulent case the effective viscosity ($\mu e=\mu+\mu t$).

Where;

μ = Laminar viscosity (fluid property)

μt = Turbulent viscosity

α = thermal diffusivity.

The governing equation for the solid field (heat sink) is only the right side of the energy equation.

$$\frac{\partial^2 T}{\partial x^2}+\frac{\partial^2 T}{\partial y^2}+\frac{\partial^2 T}{\partial z^2}=0 \quad \ldots(٣.١١)$$

٣.٣ Fins Geometries

The geometries of the simulation domain follows the geometries of the experimental test section used in the College of Engineering Heat Transfer Laboratory in University of Babylon. Experimental data are described in Chapter Four.

The general arrangements of the heat sink are given in Fig. (٣-١).

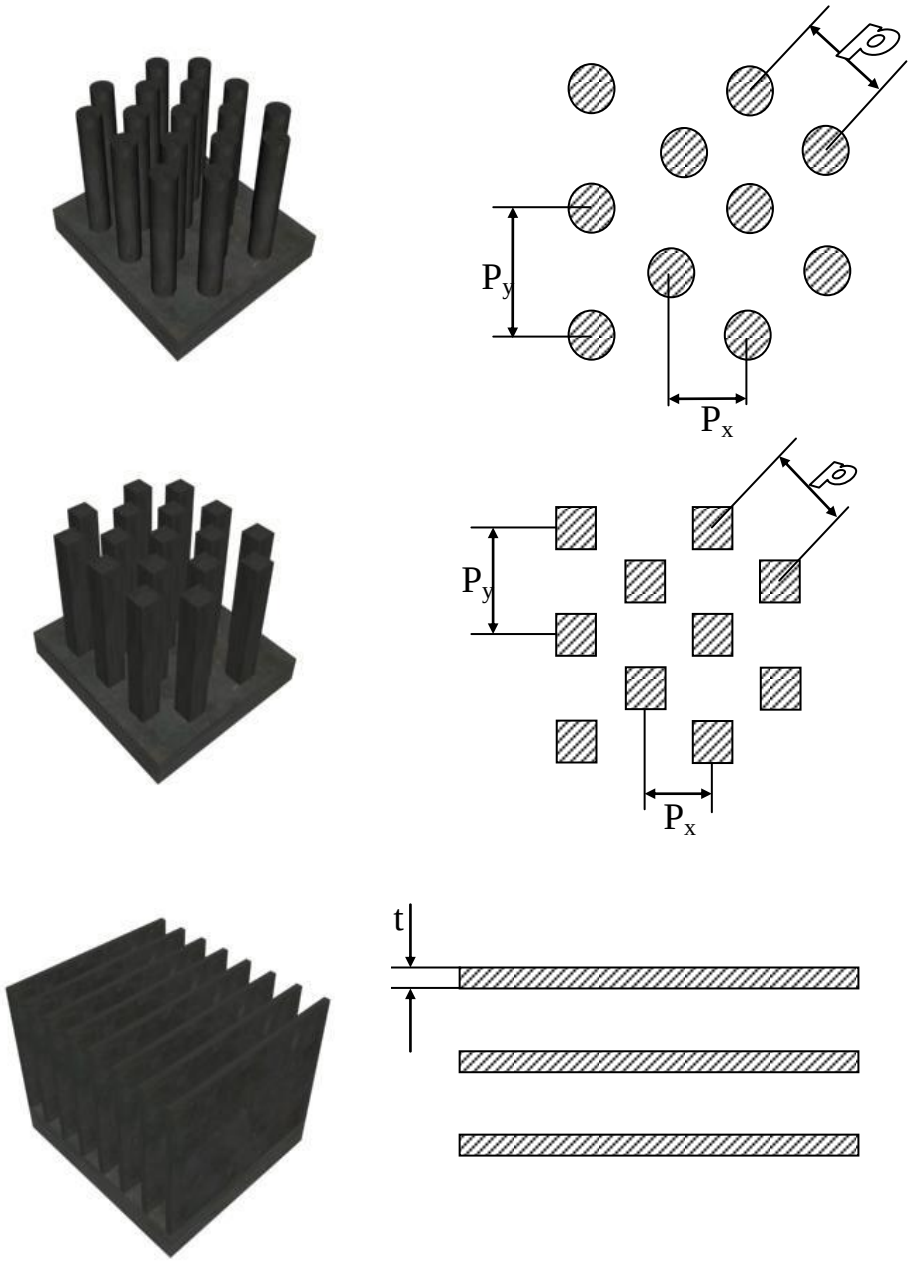

Fig (٣-١) Pin-fins and fins arrangements.

The length as well as the width of the heat sink are (٠.١) m and (٠.١١) respectively, whereas the height (H) is (٠.٠٦٨) m. The conductive base plate, which connects pin-fins, is (٠.٠١٥) m high.

The heat sinks solid structure, which is exposed to air cross-flow, consists of three types of heat sinks: cylinder, square and longitudinal fin heat sink.
The cylinder pin-fin which consists of ٥rows of aluminium pin-fins in the stream wise (*x*-direction) and ٧rows in the transverse (*y*-direction).

The diameter of the pin-fin is (d=٠.٠١٢٥) m. The pitch-to-diameter ratio in the stream wise direction is set to (P_x/d=١.٤٠٨) and in the transverse direction to (P_y/d=٢.٢٢).

For the square pin-fin which also consists of ٥ rows of aluminium pin-fin in the stream wise (*x*-direction) and ٧rows in the transverse direction (*y*-direction). The side length of the pin-fin is (L_s=٠.٠٠١) m. The pitch-to-side length in the stream wise direction is set to (P_x/L_s=١.٦) and the transverse direction to (P_y/L_s=٢.٥٢}.

The longitudinal fin heat sink consists of ٨fins of aluminium in the stream wise of (x-direction) which has the thickness (t=٠.٠٠٣٢٥) m.

The material properties are also taken from the experimental cases. The entering flow profile is uniform due to the fan placed in front of the test section.

The heat sink is heated from below by an electric resistance heater. A thermal conduction material (Zinc Oxide) placed between the heater and aluminium base sets the thermal conditions at the base bottom.

Similarly, the experimental data were taken at thermal power of (٢٠), (٣٠),and (٤٠) Watt. The numerical simulations are performed at the same thermal power.

٣.٤ The Boundary Conditions

The boundary conditions for the model equations attempt to represent the experimental conditions described previously. For the momentum transport equation, no-slip boundary conditions are implemented at all four walls to the flow direction.

The boundary condition must be applied on the areas. The model velocity varies by varying the velocity of the air at the entrance. The velocity on the surfaces of the heat sinks must be set to zero to simulate the solid walls. Also, upper, lower and side wall of the duct are given zero velocity where the duct has closed test section. The exit of the test section has not specified the air velocity; the offset pressure on the exit section must be set to zero.

The temperature field in the fluid results from a balance between thermal convection in the test stream wise direction, thermal diffusion and the convection heat transfered from the solid structure to the fluid flow. Therefore, the specified temperature for the inlet air and four walls of the duct must be applied as the boundary condition. Heat load is applied at the bottom of the heat sink as a thermal boundary condition and simulation to experimental work.

٣.٥ Numerical Solution

Thermal analysis of heat exchangers system requires the simulation of turbulent air flow, conduction, convection, advection and often radiation. Issues include, flow non-uniformity, turbulent low Reynolds Number flow as well as complex geometry. An ANSYS software package was utilized to simulate the thermal and flow behaviour of the heat sink models. Ansys software uses a hybrid approach.

An element based on Finite Element method was used for simulating conduction and convection. This is coupled with an unstructured element based finite element Computational Fluid Dynamics (CFD) code which solves the

complete Navir-Stockes equations. A unique thermal coupling method allows ANSYS software to simulate convective and conduction heat paths between disjoint element meshes on arbitrary geometry. This coupled is very complex in the ANSYS software package and does not have enough information, therefore, the solution in the present study solves the continuity and momentum equations (adiabatic flow) for three dimensional.

The theoretical results presented in this chapter are obtained by ANSYS program. This software package solves the fluid flow problem by solving momentum and continuity equation. The two equations K-ε model (turbulence model) is used to over come the turbulence in the flow. By using the finite element technique, this program analyzes the flow field through the heat sink models. There are many types of meshing controls where the boundary conditions can be changed to overcome all the actual boundary conditions.

٣.٥.١ ANSYS Program

ANSYS finite element analysis software enables engineers to perform the following tasks:

- Building computer models or transfer CAD models of structures, components, or systems.
- Applying operating loads or other design performance conditions.
- Studying physical responses such as stress levels, temperature distributions, or electromagnetic fields.
- Optimizing a design early in the development process to reduce production costs.
- Doing prototype testing in environments where it otherwise would be undesirable or impossible (for example, biomedical applications).

The ANSYS software package has a comprehensive graphical user interface (GUI) that gives the user easy, interactive access to program function commands documentation, and reference material an intuitive menu system helps users navigate through the ANSYS program. Users can input data using a mouse, a keyboard, or a combination of both.

٣.٥.٢ ANSYS GUI

The easiest way to communicate with the ANSYS program is by using the ANSYS menu system called the graphical user interface (GUI). Both beginners and experienced Ansys users use the GUI for virtually all interactive ANSYS work. The GUI provides an interface between you and the ANSYS program which commands the drive internally.

Each GUI function is a series of picks resulting in an action ultimately produces one or more Ansys commands that the program executes and record on the input history file (Job name. LOG). The GUI then enables you to perform an analysis with little or no knowledge of the Ansys commands.

٣.٥.٣ Performing a Typical ANSYS Analysis

The Ansys program has many finite element analysis capabilities, ranging from a simple, linear, static analysis to a complex, non linear, transient dynamic analysis.

The analysis guide manuals in the Ansys documentation set describe specific procedure for performing analysis for different engineering disciplines.
A typical Ansys analysis has three distinct steps;

- Build the model and mesh.
- Apply loads and obtain the solution.
- Review the results.

٣.٥.٣.١ Model and Mesh Forming

A- Solid Model Form

Heat sinks in a duct are a solid model and they must be built to simulate the experimental test. A three dimensional model for three types of heat sinks is built and meshed.

Solid models are classified into three regions;

١- ***Inlet region:***

a. Locating the key point by entering its coordinates; (the number of key points of the inlet region duct are (٨)).

b. Locating the volume of the region by joining between the key points.

٢- ***Heat Sink Region (Test Region):***

a. Locating the key point by entering its coordinates; (the numbers of key points are (٤)).

b. Locating the volume of the region by joining between the key points.

c. Locating the volume of the heat sink by entering the coordinates of each type.

d. Distinguishing between the volume of the duct and the volumes of the heat sink by the overlap command.

٣- ***Outlet Region***:

a. Locating the key point by entering it coordinate;(the number of key points of the outlet region duct are (٤)).

b. Locating the volume of the region by joining between the key points.

٣.٥.٣.٢ Solid Model Mesh

Three regions of each solid model must meshed one after another. To mesh any volume the lines of that volume must be divided first. Two factors must be noted when creating line divisions. The first factor is the line number of divisions. For fin mesh these divisions must be increased. The second one is the aspect ratio, which is the relationship among the divisions. If the entered aspect ratio number is greater than one, the length of line is increased gradually.

By using this technique, meshed volume has different mesh density as follows;

١. Inlet region which has division (٢٠) with aspect ratio (-٢). The mesh was fine toward the heat sink as in Fig. (٣-٢).

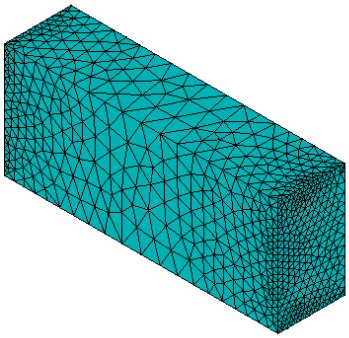

Fig. (٣-٢) Mesh of inlet region.

٢. Heat sink region which has a number of divisions (٣٠) with aspect ratio equals to one (regular mesh). The mesh is very fine in that region as in Fig. (٣-٣).

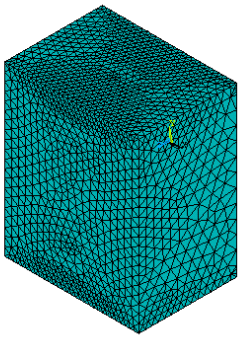

Fig. (٣-٣) Mesh of test region.

٣. Outlet region which has a number of divisions (٢٠) with aspect ratio (٣). The mesh was fine nearest the heat sink as in Fig. (٣-٤).

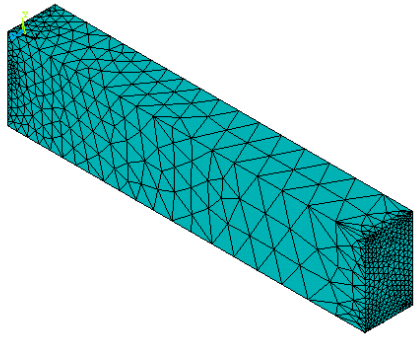

Fig. (٣-٤) Mesh of outlet region.

Free mesh is used because of irregular volume in the region of heat sinks. The aspect ratio of every element must be specified the distance between the two nodes (in the element) must be decreased when the change in the flow property is increased in this direction. Bilinear tetrahedral and three dimensional elements which were used to mesh the flow field volumes as shown in Fig. (٣-٥). The shape function equation is;

$$\Phi = Ni\,\Phi i + Nj\,\Phi j + Nk\,\Phi k + Nl\,\Phi l + Nm\,\Phi m + Nn\,\Phi n + No\,\Phi o + Np\,\Phi p$$

Where Φ: the degree of freedom.

$$\begin{aligned} Ni &= (1-s)(1-t)(1-r) \\ Nj &= (1+s)(1-t)(1-r) \\ Nk &= (1+s)(1+t)(1-r) \\ Nl &= (1-s)(1+t)(1-r) \\ Nm &= (1-s)(1-t)(1+r) \\ Nn &= (1+s)(1-t)(1+r) \\ No &= (1+s)(1+t)(1+r) \\ Np &= (1-s)(1+t)(1+r) \end{aligned} \qquad \text{...(٣.١٢)}$$

where: s, r, t are the local coordinates

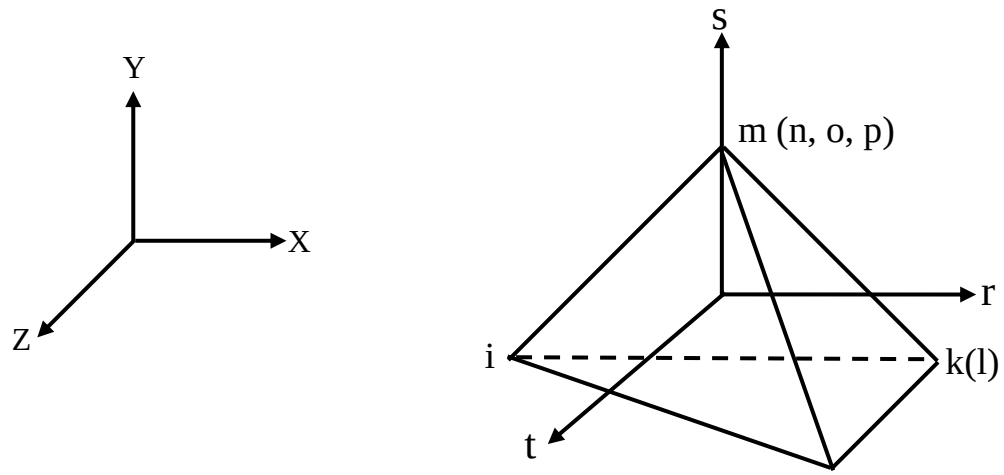

Fig. (٣-٥) Tetrahedral three dimensional elements.

٣.٥.٣.٣ Setting FLOTRAN Analysis Parameters

Options such as turbulence, incompressible flow, etc. must be in order to use them to obtain reliable solution, the options of the analysis must be chosen carefully.

The follow analysis must be steady state (time independent), turbulence (depending on Reynolds number), and adiabatic (temperature independent) to solve the momentum and continuity equations and neglecting the energy equation and incompressible (depending on the value of Mach number).

Air is the chosen fluid SI for analysis and its properties are taken from the table in the program depending on nominal temperature (٢٥ °C).

٣.٥.٣.٤ Solving the Problem

The partial differential equations solved by FLOTRAN in two equation models, the Turbulent Kinetic Energy equation is

$$\frac{\partial \rho k}{\partial t}+\frac{\partial\left(\rho v_x k\right)}{\partial x}+\frac{\partial\left(\rho v_y k\right)}{\partial y}+\frac{\partial\left(\rho v_z k\right)}{\partial z}=\frac{\partial}{\partial x}\left(\frac{\mu_t}{\sigma_k}\frac{\partial k}{\partial x}\right)+\frac{\partial}{\partial y}\left(\frac{\mu_t}{\sigma_k}\frac{\partial k}{\partial y}\right)+$$
$$\frac{\partial}{\partial z}\left(\frac{\mu_t}{\sigma_k}\frac{\partial k}{\partial z}\right)+\mu_t\phi-\rho\varepsilon+\frac{C_4\beta\mu_t}{\sigma_t}\left(g_x\frac{\partial T}{\partial x}+g_y\frac{\partial T}{\partial y}+g_z\frac{\partial T}{\partial z}\right) \quad \ldots(٣.١٣)$$

And the Dissipation Rate equation is

$$\frac{\partial \rho \varepsilon}{\partial t}+\frac{\partial\left(\rho v_x \varepsilon\right)}{\partial x}+\frac{\partial\left(\rho v_y \varepsilon\right)}{\partial y}+\frac{\partial\left(\rho v_z \varepsilon\right)}{\partial z}=\frac{\partial}{\partial x}\left(\frac{\mu_t}{\sigma_\varepsilon}\frac{\partial \varepsilon}{\partial x}\right)+\frac{\partial}{\partial y}\left(\frac{\mu_t}{\sigma_\varepsilon}\frac{\partial \varepsilon}{\partial y}\right)+$$
$$\frac{\partial}{\partial z}\left(\frac{\mu_t}{\sigma_\varepsilon}\frac{\partial \varepsilon}{\partial z}\right)+C_{1\varepsilon}\mu_t\frac{\varepsilon}{k}\phi-C_2\rho\frac{\varepsilon^2}{k}+ \quad \ldots(٣.١٤)$$
$$\frac{C_\mu\left(1-C_3\right)\beta\rho k}{\sigma_t}\left(g_x\frac{\partial T}{\partial x}+g_y\frac{\partial T}{\partial y}+g_z\frac{\partial T}{\partial z}\right)$$

$\mu_t=\rho C_\mu\frac{k^2}{\varepsilon}$	...(٣.١٥)

The final term in each equation are terms used to model the effect of buoyancy are described by **Viollet**[٤٠].

Default values for the various constants in the standard model are provided by **Lauder and Spalding**[٣٩] and are given in Standard Model coefficients.

C_1,$C_{1\varepsilon}$	C_2	C_μ	σ_k	σ_ε	σ_t	C_3	C_4
١.٤٤	١.٩٢	٠.٠٩	١.٠	١.٣	١.٠	١.٠	٠.٠

Table (٣-١) Standard Model Coefficients.

٣.٥.٣.٥ Examining the Results

Convergence is the parameter used for examining the results. As a FLOTRAN simulation proceeds, ANSYS calculates convergence monitors for each degree of freedom every global iteration. Convergence monitors are computed for velocities, pressure, turbulent kinetic energy and kinetic energy dissipation rate.

The convergence monitors are the normalized measure of the solutions rate of change from one iteration to another. Denoted by the general field variable (ϕ), and any degree of freedom, the convergence monitor is defined as follows;

$$Conv.Mon. = \frac{\sum_{i=1}^{N} \left| \Phi_i^n - \Phi_i^{n-1} \right|}{\sum_{i=1}^{N} \left| \Phi_i^n \right|} \qquad \ldots(٣.١٦)$$

Where;

N = Total number of finite element node.

n = Current global iteration number.

Φ = Degree of freedom.

Observing the rate of change of the solution and the behavior of the relevant dependent variable can monitor the solution convergence of the analysis.

٣.٥.٣.٦ Checking Results of Computer Model

To verify the results, the procedure listed below should be taken into consideration:

١. Checking the mass balance printed as parts of the result summary.

٢. Checking the boundary condition within Ansys to ensure that they are accurate.

٣. Checking if the properties are specified correctly.

٤. If the unexpected results diverge the solution, the finite element mesh may not have sufficient resolution, or significant gradients may exist near the outlets.

Chapter 4

Experimental Work

٤.١ Introduction

Heat exchanger can be found in a number of different industrial sectors where the need to transport heat between existing media.

Consequently, wide spread use of heat exchangers has caused development to take place in a piecemeal fashion in a number of rather unrelated area. The technology of heat exchangers, familiar in one sector, has progressed slowly across the boundaries of the different sectors.

The conduction-convection heat transfer for forced convection forms the basis of most industrial heat exchangers' related equipment. The measurement and the experimental work for such circumstances is achieved in heat transfer lab in Babylon University by studying the temperature profiles and velocity distribution in an air duct with associated three types of extended heat transfer surfaces in the present study.

The horizontal duct is so constructed that the air temperature and velocity can be readily measured, and a variety of "plug-in" modules of heated solid surfaces of known dimensions is presented to the air stream for detailed study. A fan situated at one side of the duct provides the air stream for forced convection experiments.

An independent bench-mounted console contains temperature measurement, power control, and fan speed control circuits with appropriate instrumentation. Temperature measurement, to the resolution of (٠.١) ^{o}C, is used thermostat sensors with direct digital read-out in ^{o}C. Air velocity is measured with a portable anemometer mounted on the duct.

The power control circuit provides a cautiously variable, electrical out put of (٠-١٠٠) Watts with a direct read out in watts.
Using these instrumentation provided forced convective heat transfer coefficients are determined for:

١. An array of fins (finned heat sink)
٢. An array of cylinders (pinned heat sink)
٣. An array of squares (pinned heat sink)

Each module may be used independently, on the bench, to determine forced convection coefficient for horizontal flow.

٤.٢ Experimental Apparatus

The main aim of the research is to specifying a better performance and heat dissipation of three types of heat sinks by studying the velocity and temperature distribution and locating the heat transfer coefficient for several air speed and heat flux. All these parameter required building up the main experimental rig.

Fig. (٤-١) shows experimental apparatus consisting of three types of heat sinks, centrifugal fan, test section, control system for power supply to heat source and temperature measurement of the base plate of heat sink, and portable anemometer, a data acquisition system to be used with PC to control the test section and all measurement. All requirements are shown in Fig.(٤-٢). The experiments were carried out in one type of inlet and outlet region.

One heat sink location in the duct of several inlet velocities and heat fluxes are used in this study. The duct was constructed from aluminum material of height (٠.٠٧٣) m, width (٠.١٢٥) m and length (١) m.

The cooling fluid is air supply by centrifugal fan with inlet velocity (٢), (٣), (٤), and (٦) m/s. The main rig consists of three types of heat sinks which are connected with control system to change the power supply (heat flux) for each one (٢٠),(٣٠), and (٤٠) Watt. The temperature measurements in rig are controlled by data-acquisition system with (PC).

Velocities at different positions are measured by a portable anemometer. Fig. (٤-١) shows the experimental apparatus consisting of centrifugal fan. Test section control system for power supply heat flux and thermocouples for temperature measurement in flow field and on the heat sinks, and portable anemometer to measure the velocity at a selector positions are shown in Figs. (٤-٣), (٤-٤), (٤-٥).

Moreover a new positions for measured velocity and temperature on the heat sink have been chosen to give more accurate results.

٤.٢.١ Interface Cart and Software Driver

Interface cart is logically used to change the measured data (temperature) from test section to PC. To take all parameters above building software by visual basic version (٦.٠) was occurred to control the test section from PC. The software driver consists of several forms and some function. These procedures are used for the dynamic-linked libraries (abbreviated as.dll) available from other resources to access the available centronic ports because VB (٦.٠) doesn't support any commands for port accessing.

٤.٣ Measurement Procedure

Before starting the reading, two tests are made to check the instrumentation. The first test is to ensure that the velocity reading of the portable anemometer is zero and its reading of the temperature is corrected with the thermocouple reading before running.

The second test is to make sure that the thermocouple was correctly attached to the surface of the fins by reading the sensor number in the PC. If there is any significant difference for anyone of the thermocouples. The thermocouples are not correctly attached to the surface.

٤.٣.١ Velocity Measurement

The velocity had been measured at the entrance of the duct to select a suitable velocity value which was (٢), (٣), (٤), and (٦) m/s. Also measured velocity and temperature in the selecting position as shown in Figs (٤-٣), (٤-٤) and (٤-٥) marked by ($A_{١-١}$, $B_{١-١}$, $C_{١-١}$, $D_{١-١}$…etc) which was given its coordinates (x , y, z) in the test section (heat sink) which gave us body contour for the velocity and temperature distribution in the test section .

Fig. (٤-٣) represents the position for measuring the air velocity and temperature for the cylindrical pin-fin heat sink, Fig. (٤-٤) represents the position of measuring the air velocity and temperature for the square pin-fin heat sink. Fig. (٤-٥) represents the positions of measuring the air velocity and temperature for the longitudinal fin heat sink.

The velocity measured by portable anemometer is shown in Fig. (٤-٦) which gives the digital reading of air velocity in one direction. It also gives us the temperature of air at the same position.

٤.٣.٢ Temperature Measurement

In all industrial plants the measurement of temperature is of crucial importance in monitoring the performance and correct functioning of the process involved. The choice of the most suitable temperature sensing device in any given situation is therefore of particular significance in the design, operation and maintenance of the plant.

The ever increasing cost of using energy also places considerable emphasis on the measurement of temperatures to ensure that optimum efficiencies are being obtained.

In the present study tow positions of temperature measurement were needed. The first position in the core of heat sink to measuring air flow temperature, The second position is the surface of pin or fin and the base of heat sinks, this positions are marked by ($S_١$, $S_٢$, $S_٣$, $S_٤$, $S_٥$ ….etc) as describes in Figs (٤-٣), (٤-٤) and (٤-٥). Thermocouple type (**K**) are used because it was overcome temperature range which needed in the study and available in the Heat Transfer Lab.

The calibration of thermocouple type (K) was occur by using Temperature Measurement Unit by compare its reading with a platinum resistance thermometer. Table (٤-١) gives information of thermocouple type as shown below.

Thermocouple Type	Name of Materials	Useful Application Range
B	Platinum ٣٠٪ Rhodium(+) Platinum ٦٪ Rhodium(-)	١٣٧٠-١٧٠٠ ^{o}C
C	Tungsten ٥٪ Rhenium (+) Tungsten ٢٦٪ Rhenium (-)	١٦٥٠-٢٣١٥ ^{o}C
E	Chromium (+) Constantan (-)	-٢٠٠-٩٠٠ ^{o}C
J	Iron (+) Constantan (-)	٠-٧٥٠ ^{o}C
K	Chromium (+) Aluminum (-)	-٢٠٠-١٢٥٠ ^{o}C
N	Nicrosil (+) Nisil (-)	٦٥٠-١٢٦٠ ^{o}C
R	Platinum ١٣٪ Rhodium (+) Platinum (-)	٨٧٠-١٤٥٠ ^{o}C
S	Platinum ١٠٪ Rhodium (+) Platinum (-)	٩٨٠-١٤٥٠ ^{o}C
T	Copper (+) Constantan (-)	-٢٥٠-٣٥٠ ^{o}C

Table (٤-١) Thermocouple Reference[٤١].

Temperature measurement in the heat sink was made by two ways:

١. Temperature measured by the portable anemometer associated with measured velocity. This instrument enables us to measure temperature through the heat sinks at various locations by using three dimensional transverse mechanism. Body contours for temperature distribution for three dimensional of heat sinks can be plotted.

٢. Temperature measurement at various locations in the surface and base of heat sinks was determined by the use of an insulated thermocouple type **K** (٠.٢٧) mm Chromium-Aluminum thermocouple wire. The thermocouple wire was cut into pieces, each pieces of the wire was skinned from both ends and one of the ends was spot-welded forming a spherical bead. In all experiments we used (١٥) thermocouples on the surface of fins to determine the temperature value on he surface of fins as shown in Fig. (٤-٧).

All measured data was controlled by using data-acquisition system to convert all analog measurement reading to digital reading in (PC.) and recorded this data in file during (١٠) s.

To check that all experiments will be in steady-state condition, choose some points to study their temperature value during the time, as shown in Fig.(٤-٨).

Wherever its found that the solution will need about (٢٠) min to receive a steady state condition, all data are recorded after (٢٠) min.

٤.٣.٣ Thermal Conductivity Measurement

The thermal conductivity of the material (Aluminum) used for manufacturing heat sinks was measured by using the instrument shown in Fig. (٤-٩).The instrument was manufactured by P.A Hilton Company LTD (England). The theoretical basic for the instrument is the Fourier Law where cylindrical sample is heated by using an electrical heater. After this, the temperature was read over the sides of the sample by digital thermocouples.

The distance between every two thermocouples was (١٠) mm. This thermocouple read the change in temperature over the sides of the sample. Through the temperature recorded by the instrument, the curve shown in

Fig. (٤-١٠) can be plotted which explains the temperature gradient ($\Delta T/\Delta X$) applied in the Fourier Law to measure (k).

$$q = -k\,A\frac{\Delta T}{\Delta X} \qquad \text{...(٤-١)}$$

where

q; heat flow (Watt) [measured directly from the instrument. A; Area perpendicular to heat flow (m^2). $\Delta T/\Delta X$; Temperature gradient, and k; Thermal conductivity.

q (Watt)	T_h (°C)	T_c (°C)	k (Watt/m. °C)
١٠	٣٢.١	٢٨	١٥٥.٢٧
١٥	٣٧.٦	٣١.٥	١٥٦.٥٥
٢٠	٤٤.١	٣٦	١٥٧.١٩
٢٥	٥١.٤	٤٠.٢	١٥٦.٠٣
٣٠	٥٦.٧	٤٤.٥	١٥٦.٥٥
٣٥	٦١.٥	٤٧.٣	١٥٦.٩١
٤٠	٦٧.٧	٥١.٤	١٥٦.٢٣

Table (٤-١) show the test reading to measure thermal conductivity.

By taking the average value of the thermal conductivity from the above table, the resulting value of $k \approx$ ١٥٦ Watt/m.^{o}C.

٤.٤ Errors

The thermocouple calibration is shown in Fig. (٤-١١), with an error of less than (٠.٥) ^{o}C where the thermocouple is pinned to the surface of the fins to measure temperature. The thermocouple was connected with (PC) by interface cart to convert all analog measurement data to digital data from (PC) in each experiment with an error of less than (٠.٠٠٥ %) ^{o}C.

The anemometer temperature was calibrated with the thermocouple temperature, as in Fig. (٤-١٢), with error less than (١٠٥) ^{o}C.

The calibration process is very sensitive to the probe alignment, probe support and any blockage so the procedure is repeated more times that get

smoothing curves where the polynomial curve-fit method fourth-order was used. The accuracy of processed data shown in table (٤-٢) was good with a range of errors of approximately not exceeded (± ٢.٥٪)[٤٢].

Velocity Vector R in (m/sec)		
Actual	Measured	Error %
١٥.٦	١٥.٩	١.٩
١٥.٩	١٦.١	١.٢
١٥	١٤.٨	١.٣
١٥.٧	١٦	٢.٥
١٥.١	١٤.٩	١.٣
١٥.٨	١٦	١.٢
١٥.٩	١٦.٣	٢.٥
١٥	١٤.٧	٢
١٥.١	١٥.٤	١.٩

Table (٤-٢) Anemometer measurement errors.

Fig. (٤-٢) Photograph of test section.

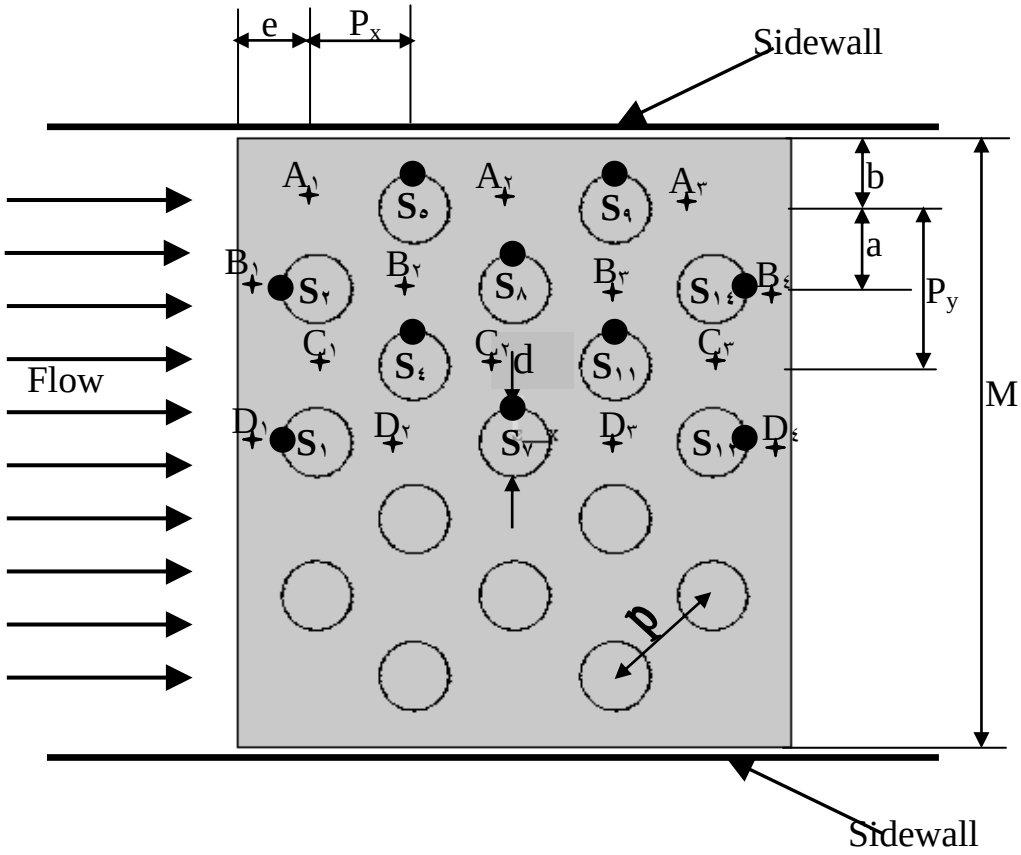

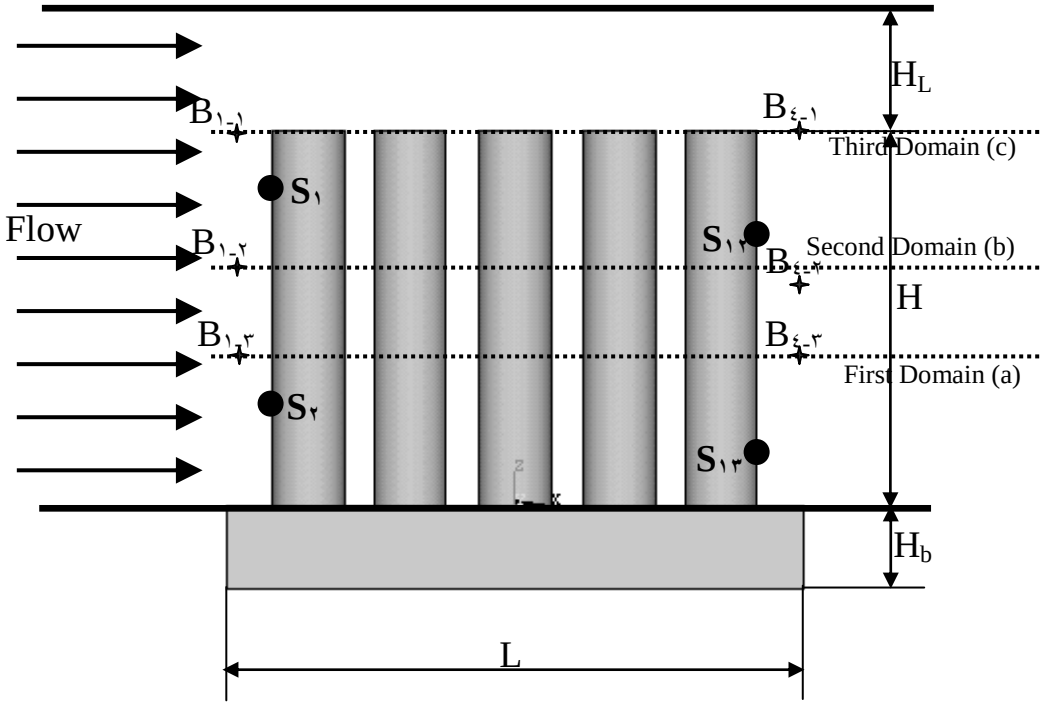

Fig. (٤-٣) Positions of temperature and velocity measurement for cylindrical pin-fin.

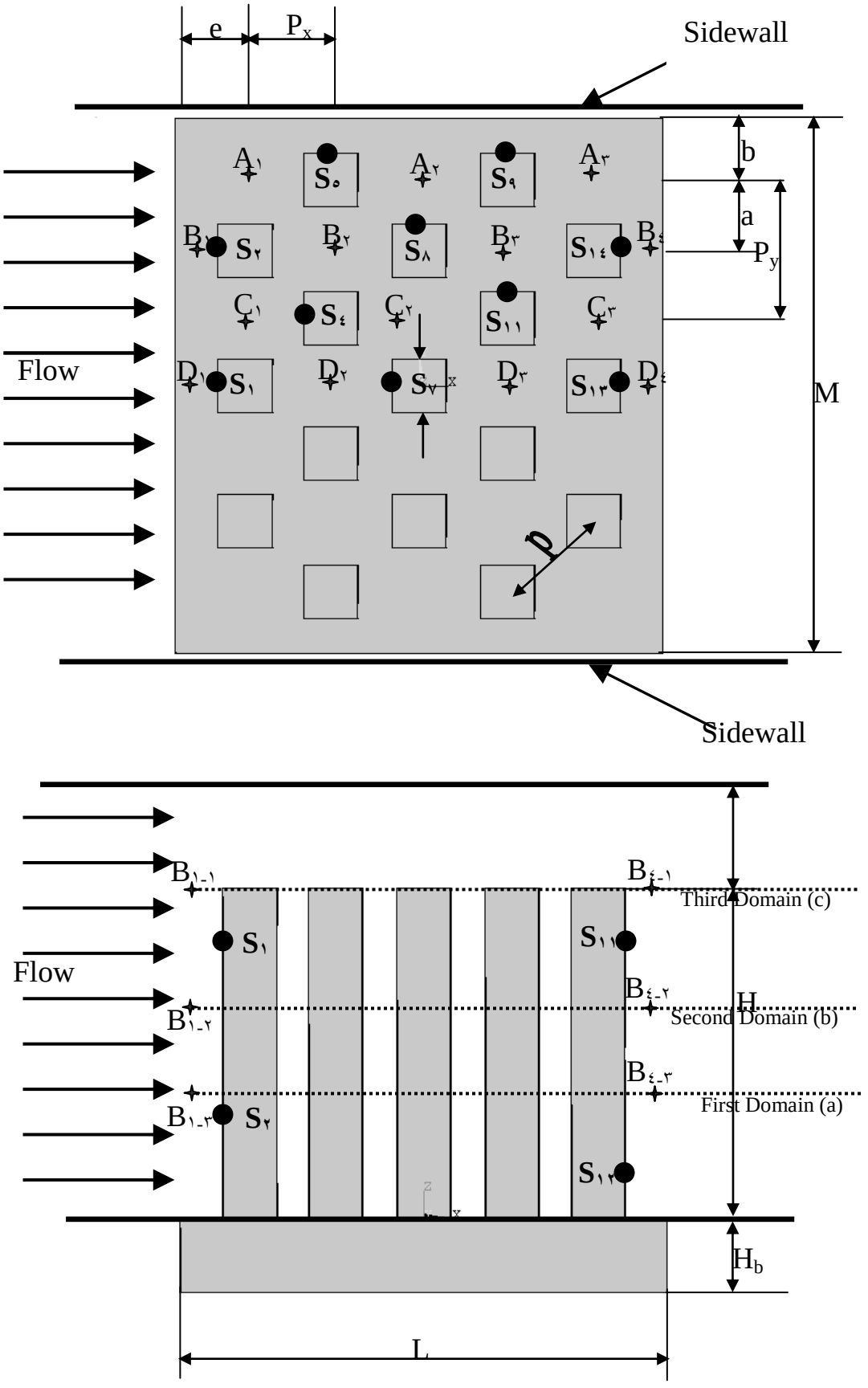

Fig. (٤-٤) Positions of temperature and velocity measurement for square pin-Fin.

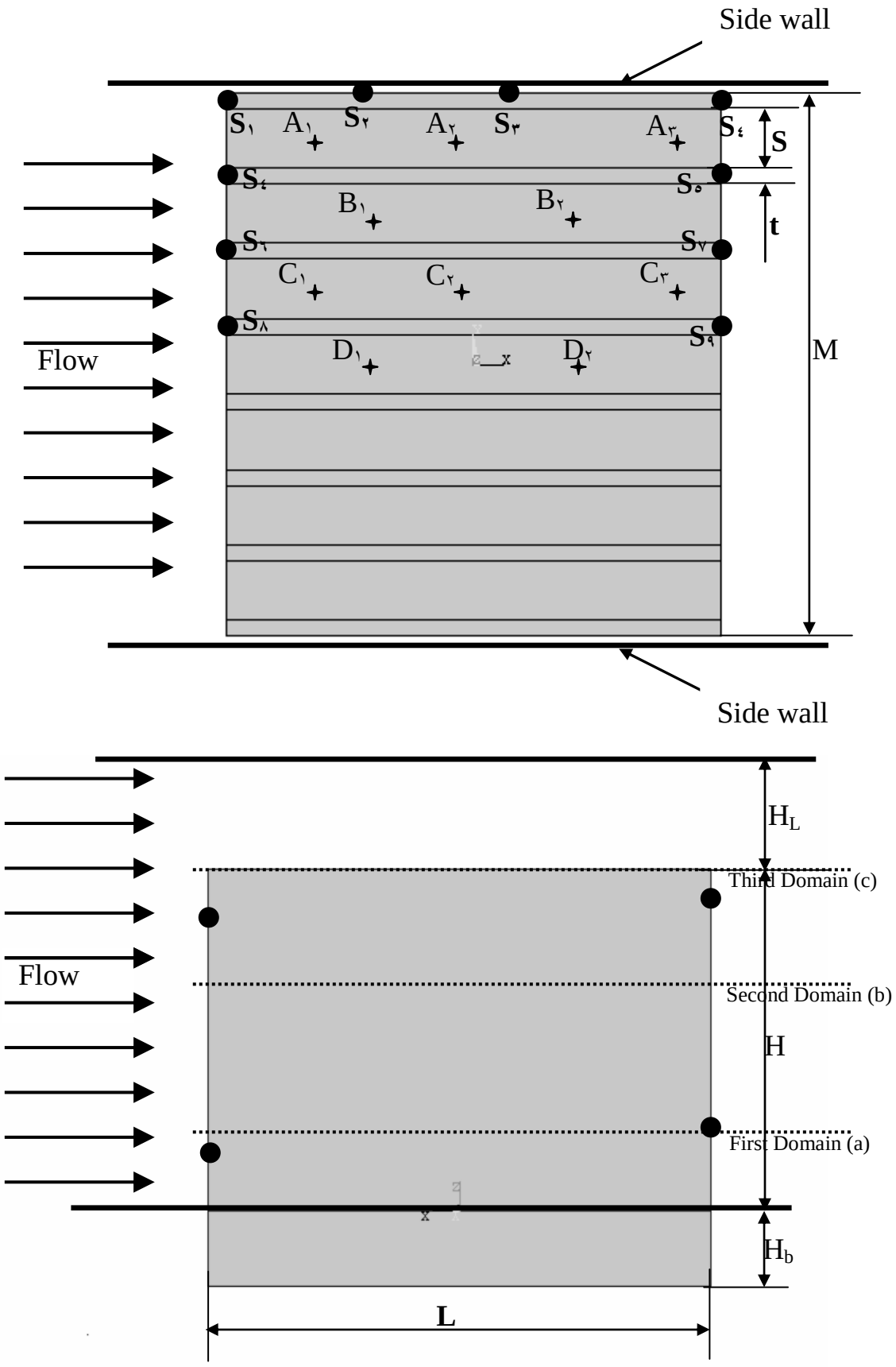

Fig. (٤-٥) Positions of temperature and velocity measurement for longitudinal fin.

Parameters	Dimensions
H, pin-fin height	٦٨ mm
H_b, sink base thickness	١٥ mm
M, sink width	١١٠ mm
L, sink length	١٠٠ mm
d, cylinder pin diameter	١٢.٥ mm
l, square pin side distance	١١ mm
P_x, pitch stream wise direction	١٧.٦ mm
P_y, pitch transverse direction	٢٧.٧٥ mm
t, fin thickness	٣.٢٥ mm
P, pitch distance	٢٢.٨ mm
H_L, by-pass distance	٥ mm
S, fin gap distance	١٢ mm
e, inlet distance X-direction	١٤.٢٥ mm
b, inlet distance Y-direction	١٢.٧٥ mm
$A_{١-١}$, $B_{١-١}$, $C_{١-١}$, $D_{١-١}$,….etc	Positions of temperature and velocity measurements in the air flow.
$S_١$, $S_٢$, $S_٣$, $S_٤$, $S_٥$,….etc	Positions of temperature sensors.

Table (٤-٣): Values of geometrical parameters.

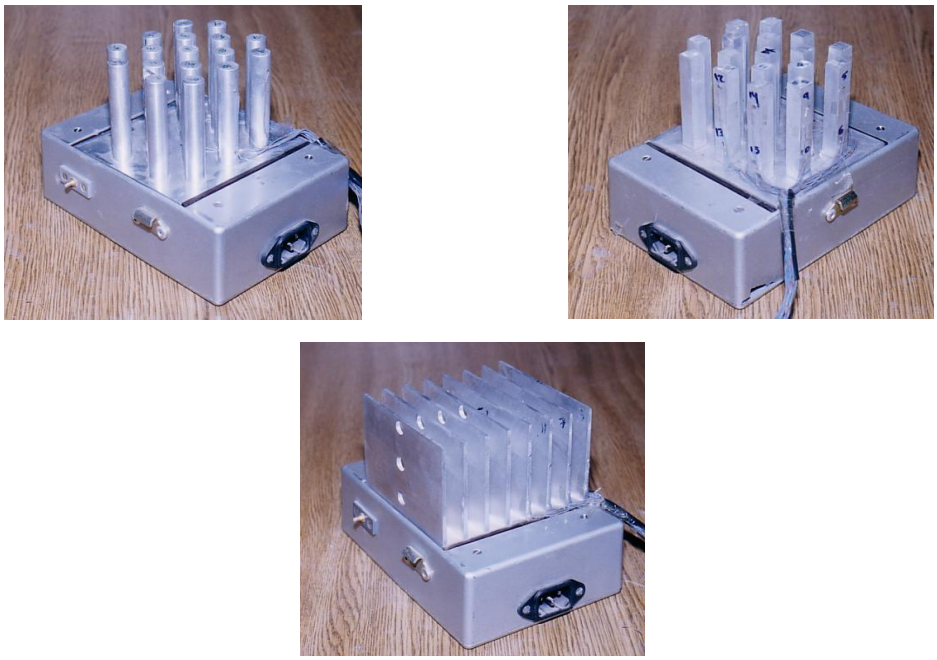

Fig. (٤-٧) Measurement of surface temperature.

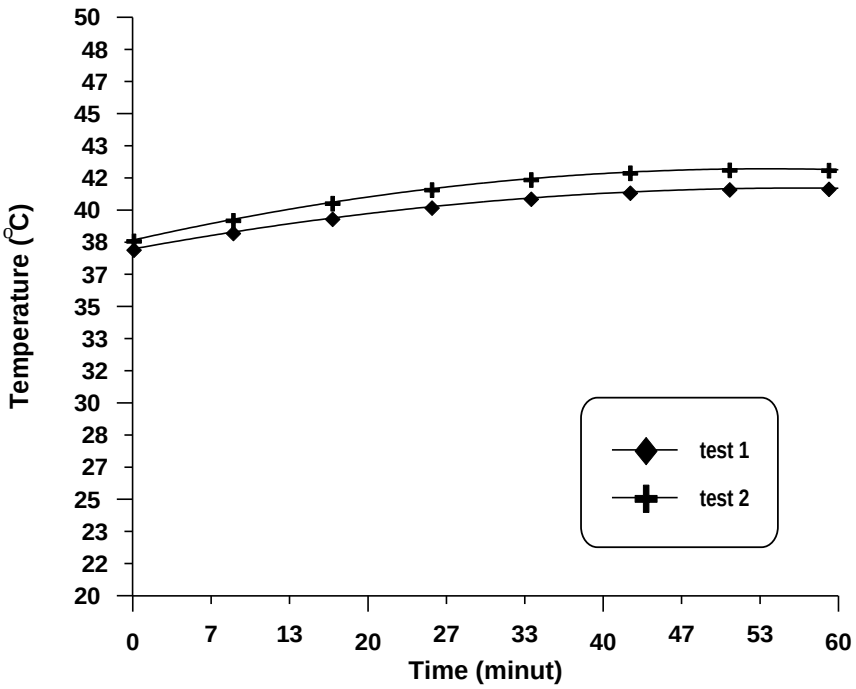

Fig. (٤-٨) The time requirement to arrive steady state condition.

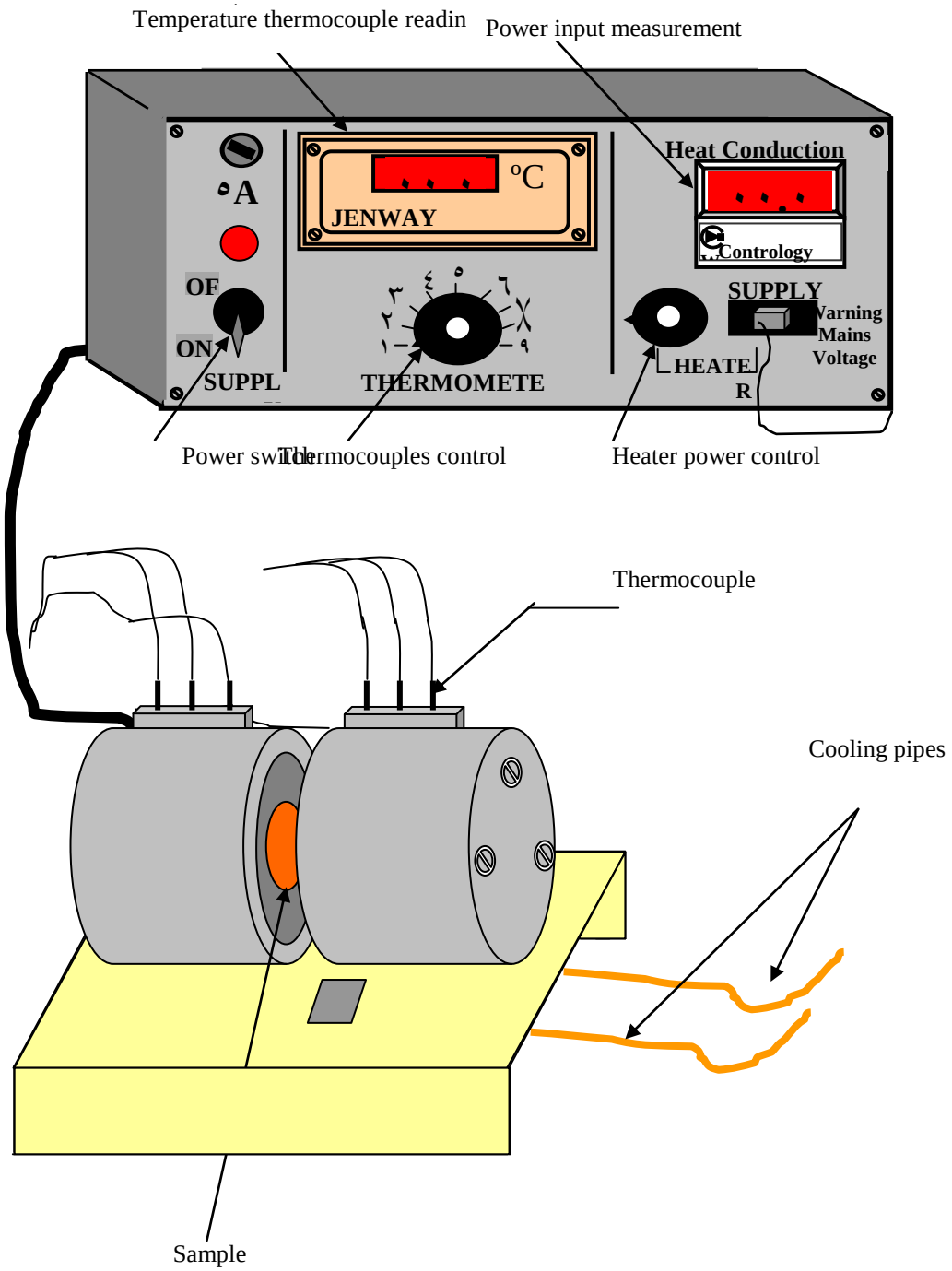

Fig. (٤-٩) Apparatus of thermal conductivity

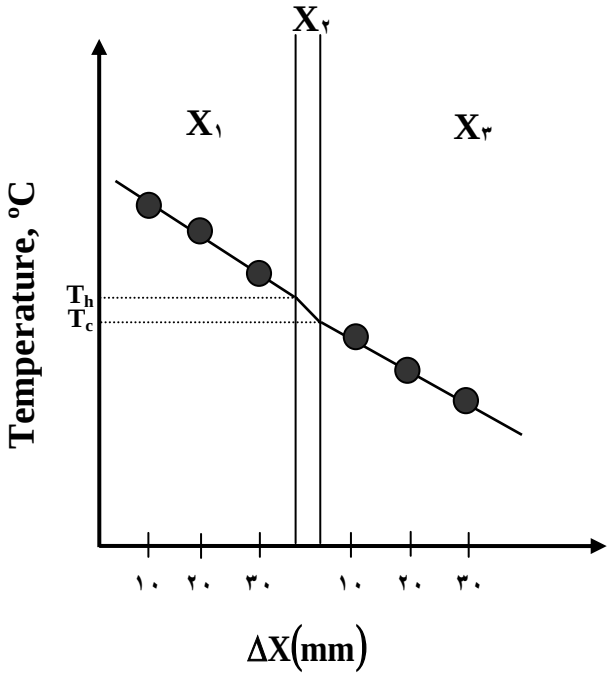

Fig. (٤-١٠).Temperature gradient $(\Delta T/\Delta X)$

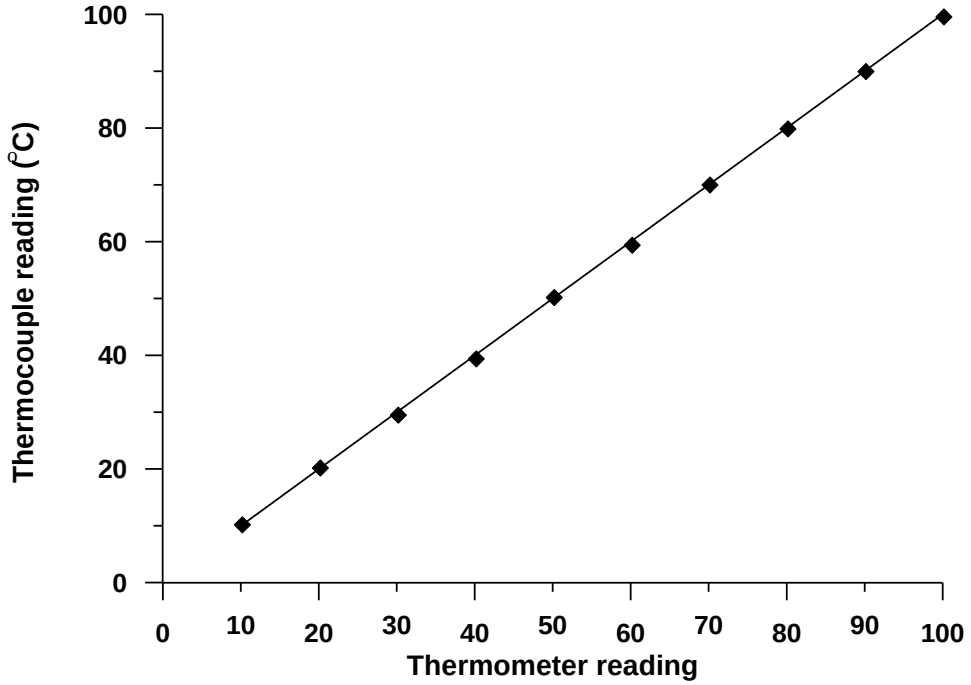

Fig .(٤-١١) Calibration curve of thermocouple type K,

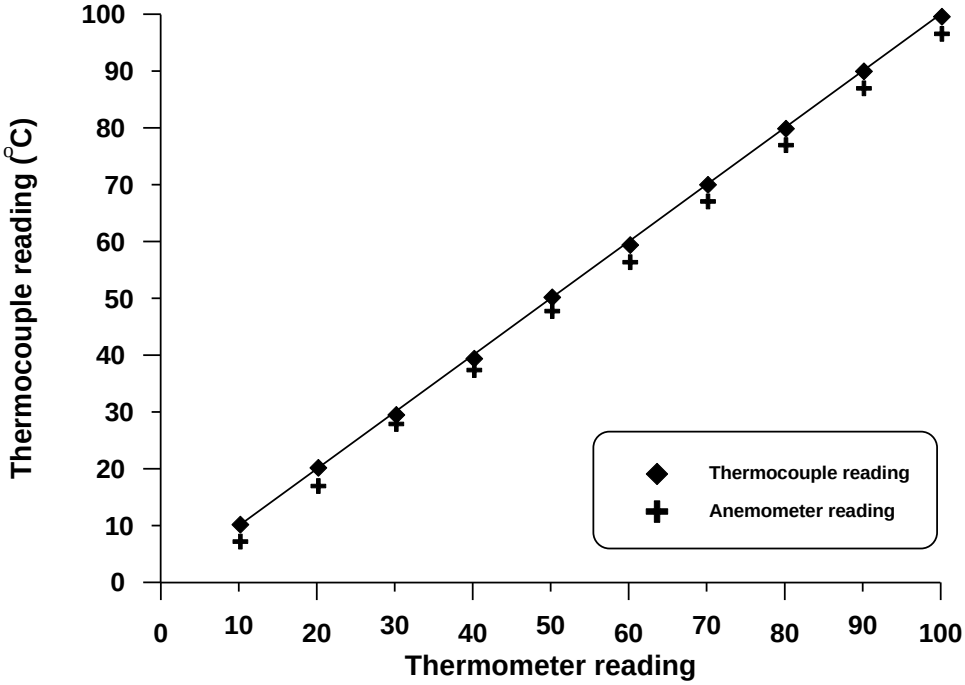

Fig. (٤-١٢) Calibration curve of anemometer thermocouple.

Chapter 5

Results and Discussion

٥.١ Experimental Results

Four types of experiments are carried out in this study:

A- Measurement of thermal resistance for the three types of heat sinks and for all conditions which included four different inlet velocity (٢), (٣), (٤), and (٦) m/s and three different heat flux (٢٠), (٣٠), and (٤٠) Watt.

B- Measurement of local heat transfer coefficient for the three types of heat sinks and for all conditions.

C- Measurement of velocity distribution for each heat sink and for all conditions at (*z*= ٠.٠٢٢٦) m , (*z*=٠.٠٤٥) m , and (*z*= ٠.٠٦٨) m as describe in Figs (٤-٣), (٤-٤) and (٤-٥).

D- Measurement of temperature distribution for each heat sink and for all conditions at (*z*= ٠.٠٢٢٦) m , (*z*= ٠.٠٤٥) m , and (*z*= ٠.٠٦٨) m as describes in Figs (٤-٣), (٤-٤) and (٤-٥).

٥.١.١ Thermal Resistance

The total thermal resistance is primary thermal performance parameter for the heat sink which is considered in this study as:

$$R_{th} = \frac{(T_B - T_\infty)}{q_{conv}} \qquad \text{...(٥.١)}$$

where:

T_B : Base temperature of heat sink

T_∞ : Ambient temperature

q_{conv} : Heat convected through the heat sink which is given by

$$q_{conv} = q_{total} - q_{loss} \quad \text{...(٥.٢)}$$

where:

q_{total} : Total amount of power supplied to heat sink.

q_{loss}: Total heat losses due to conduction and radiation.

The heat extract through the heat sink which was reported as (٨٠ %)of the total losses was due to forced convection [٣٧].

Fig. (٥-١) shows the effect of increasing velocity on the thermal resistance for each heat sink and for different heat loads.

The results show that the thermal resistance of square pin-fin is higher than the thermal resistance for cylindrical pin-fin. Thermal resistance for cylinder pin-fin heat sink is higher than for longitudinal fin heat sink.

Same behavior is obtained for all heat loads. This is due to the fact that velocity distribution was more uniform through the longitudinal fin heat sink which increases the heat transfer coefficient and decreases the base temperature and decreases the thermal resistance. Also, the areas of convection for longitudinal fin heat sink is higher than the area of convection for cylindrical and square pin-fin.

The difference between curves reaches a minimum value at maximum studied velocity due to higher mass of air across the heat sinks.

Fig. (٥-٢) shows the relative thermal resistance which was obtained by dividing the thermal resistance to the surface area of convection for each type of heat sink compared with the results obtained by Arnold [٣٥].

Fig. (٥-٢) illustrates a good agreement obtained in calculating the steady state by experimental results.

The results show that the relative thermal resistance of cylindrical pin-fin is higher than the relative thermal resistance for square pin-fin, and the relative thermal resistance for square pin-fin is higher than that for longitudinal fin.

This is due to the surface area of convection heat transfer where the longitudinal fin heat sink has maximum surface area of convection which is equal to (١١٤٩.٣٦) cm^2. The surface area of convection for square pin-fin is equal to (٥٢٩.٢١) cm^2, and for the cylinder pin-fin it is equal to (٤٧٤.٨٢٢) cm^2 while the three types of heat sinks have the same area of conduction which was equal to (٣.٢٥) cm^2.

The longitudinal fin maintains large expose surface area available for heat transfer.

Figs. (٥-٣), (٥-٤) , (٥-٥) and (٥-٦) show the temperature rise (T_B-T_∞) with heat flux for velocity (٢), (٣), (٤), and (٦) m/s respectively.

The temperature rise for square pin-fin is higher than the temperature rise for the cylinder pin-fin.

The temperature rise for the cylindrical pin-fin is higher than the temperature rise for the longitudinal fin heat sink. This is due to the fact that the heat convected from the longitudinal fin is higher than the heat convected from cylindrical and square pin-fin, and the heat convected from cylindrical pin-fin is higher than the heat convected from square pin-fin, therefore, the base temperature (T_B) for longitudinal fin is lower than the base temperature of cylindrical and square pin-fin.

The Figs. (٥-٣), (٥-٤) , (٥-٥) and (٥-٦) show that the temperature rise increases with the increase of heat flux due to the increase of the base temperature.

The value of temperature rise was minimum for maximum velocity because the increases of velocity decreases the base temperature.

٥.١.٢ Local Heat Transfer Coefficients

In the present study, the local heat transfer coefficient is calculated according to the following equations:

$$\frac{T-T_\infty}{T_b-T_\infty}=\frac{\cosh m(H-x)+\left(\frac{h}{km}\right)\sinh m(H-x)}{\cosh mH+\left(\frac{h}{km}\right)\sinh mH} \qquad \ldots(٥.٣)$$

$$q=\sqrt{hpkA}(T_b-T_\infty)\frac{\sinh mH+\left(\frac{h}{km}\right)\cosh mH}{\cosh mH+\left(\frac{h}{km}\right)\sinh mH} \qquad \ldots(٥.٤)$$

The above equations are solved for the two unknown h and T_b for each pin-fin[٤٣].

The change of local heat transfer coefficient of each heat sink is plotted for all conditions in Figs. (٥-٧) to (٥-١٨).The local heat transfer coefficient for longitudinal fin heat sink for all cases is larger than that for cylinder and square pin-fin. Also the local heat transfer coefficient for cylinder pin-fin in all cases is larger than that for square pin-fin. This is due to the velocity distribution on each heat sink. The velocity distribution in the longitudinal fin was more uniform along the heat sink from that in cylinder and square pin-fin.

Fig. (٥-٧) shows the minimum local heat transfer coefficient where the heat flux (٢٠) Watt and velocity (٢) m/s. Fig. (٥-١٨) shows the maximum local

heat transfer coefficient where conditions are (٤٠) Watt heat flux and (٦) m/s velocity.

The local heat transfer coefficient is increased with the direction of flow in longitudinal heat sink while the local heat transfer coefficient is decreased with the flow for both cylindrical and square pin-fin. This is as a result of thermal boundary layer development from the entrance of the heat sink towards the exit. This boundary layer is developed in the case of longitudinal heat sink because the flow has no restriction on its flow.

The heat sink has no clearance above it and no large space in the two sides of the heat sink. Also with increasing distance from the leading edge the effect of heat transfer penetrates further into the free stream and the thermal boundary layers grow. Therefore the thermal boundary layer is more effective in longitudinal fin heat sink while the thermal boundary layer is less effective in pin-fin because of the small area of attach.

Figs. (٥-١٩) and (٥-٢٠) show the local heat transfer coefficient along flow direction for (٩-Cross Cut fin) and (١٢-Cross Cut fin) respectively.. For (١٢-fin) heat sink is generally higher than the those for (٩-fin) heat sink due to the increased surface area [٣٤]. These Figs. are used to compare the behaviour of the local heat transfer coefficient through the geometry of heat sinks. A good agreement behaviour is obtained. Figs. (٥-١٩) and (٥-٢٠) show the same behaviour of local heat transfer coefficient obtained from the experimental results.

A comparison of the average Nusselt number variation with Reynolds number for three types of heat sink are shown in Figs. (٥-٢١),(٥-٢٢) and (٥-٢٣).

For clarity, the results are plotted on three graphs for different heat flux (٢٠), (٣٠) and (٤٠) Watt. For each geometry ,four simulations were carried out

by varying inlet air velocity. The curves represent the lines of best fit through the four points obtained in the simulations.

It can be noted that the longitudinal fin heat sink shape yields the highest Nusselt number at all Reynolds numbers in the range considered here. The lowest Nusselt number is for the square pin-fin heat sink. Fig. (٥-٢١) obviously shows that the heat flux (٢٠) Watt leads to the Nusselt number which is much lower than the other heat fluxes (٣٠) and (٤٠) Watt. It is interesting to note that the staggered cylinder pin-fin is better than the staggered square pin-fin.

٥.١.٣ Velocity Distribution

Fig. (٥-٢٤) shows the effect of air flow velocity for experimental and theoretical results, where significant flow By-Pass is seen with square pin-fin heat sink. This is of no surprise since the cross-section of this heat sink represents more of an obstruction for air flow. Also, Cylinder pin-fin induced more flow By-Pass than the straight fin, suggesting increase turbulence and pressure drop for ail heat sinks, The largest mount of By-Pass is at maximum air velocity. The theoretical results was lower than experimental results this is for adiabatic flow were studied for theoretical results.

In the experimental results we can read the velocity of air in the *x*-direction (v_x=*u*) at given local coordinates (*x* , *y*) by using portable anemometer at three domains of *z*-direction (*z*=٠.٠٢٢٦ m) from the base which marked **(a)**, (*z*=٠.٠٤٥٣ m) from the base which marked **(b)** and (*z*=٠.٠٦٨ m) from the base which marked **(c)**. This results enable us to give a good picture of velocity distribution.

This section presents the velocity profiles only for inlet velocity (٢) m/s and thermal power (٢٠) Watt. Figs. (٥-٢٥) to (٥-٢٧) show the body contour of velocity distribution for each heat sink and for three domains.

Fig. (٥-٢٥) shows the velocity distribution for cylinder pin-fin heat sink at three domains with entrance velocity which is equal to (٢) m/s.

Fig. (٥-٢٥ a) shows the velocity distribution at first domain where (z=٠.٠٢٢٦ m) nearest the base.

Fig. (٥-٢٥ b) shows the velocity distribution at the second domain where (z=٠.٠٤٥٣ m) middle the distance of heat sink.

Fig. (٥-٢٥ c) shows the velocity distribution at the third domain where (z=٠.٠٦٨ m) at the tip of heat sink.

These Figs. (٥-٢٥ a, b and c) show the maximum velocity at the two sides of heat sink. This occurs because the air flow tries to take the straight paths which have no restriction on it to exit from the heat sink.

This phenomenon decreases the cooling of heat sink. Therefore ,the space in the two sides of heat sink must be small. It also forces the air to pass through heat sink. These Figs. show the large deformation which is different in value of velocity during the core of heat sink. In the middle end of heat sink minimum velocity occurs. The maximum values of velocity noticed for body contour have the second domain where (z=٠.٠٤٥٣) m because this domain is at the middle distance of the channel.

Fig. (٤-٢٦) shows the velocity distribution for square pin-fin heat sink at three domains with entrance velocity which is equal to (٢) m/s.

Fig. (٥-٢٦ a) shows the velocity distribution for square pin-fin heat sink at first domain (z=٠.٠٢٢٦) m.

Fig. (٥-٢٦ b) shows the velocity distribution at the second domain where (z=.٠٤٥٣) m.

Fig. (٥-٢٦ c) shows the velocity distribution at third domain where (z=٠.٠٦٨) m.

From these Figs. we can show the difference between velocity distribution for cylinder and square pin-fin heat sink, which is due to the shape of pin-fin. The air flow around is more improved distribution from the square pin-fin. Square

pin-fin has a sharp angle in four corners which promote dead zone behind each pin. The values of velocity for square pin-fin is smaller than those for cylinder pin-fin.

For square pin-fin heat sink of the second domain has large values of velocity because it was in the middle distance of the channel.

Fig. (٥-٢٧) shows the velocity distribution for longitudinal fin heat sink at three domains with entrance velocity which is equal to (٢) m/s.
Fig. (٥-٢٧ a) shows the velocity distribution at first domain where (z=٠.٠٢٢٦) m.
Fig. (٥-٢٧ b) shows the velocity distribution at the second domain where (z=٠.٠٤٥٣) m.
Fig.(٥-٢٧ c) shows the velocity distribution at the third domain where (z=٠.٠٦٨) m.

Figs. (٥-٢٧ a, b and c), we can show that a large difference between the velocity distribution on longitudinal fin heat sink and both cylinder and square pin-fin. This is due to the geometry of fins and its arrangement.

In longitudinal fin heat sink the air flow enters the grooves between fins. This process is like the flow over flat plate. When velocity enters the grooves the velocity boundary layer starts to grow on the surface of fin on the other surface the velocity boundary layer starts to grow also. At the distance from the leading edge the two boundary layers were attached and the velocity at this point reaches its maximum. These grooves represent a good straight path to the air flow to move on it. The value of velocity increases toward the flow in this type of heat sink. For this reason the velocity distribution for longitudinal fin heat sink is more uniform than that in cylindrical and square pin-fin heat sink. There are also no large different between the inlet and outlet heat sink velocity.

For longitudinal fin heat sink the maximum value of velocity can be shown in the second domain because this domain in the middle distance of the channel.

٥.١.٤ Temperature Distribution

In the experimental results we can read the temperature of air at given local coordinates (x , y) at the core of heat sink by using portable anemometer at three domains of z-direction (z=٠.٠٢٢٦) m, (z=٠.٠٤٥٣) m and (z=٠.٠٦٨) m.
The detailed temperature fields at different inlet velocity, give an insight into the heat transfer conditions in the studied heat sink.

It should be also noted that different heating powers (٢٠), (٣٠) and (٤٠) Watt are used on the base-plate, there exists a similarity in force convection heat removal from the heat sink structure.

Namely, higher heat input causes higher absolute temperature levels, whereas, the form of isothermal changes only slightly, due to the modification in air properties. Therefore, this section describes the temperature fields only for (٢) m/s inlet velocity and for thermal power (٢٠) Watt. The temperature is in Celsius scale.

The measured temperature increase through the heat sinks are plotted in Figs. (٥-٢٨), (٥-٢٩), (٥-٣٠), and (٥-٣١). For three types of heat sinks and for different heat loads, For all Figs. The longitudinal fin heat sink shows the lowest temperature increase. Also, the temperature increase decreases with increase velocity therefore Fig. (٥-٣١) show the lowest temperature increase for three types of heat sinks because the air velocity was maximum (٦) m/s.

Figs. (٥-٣٢) to (٥-٣٤) show the Isothermal contour of temperature distribution for each heat sink and for three domains.

Fig. (٥-٣٢) shows the Isothermal contour temperature field for cylindrical pin-fin heat sink at three domains.

Fig. (٥-٣٢) marked with (a) present the temperature field in the first domain, whereas fig. (٥-٣٢) marked with (b) reveals the temperature field in the second domain and fig. (٥-٣٢) marked (c) presents temperature field in the third domain.

It is evident that the lowest temperature in the air stream is at the beginning of the heat sink for this type of heat sink; this is on the left side. The temperature raises as the air passes through the heat exchanging structure. Therefore the highest temperatures are noted at the exit; this is on the right side. The lowest temperature in the domain is in the third domain which is the upper domain and the highest on the bottom (first domain) close to the base-plate.

Because the heat flux is a vector perpendicular to the isotherms, a qualitative picture of heat flow can be extracted from the calculated temperature fields. It can be seen in this fig. that most of the heat is transfered from the solid to fluid in the first half of the test section. The highest heat fluxes appear in the middle left corner, where the temperature gradients are the highest.

The second half of the heat sink does not participate in the heat transfer process. From these Figs. (٥-٣٢), it is revealed that in the nearest to the base-plate the temperature field is not fully developed. This means that the air which enters the test section is quickly heated due to the nearest to the base-plate and leaves the heat sink at the temperature nearest to the base temperature. With increasing distance from the base-plate temperature field becomes more developed.

This phenomenon also occurs with inlet velocity increasing where at low velocity the temperature field is not fully developed.

This means that air, which enters the test section, is quickly heated due to its low velocity and leaves the heat sink at the temperature of the solid-phase, unable to receive additional heat from the source.

With increasing inlet velocity, the state of thermal saturation diminishes. This means that, with increasing inlet velocity, the air flow leaves the heat sink at

lower exit temperature. Such coolant flow is thermally unsaturated, still capable of heat removal. Nevertheless, as the average temperature decreases, the role of heat conducting base-plate increases. This causes further reduction in the air and structure temperatures at the simulation domain exit.

٥. ٢ Theoretical Results

The theoretical results are divided into three parts.

١- Body contour represents the velocity distribution in the *x*-direction (*v*=*u*) for three types of heat sinks at three domains: (*z*=٠.٠٢٢٦) m , (*z*=٠.٠٤٥٣) m and (*z*=٠.٠٦٨) m with inlet velocity (٢) m/s.

٢- Body contour represents the velocity distribution (average velocity or resultant velocity) for three types of heat sinks and for three domains: (*z*=٠.٠٢٢٦) m, (*z*=.٠٤٥٣) m and (z=٠.٠٦٨) m with inlet velocity which is equal to (٢) m/s.

٣- Vector plot for three types of heat sink at the middle distance of the height of fins.

٥-٢-١ Velocity Distribution *v*= u

Fig. (٥-٣٥) shows the velocity distribution for cylinder pin-fin heat sink at the three domains with inlet velocity which is equal to (٢) m/s.

Fig. (٥-٣٥ a) shows the velocity distribution at the first domain where (*z*=٠.٠٢٢٦)m.

Fig. (٥-٣٥ b) shows the velocity distribution at the second domain where (*z*=٠.٠٤٥٣) m.

Fig. (٥-٣٥ c) shows the velocity distribution at the third domain where (*z*=٠.٠٦٨) m.

Figs. (٥-٣٥ a, b and c) show a good agreement with the velocity distribution obtained by experimental work.

The results of theoretical work gives us a clearer picture than that obtained from experimental results. This is due to the fact that the solution of the governing equation occurs in each node in the test section. The test section contains a lot of nodes and elements, therefore, the solution is more accurate. Fig. (٥-٣٥) show that the maximum velocity occurs on each side of heat sink which can namely Side-bypass. Therefore ,the Side-by pass of air should be minimized to improve the heat dissipation.

Fig. (٥-٣٦) shows the velocity distribution for square pin-fin heat sink at three domains with inlet velocity (٢) m/s.

Fig. (٥-٣٦ a) shows the velocity distribution at the first domain where (z=٠.٠٢٢٦) m.
Fig. (٥-٣٦ b) shows the velocity distribution at the second domain where (z=٠.٠٤٥٣) m.
Fig. (٥-٣٦ c) shows the velocity distribution at the third domain where (z=٠.٠٦٨) m.

Figs. (٥-٣٦ a, b and c) show a good agreement with the velocity distribution obtained by experimental work. The results of theoretical work gives a clearer picture than that obtained from experimental work.

Fig. (٥-٣٧) shows the velocity distribution for longitudinal fin heat sink at three domains with inlet velocity (٢) m/s.

Figs. (٥-٣٧ a, b and c) show the maximum velocity that occurs in the grooves of longitudinal fin heat sink this phenomena increase heat dissipation from the fins.

٥-٢-٢ Resultant Velocity Distribution (V_{sum})

Figs. (٥-٣٨) , (٥-٣٩) and (٥-٤٠) show the resultant velocity of three domains of each heat sink cylinder , square and longitudinal fin heat sinks where resultant velocity from the theoretical work.

.

$v_{sum} = \sqrt{u^2 + v^2 + w^2}$	...(٥.٥)

٥-٢-٣ Vector Velocity Distribution

.

Figs. (٥-٤١), (٥-٤٢) and (٥-٤٣) show the vector plot for three types of heat sinks at the middle simulation domain (z=٠.٠٤٥٣) m.

Figs. (٥-٤١), (٥-٤٢), and (٥-٤٣) show the different behaviour of flow through heat sink. Notice the symmetry of flow for each heat sink. This is due to the nearest from the exact solution. The distribution of flow is quite different for each heat sink. For cylinder and square pin-fin, the first two rows of pins and the side rows are the most effective because the maximum velocity occurs at these positions. This is also evident for longitudinal fin heat sink which is the most effective whereas the cylinder and square pin-fin heat sink.

٥. ٢. ٤ Experiments

Experiments were conducted to measure the velocity and temperature contours for three types of heat sinks for different inlet velocity and heat flux.

In all experiments the average inlet velocity at the entrance of the duct was (٢),(٣),(٤), and (٦) m/s. The Reynolds numbers based on hydraulic diameter of inlet region was (١٠٥٤٣), (١٥٨١٥), (٢١٠٨٧), (٣١٦٣١) respectively. For three

values of heat flux (٢٠), (٣٠), (٤٠) Watt to study thermal resistance of each heat sink and flow characteristics.

Table (٥-١A,B,C) specify the experimental tests and the base temperature of heat sinks which was carried out in experimental work.

Heat Flux / Velocity	Q=٢٠ watt	Q=٣٠ watt	Q= ٤٠ watt
$V_{١}$= ٢m/s	٤٥.٦°C T_{∞}=٣٦.٢١٤	٤٩.٤°C T_{∞}=٣٦.٢١٤	٥٢.٣°C T_{∞}=٣٦.٢١٤
$V_{٢}$= ٣m/s	٤٣.٨°C T_{∞}=٣٦	٤٨.٣°C T_{∞}=٣٦	٥٠.٧°C T_{∞}=٣٦
$V_{٣}$= ٤m/s	٤٤°C T_{∞}=٣٧.٠٣٠	٤٦°C T_{∞}=٣٧.٠٣٠	٤٨°C T_{∞}=٣٧.٠٣٠
$V_{٤}$= ٦m/s	٤٥.٥°C T_{∞}=٣٨.٤٥٨	٤٧.٦°C T_{∞}=٣٨.٤٥٨	٥٠.٣°C T_{∞}=٣٨.٤٥٨

Table (٥-١A) Base Temperature of
Longitudinal Fin Heat Sink.

Heat Flux / Velocity	Q=٢٠ watt	Q=٣٠ watt	Q= ٤٠ watt
$V_{١}$= ٢m/s	٤٣.٨°C T_{∞}=٣٤.١٨	٤٩.٣°C T_{∞}=٣٤.١٨	٥٣.٨°C T_{∞}=٣٤.١٨
$V_{٢}$= ٣m/s	٤٤.٨°C T_{∞}=٣٦.٥٥٩	٥٠.٢°C T_{∞}=٣٦.٥٥٩	٥٣°C T_{∞}=٣٦.٥٥٩
$V_{٣}$= ٤m/s	٤٤.٣°C T_{∞}=٣٧.٠٣٠	٤٦.٥°C T_{∞}=٣٧.٠٣٠	٤٧.٦°C T_{∞}=٣٧.٠٣٠
$V_{٤}$= ٦m/s	٤٣.٨°C T_{∞}=٣٧.٤٣٩	٤٥.٦°C T_{∞}=٣٧.٤٣٩	٤٧.٤°C T_{∞}=٣٧.٤٣٩

Table (٥-١B) Base Temperature of
Cylindrical Pin-Fin Heat Sink

Heat Flux / Velocity	Q=٢٠ watt	Q=٣٠ watt	Q= ٤٠ watt
$V_{١}$= ٢m/s	٤٦.٧°C T_{∞}=٣٥.٥٣٩٧	٥١.٨°C T_{∞}=٣٥.٥٣٩٧	٥٦.٢°C T_{∞}=٣٥.٥٣٩٧
$V_{٢}$= ٣m/s	٤٦.٨°C T_{∞}=٣٦.٢١٤	٥٠.٨°C T_{∞}=٣٦.٢١٤	٥٤.٣°C T_{∞}=٣٦.٢١٤
$V_{٣}$= ٤m/s	٤٥.١°C T_{∞}=٣٧.٠٣٠	٤٧.٢°C T_{∞}=٣٧.٠٣٠	٤٨.٨°C T_{∞}=٣٧.٠٣٠
$V_{٤}$= ٦m/s	٤٤.٣°C T_{∞}=٣٧.٢٣٤	٤٦.٣°C T_{∞}=٣٧.٢٣٤	٤٧.٩°C T_{∞}=٣٧.٢٣٤

Table (٥-٢C) Base Temperature of
Square Pin-Fin Heat Sink.

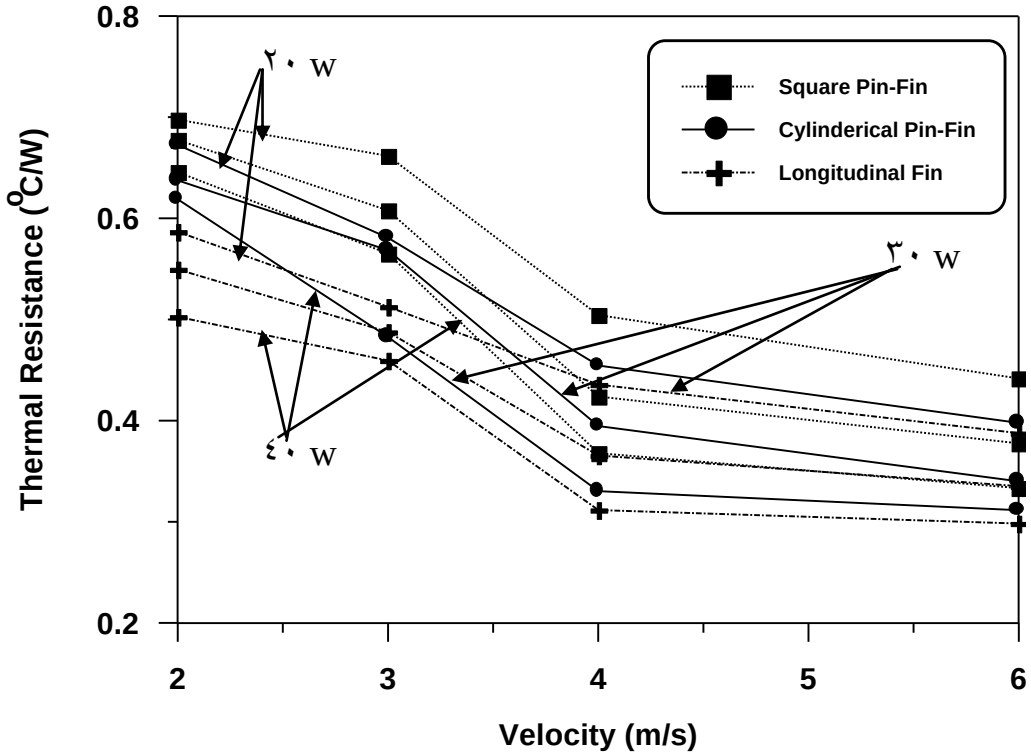

Fig.(٥-١) Thermal Resistance vs. Air Velocity for different heat fluxes.

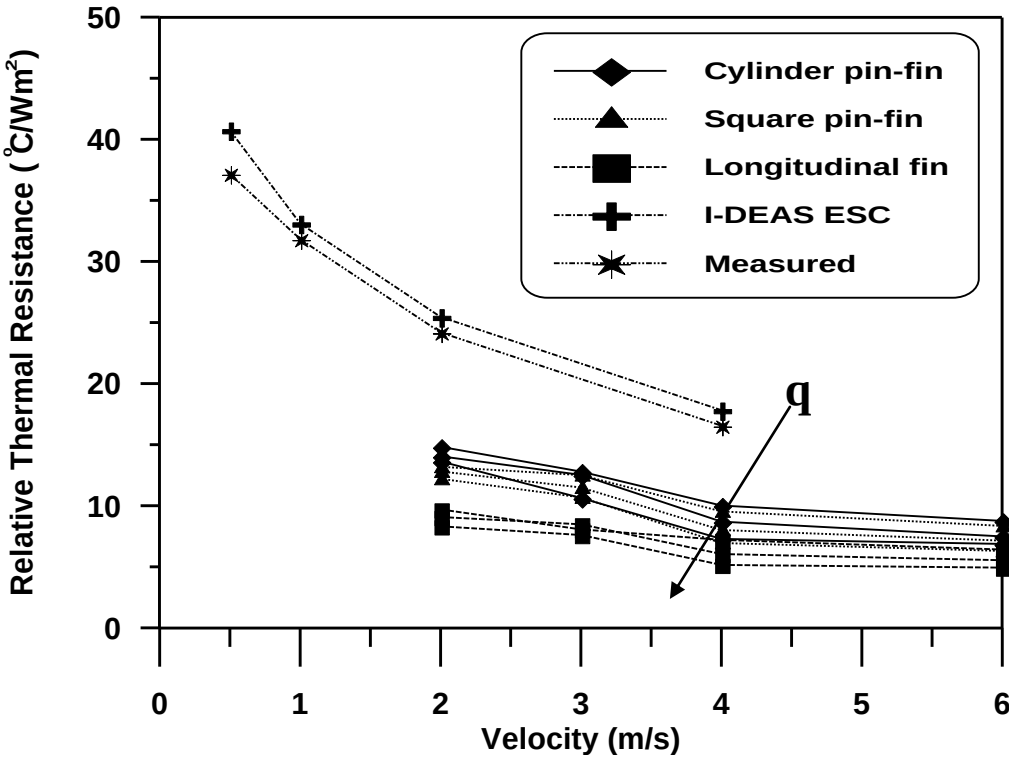

Fig.(٥-٢) Comparison of Relative Thermal Resistance vs. Air Velocity

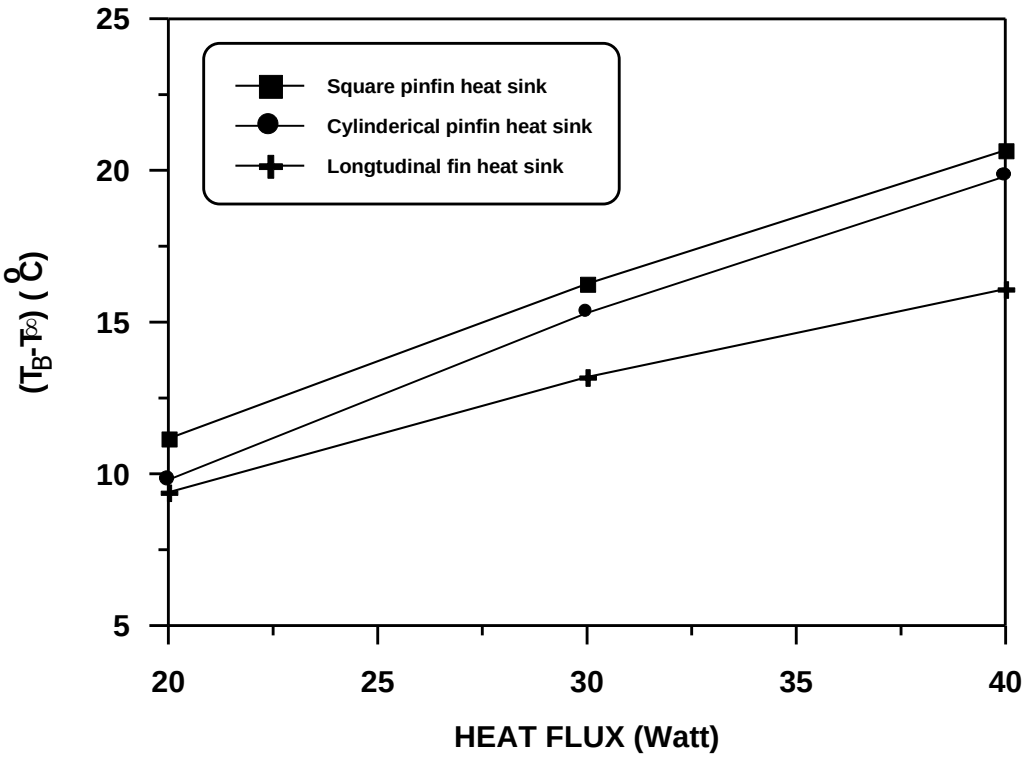

Fig.(٥-٣) Temperature Rise vs. Heat Flux for Inlet Velocity (٢) m/s.

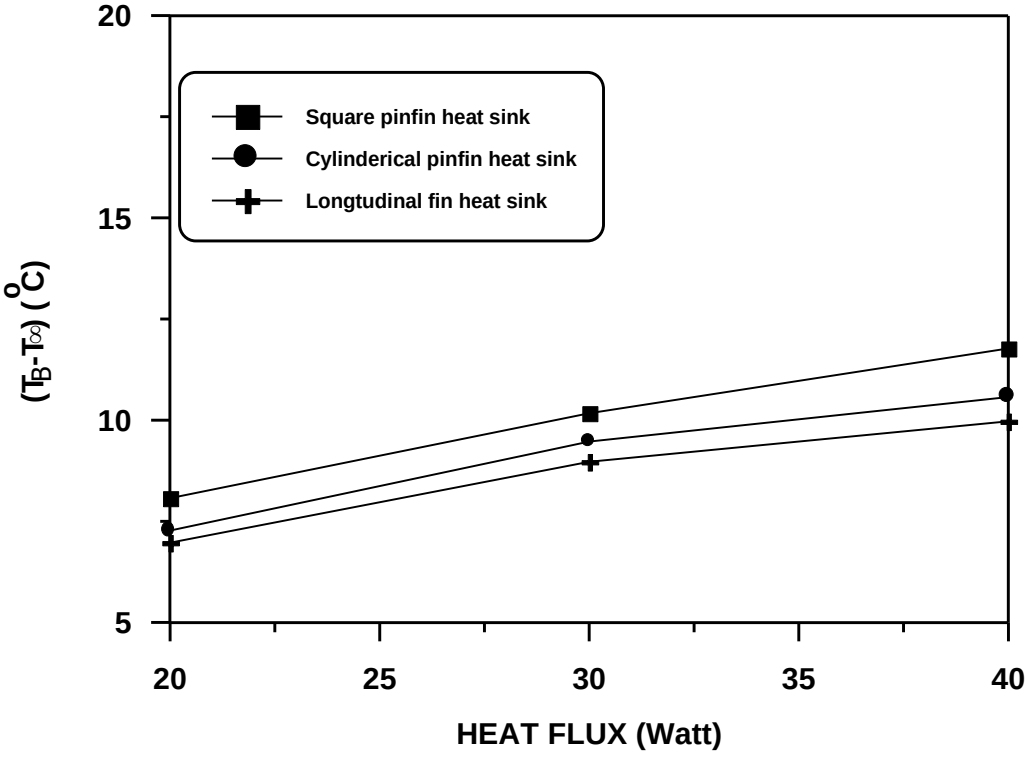

Fig.(٥-٤) Temperature Rise vs. Heat Flux for Inlet Velocity (٣) m/s.

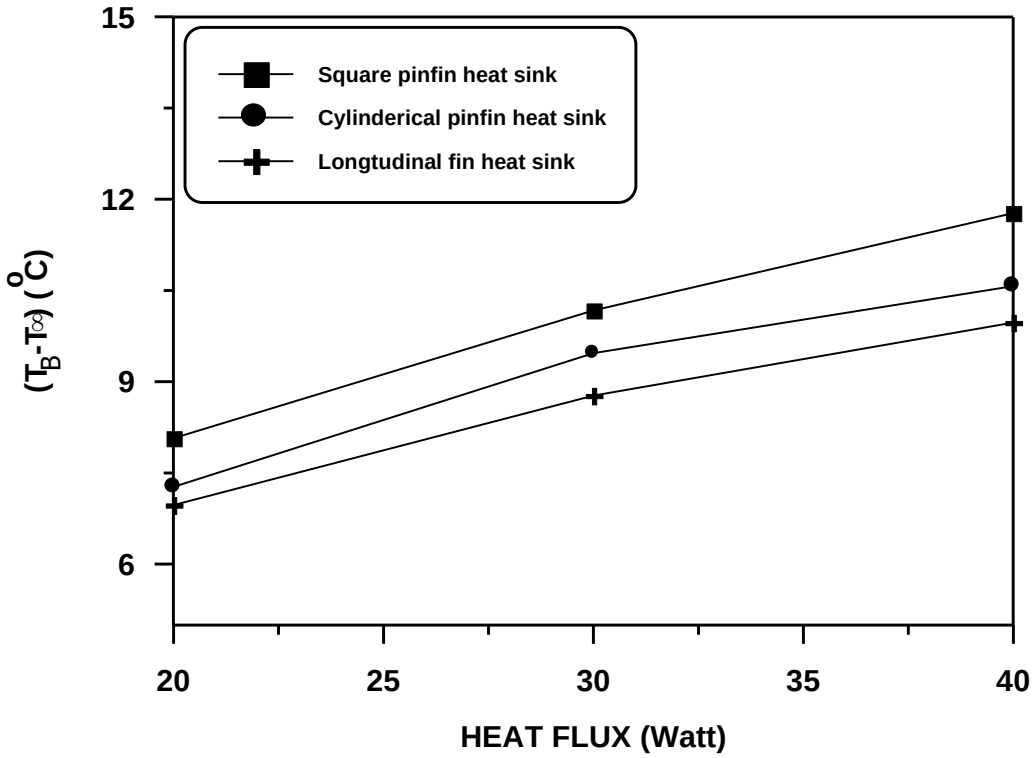

Fig.(٥-٥) Temperature Rise vs. Heat Flux for Inlet Velocity (٤) m/s.

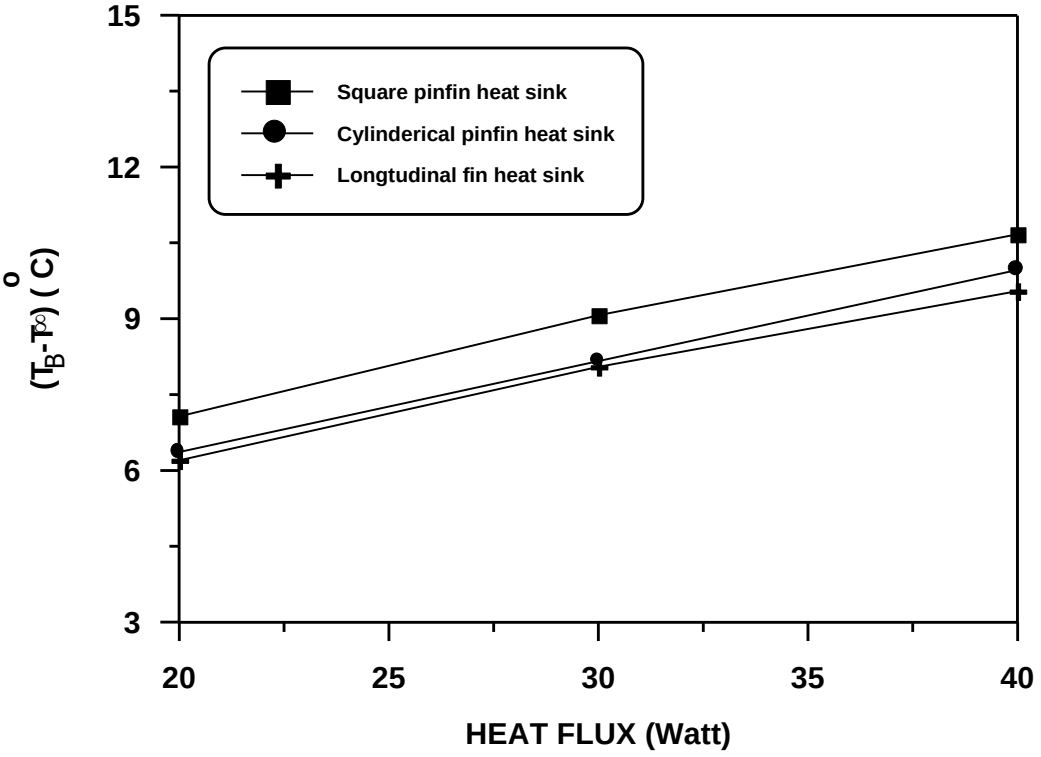

Fig.(٥-٦) Temperature Rise vs. Heat Flux for Inlet Velocity (٦) m/s.

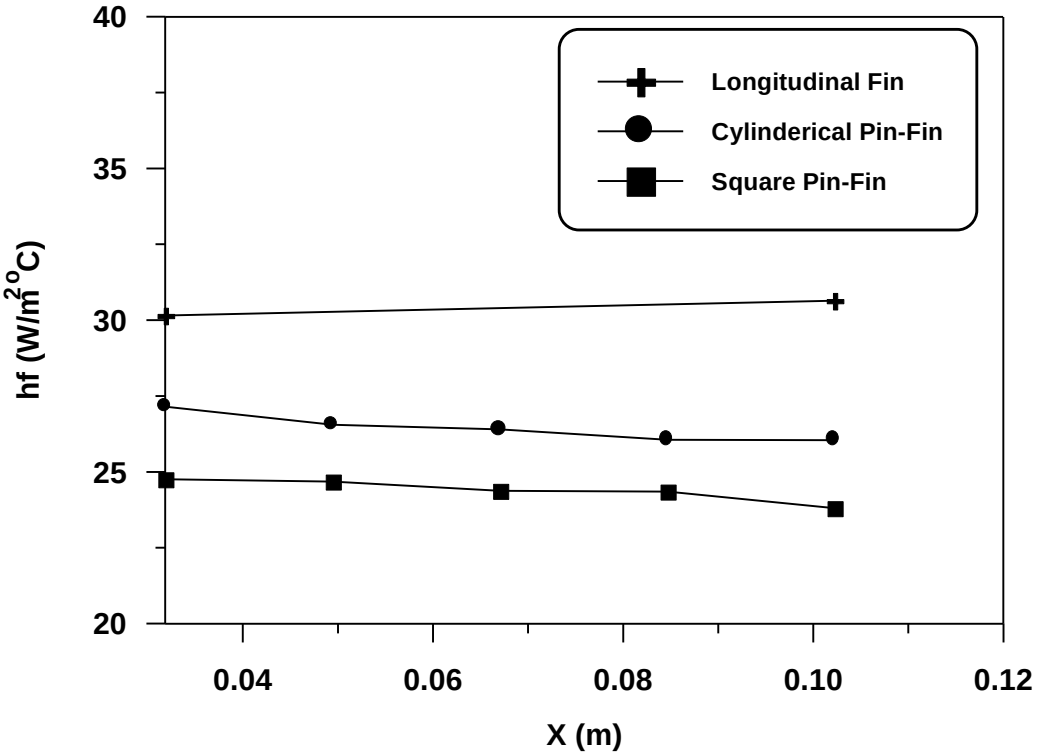

Fig.(٥-٧) Local Heat Transfer Coefficient along Flow Direction for Velocity (٢) m/s and Heat Flux (٢٠) Watt.

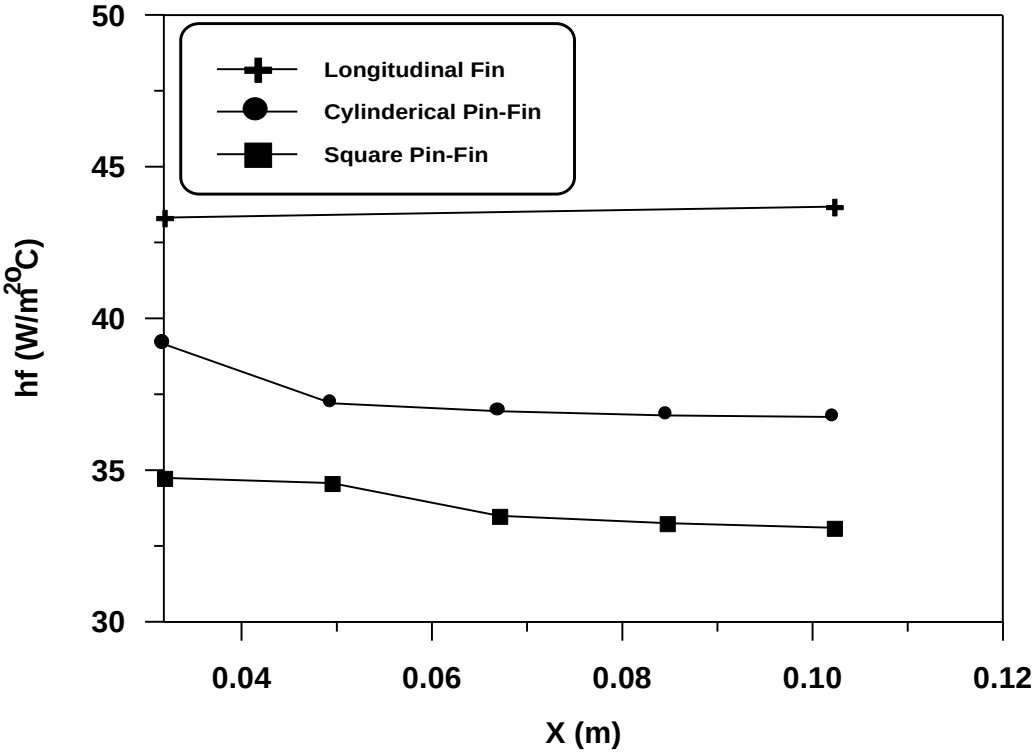

Fig.(٥-٨) Local Heat Transfer Coefficient along Flow Direction for Velocity (٢) m/s and Heat Flux (٣٠) Watt.

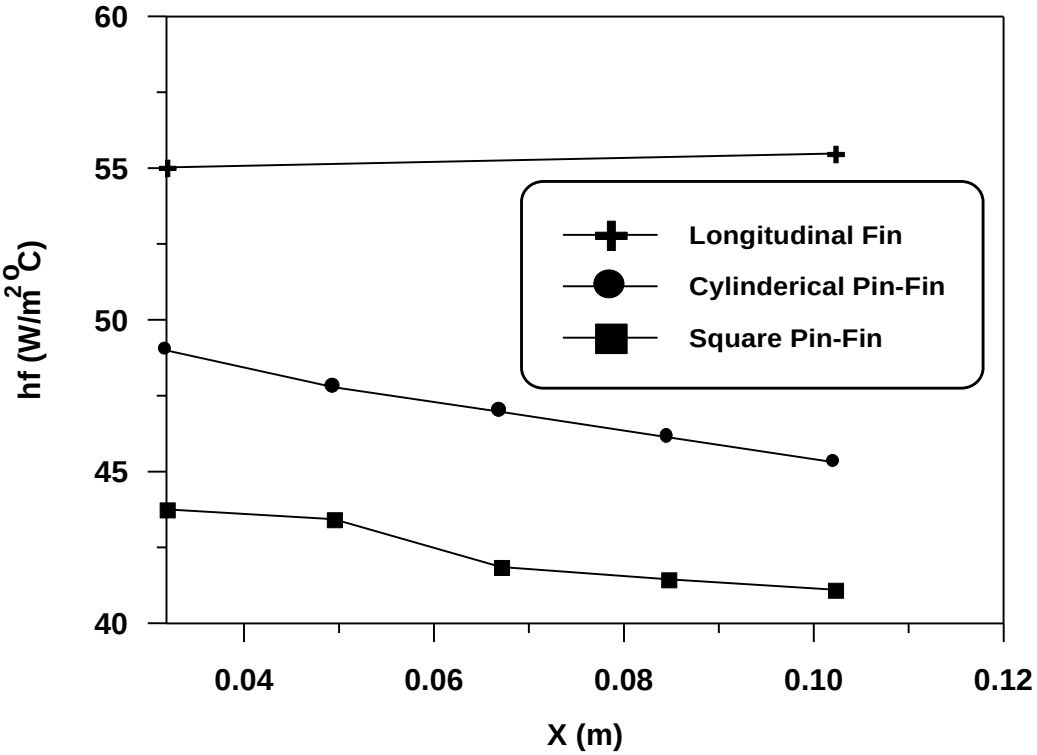

Fig.(٥-٩) Local Heat Transfer Coefficient along Flow Direction for Velocity (٢) m/s and Heat Flux (٤٠) Watt.

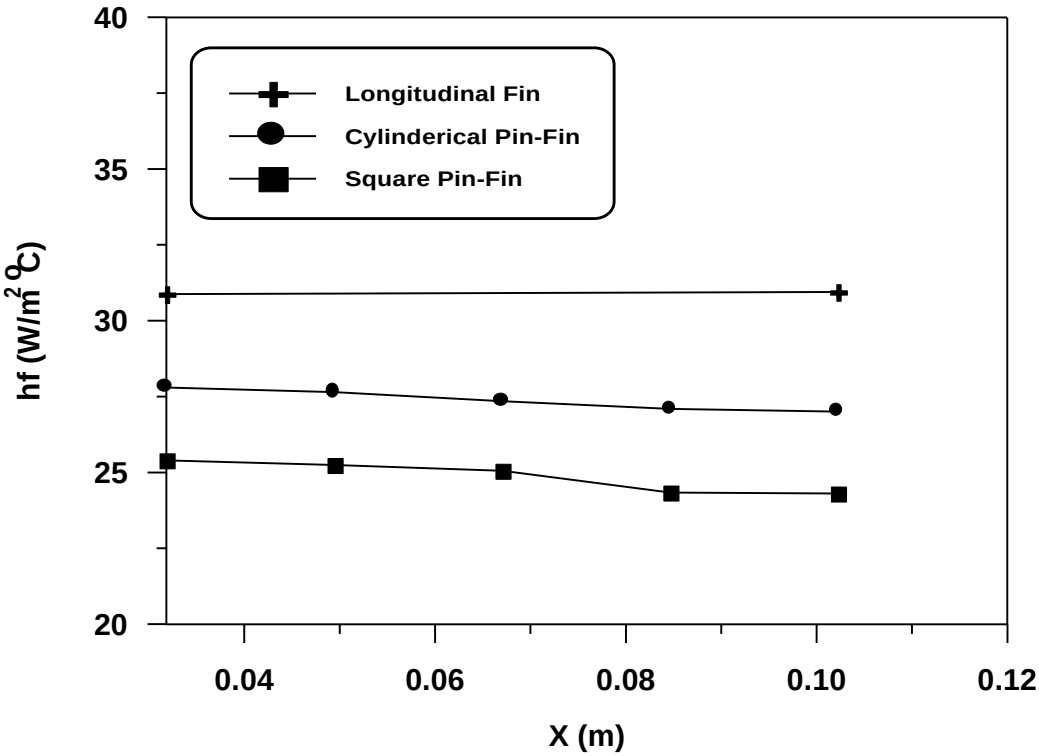

Fig.(٥-١٠) Local Heat Transfer Coefficient along Flow Direction for Velocity (٣) m/s and Heat Flux (٢٠) Watt.

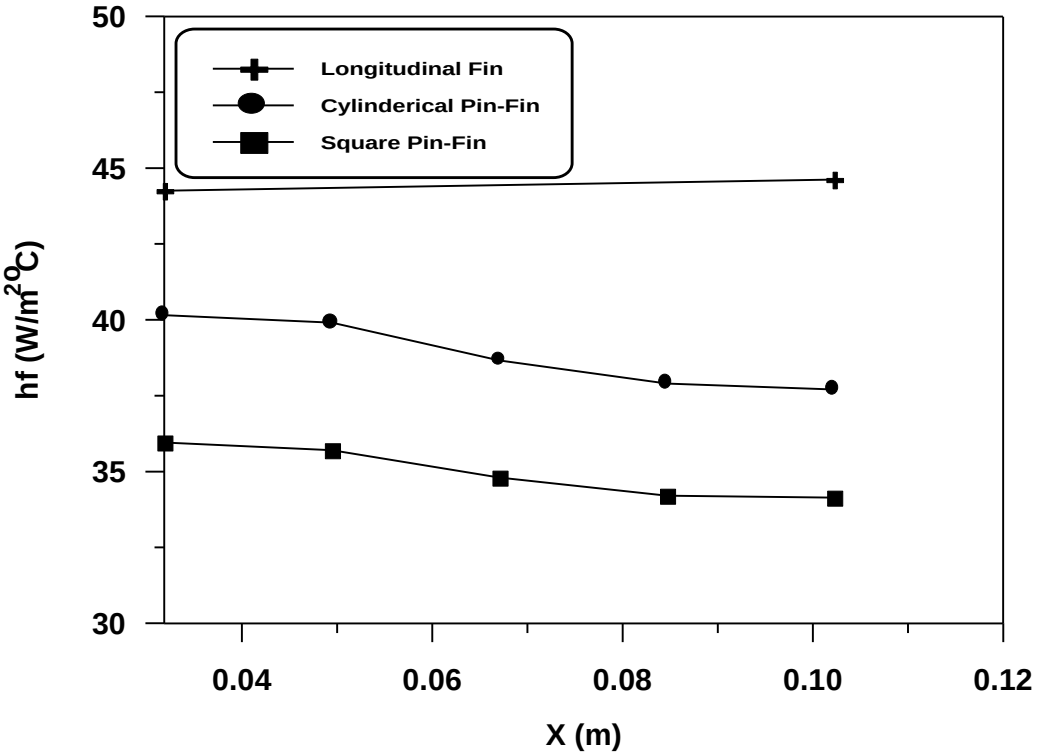

Fig.(٥-١١) Local Heat Transfer Coefficient along Flow Direction for Velocity (٣) m/s and Heat Flux (٣٠) Watt.

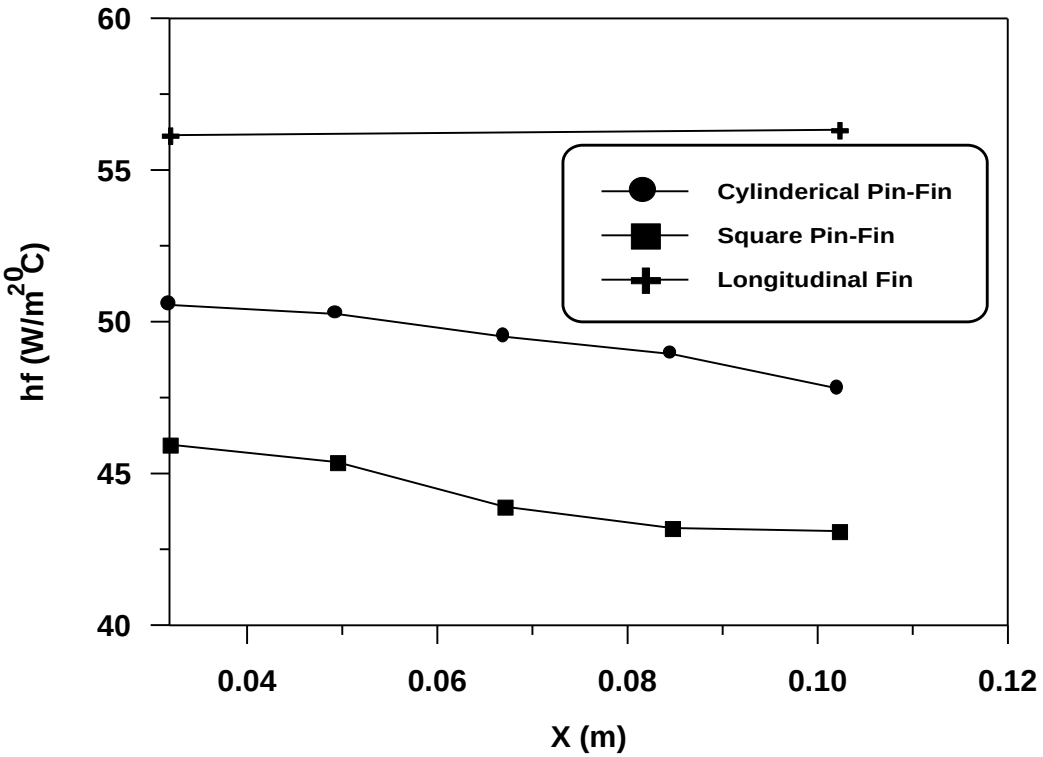

Fig.(٥-١٢) Local Heat Transfer Coefficient along Flow Direction for Velocity (٣) m/s and Heat Flux (٤٠) Watt.

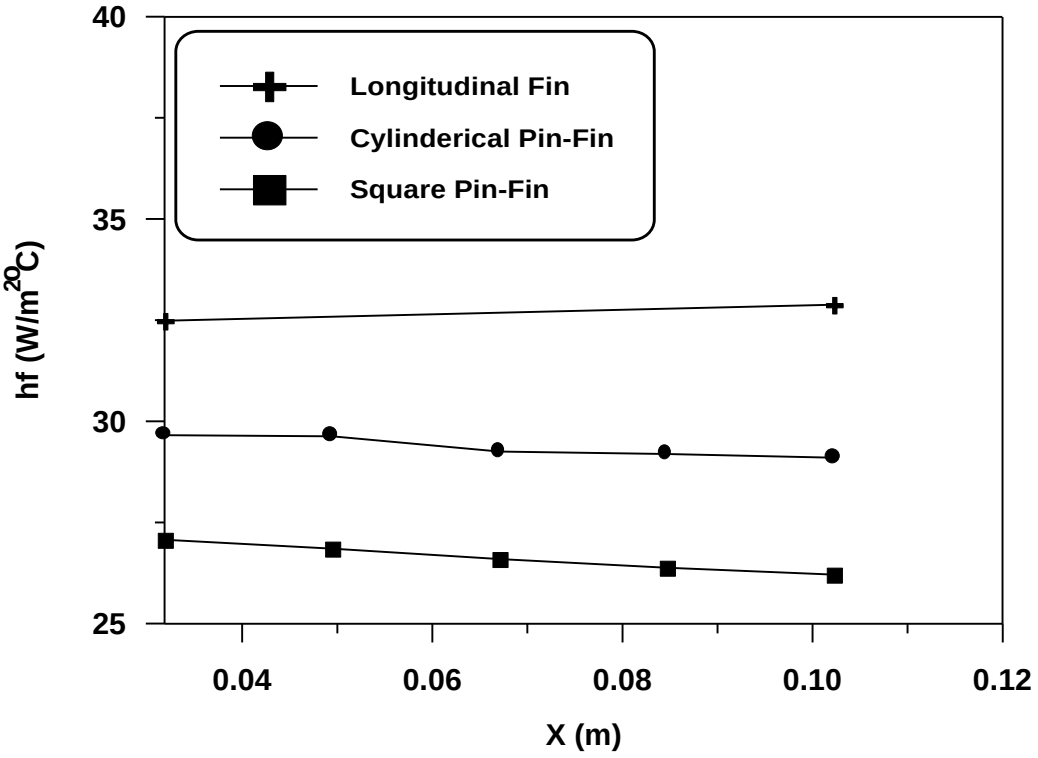

Fig.(٥-١٣) Local Heat Transfer Coefficient along Flow Direction for Velocity (٤) m/s and Heat Flux (٢٠) Watt.

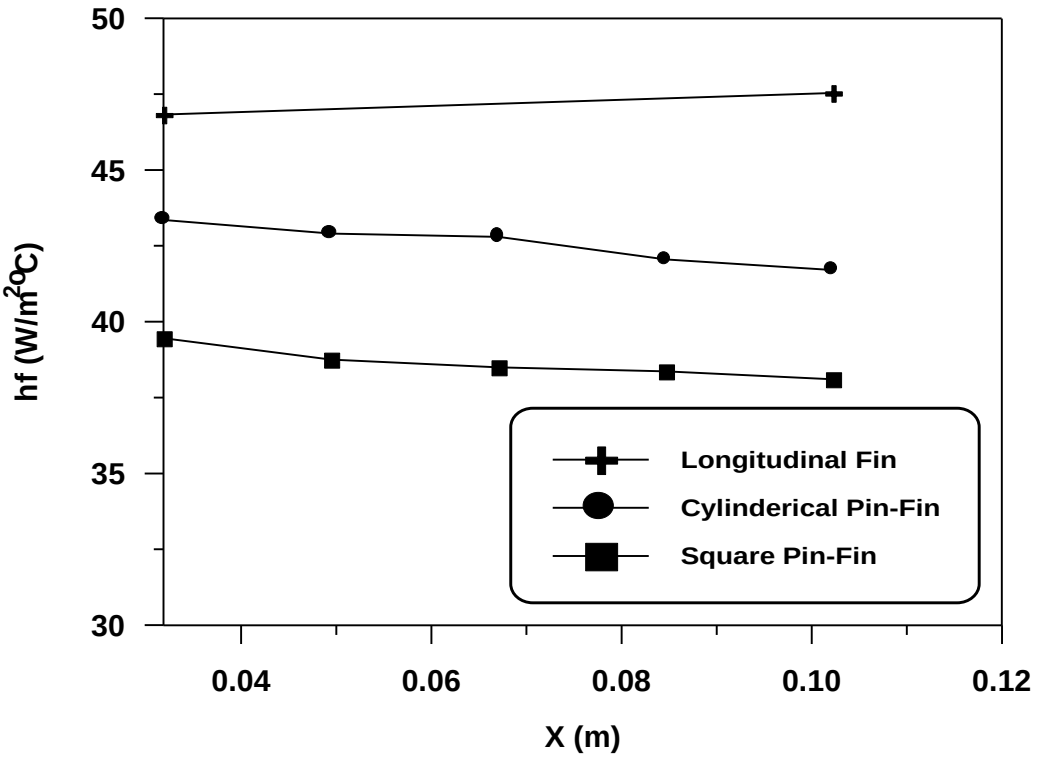

Fig.(٥-١٤) Local Heat Transfer Coefficient along Flow Direction for Velocity (٤) m/s and Heat Flux (٣٠) Watt.

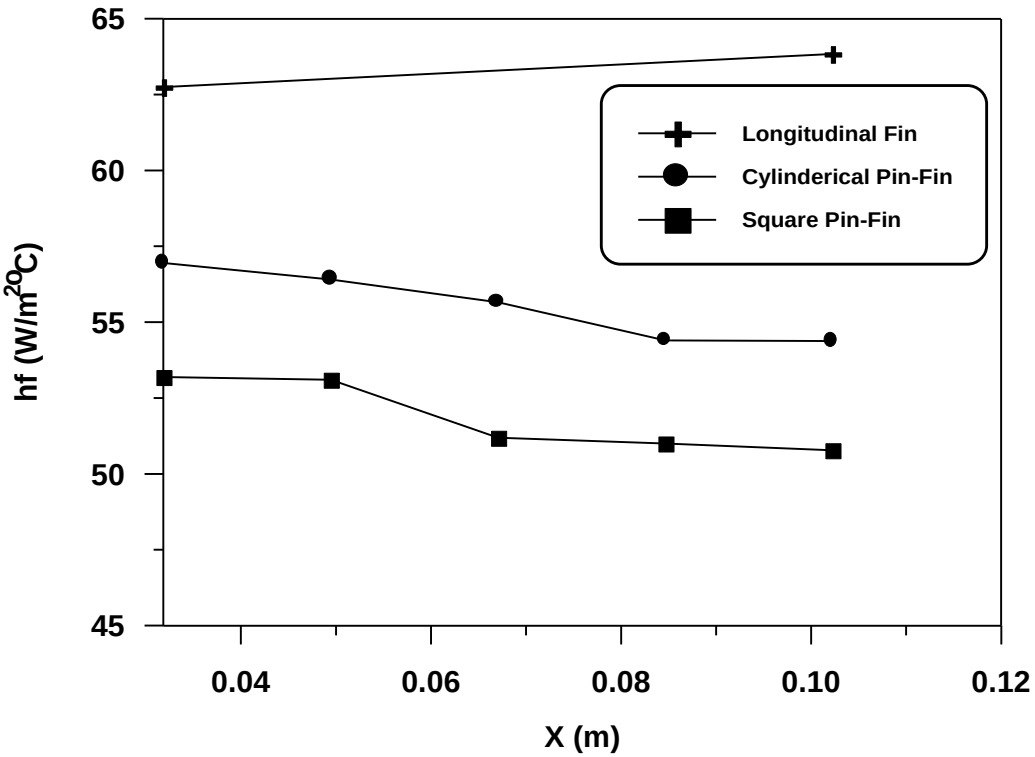

Fig.(٥-١٥) Local Heat Transfer Coefficient along Flow Direction for Velocity (٤) m/s and Heat Flux (٤٠) Watt.

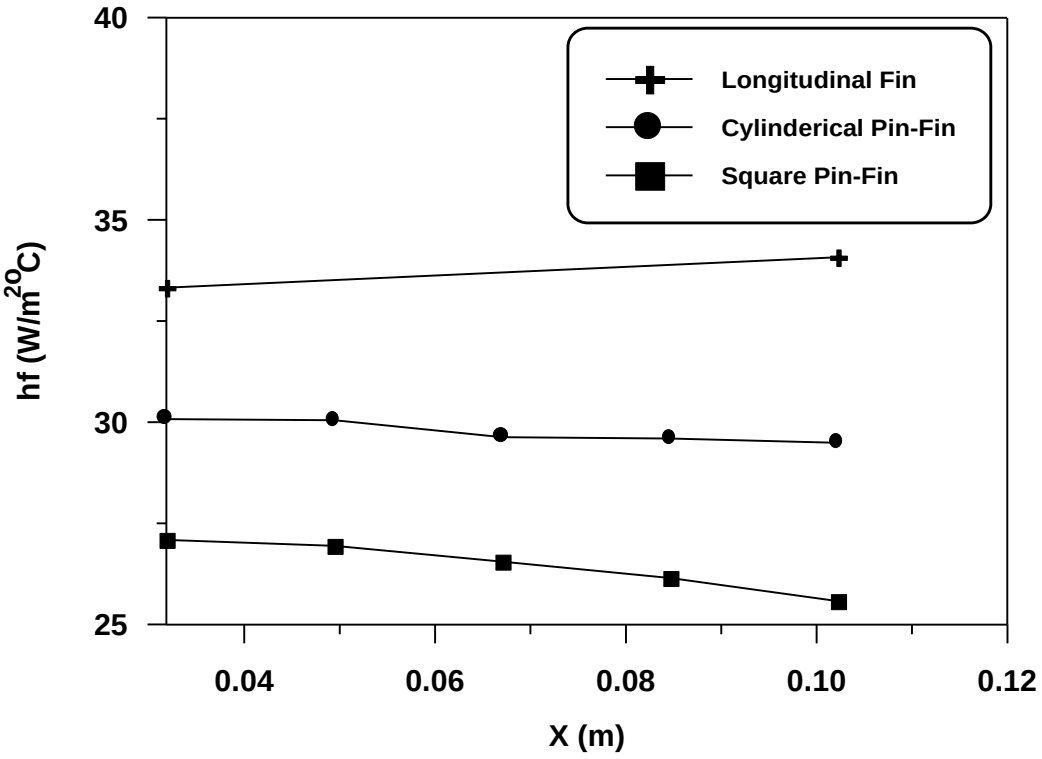

Fig.(٥-١٦) Local Heat Transfer Coefficient along Flow Direction for Velocity (٦) m/s and Heat Flux (٢٠) Watt.

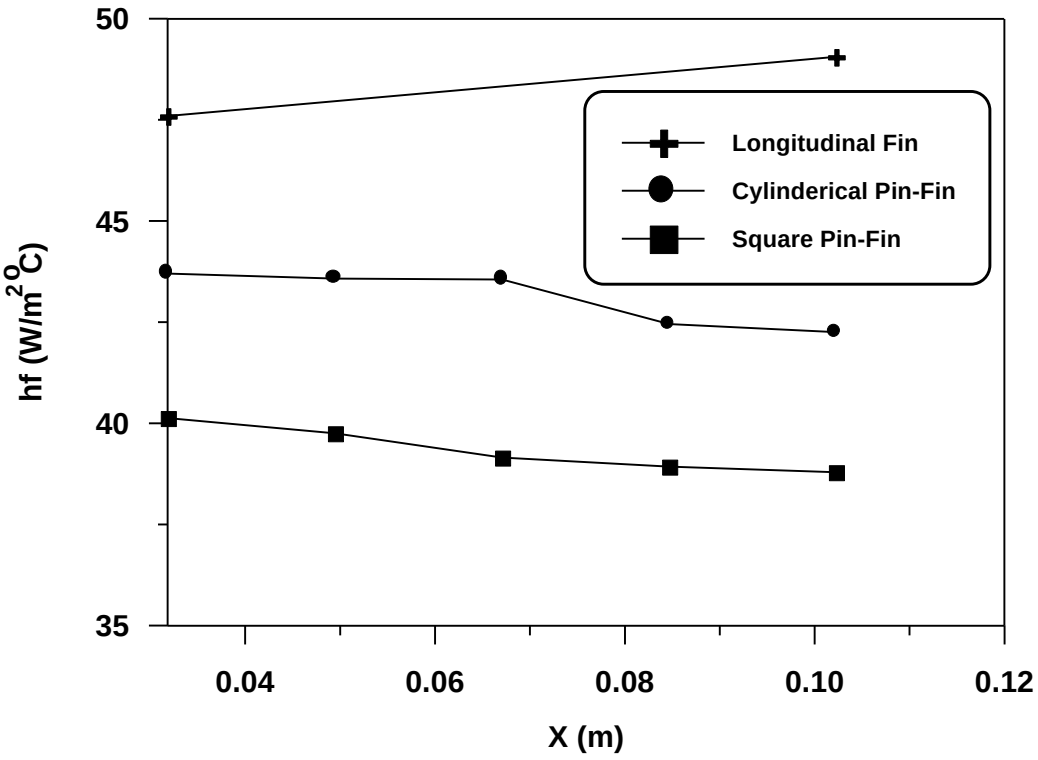

Fig.(٥-١٧) Local Heat Transfer Coefficient along Flow Direction for Velocity (٦) m/s and Heat Flux (٣٠) Watt.

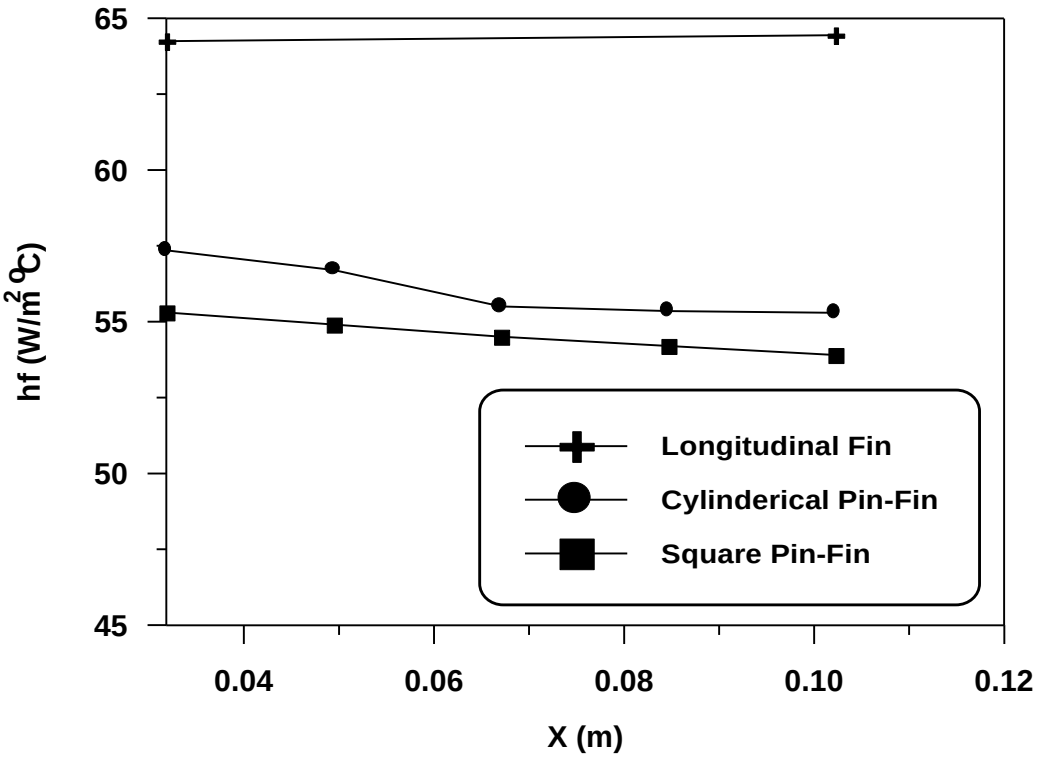

Fig.(٥-١٨) Local Heat Transfer Coefficient along Flow Direction for Velocity (٦) m/s and Heat Flux (٤٠) Watt.

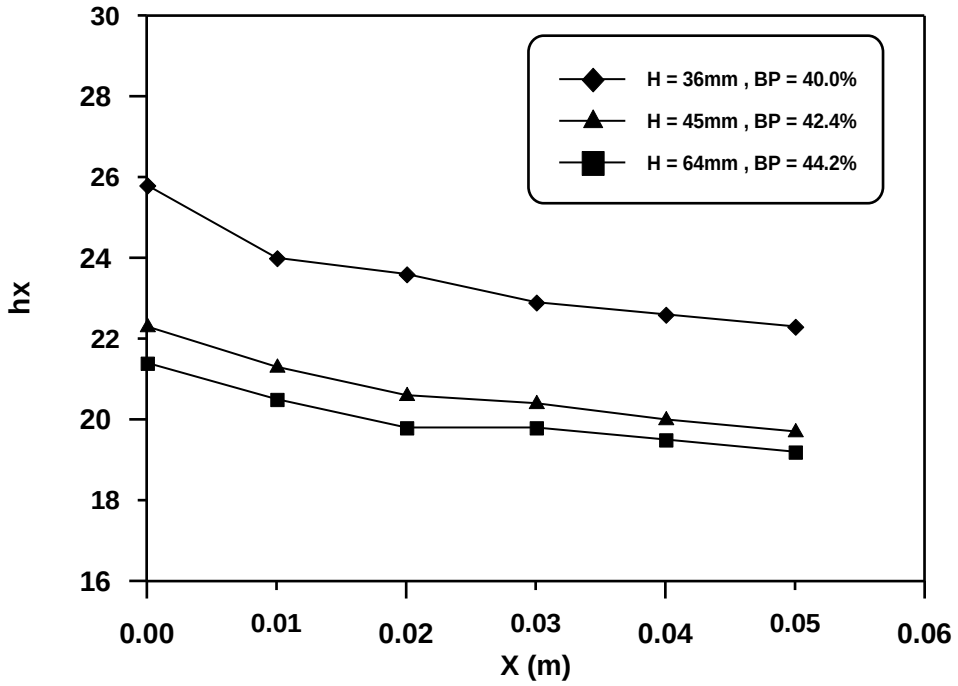

Fig.(٥-١٩) Local Heat Transfer Coefficient along Flow Direction for (٩-Cross Cut Fin) Heat Sink Re_L=٧٠٠٠ Ref(٣٤).

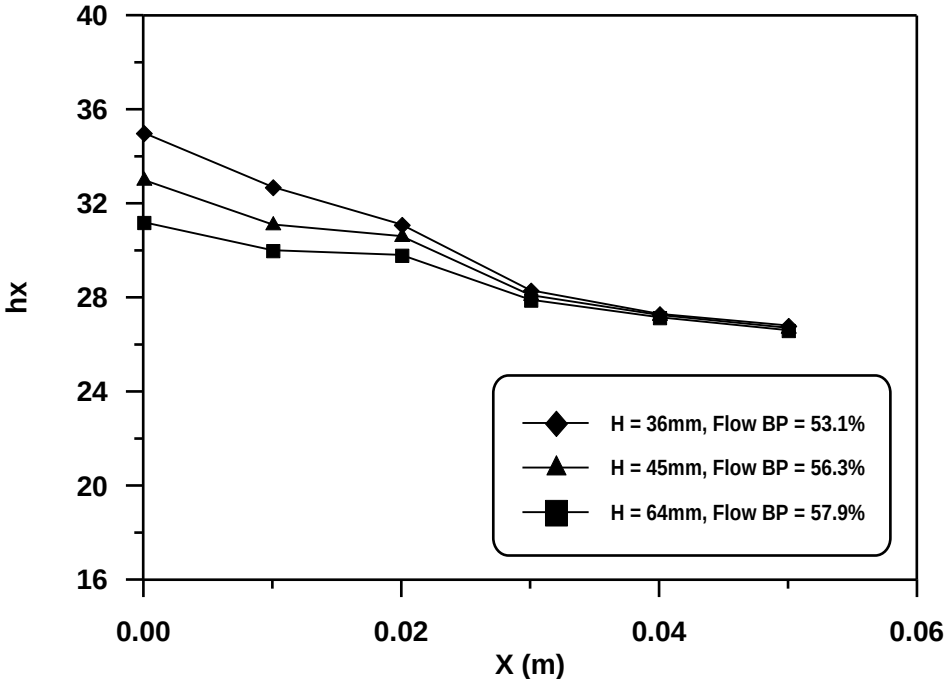

Fig.(٥-٢٠) Local Heat Transfer Coefficient along Flow Direction for (١٢-Cross Cut Fin) Heat Sink Re_L=٧٠٠٠ Ref(٣٤).

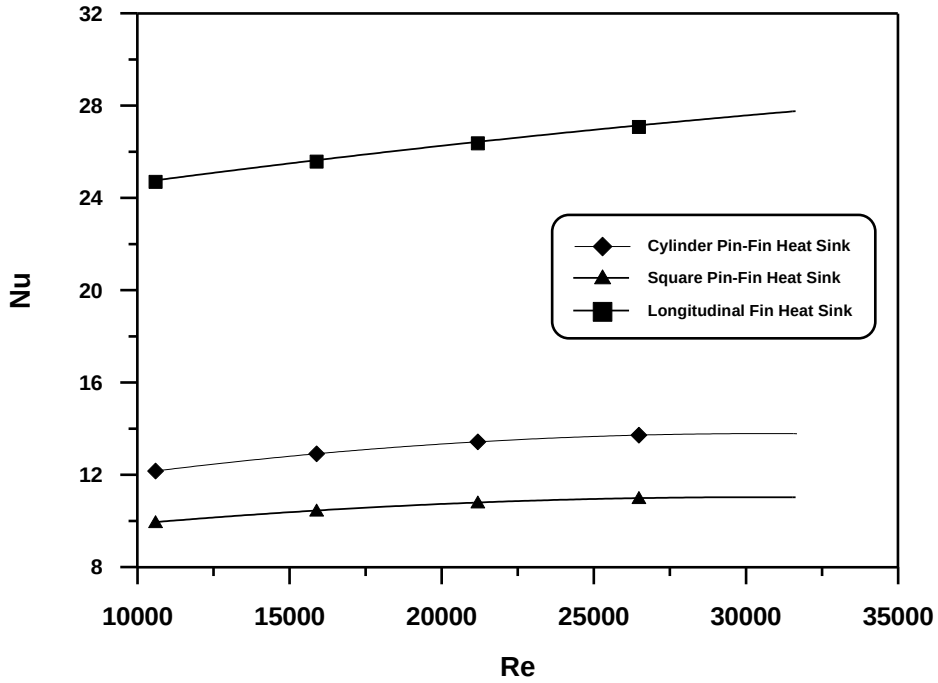

Fig.(٥-٢١) Reynolds Number vs. Nusselt Number For Heat Flux (٢٠) Watt.

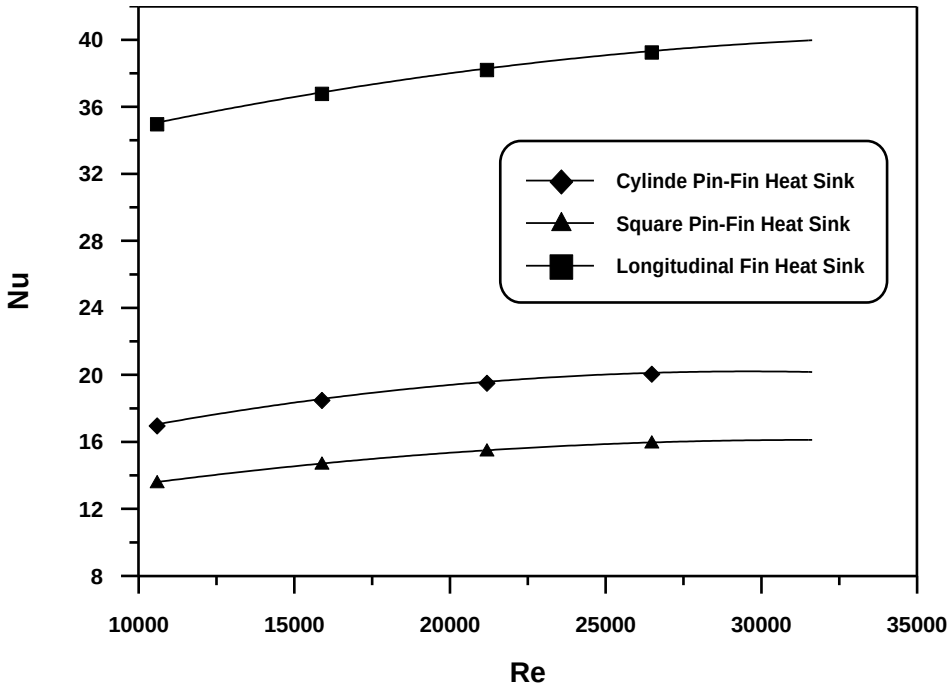

Fig.(٥-٢٢) Reynolds Number vs. Nusselt Number For Heat Flux (٣٠) Watt.

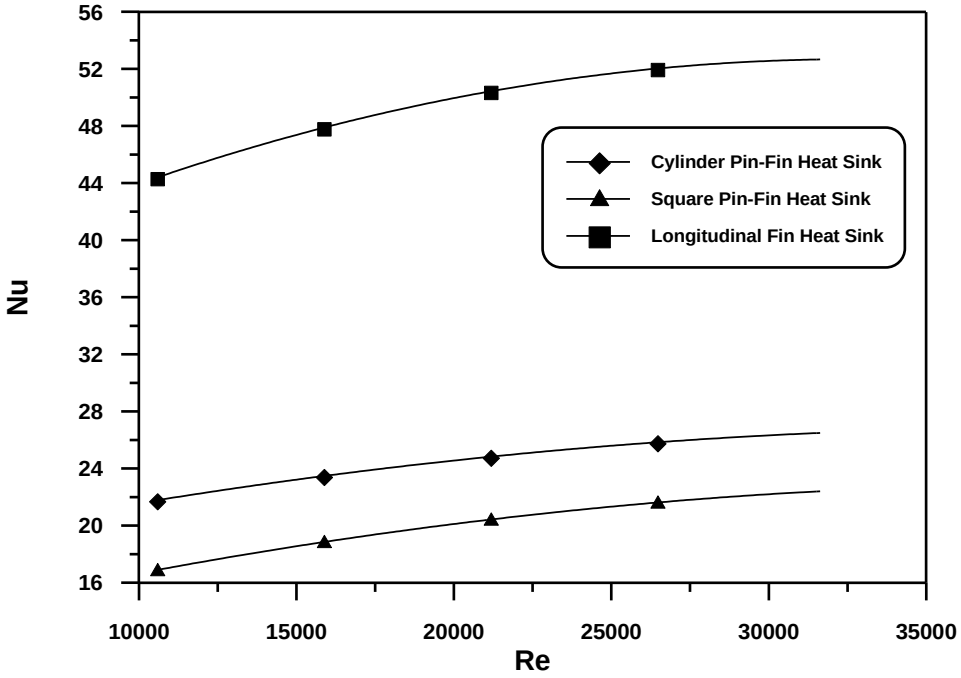

Fig.(٥-٢٣) Reynolds Number vs. Nusselt Number For Heat Flux (٤٠) Watt.

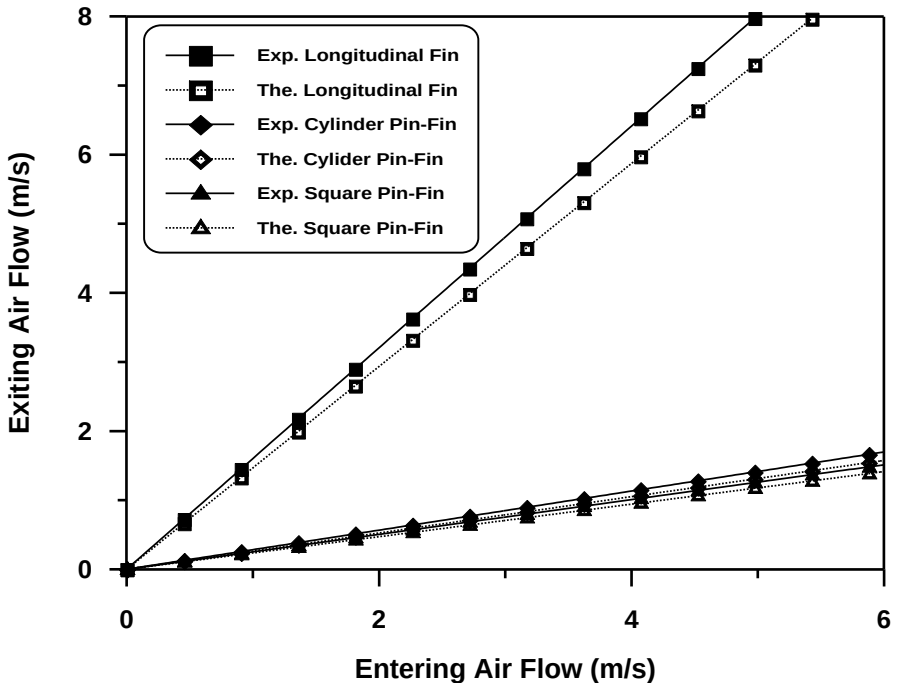

Fig. (٥-٢٤) Dynamic Correlation of Effective Air Flow through a Heat Sinks.

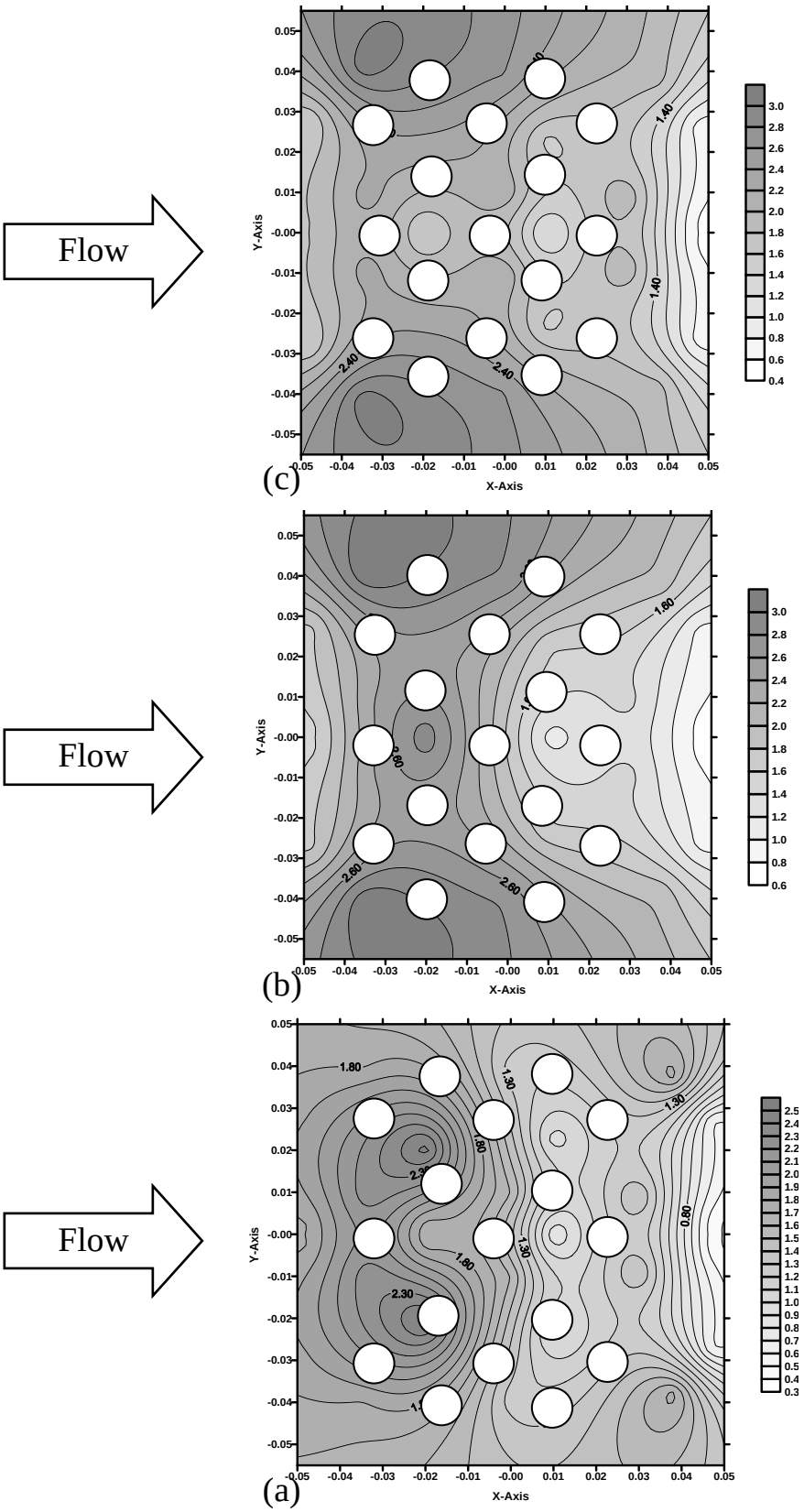

Fig. (٥-٢٥) Velocity Contour Map for Cylinder Pin-Fins in The First Domain (a), Second Domain (b), and Third Domain (c).

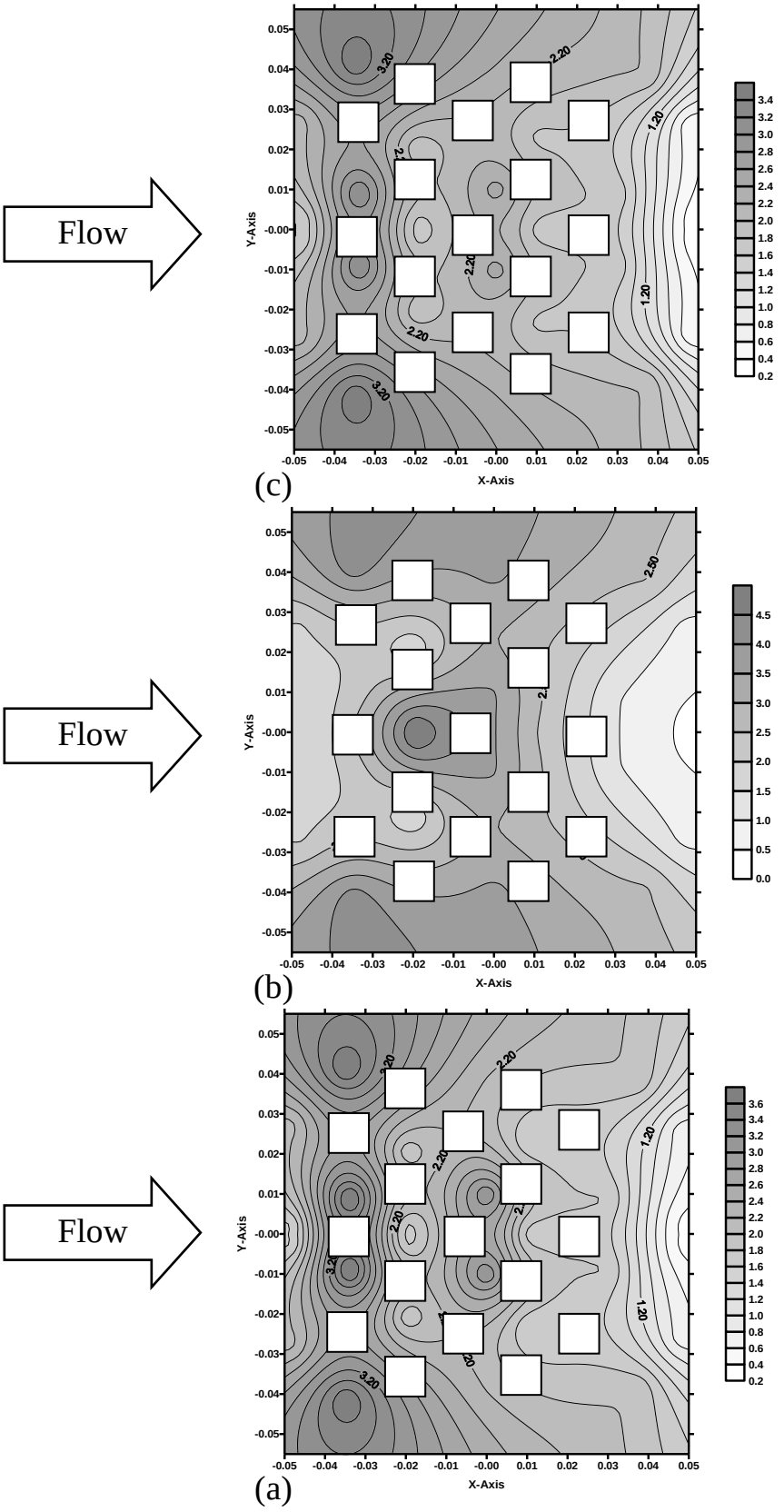

Fig. (٥-٢٦) Velocity Contour Map for Square Pin-Fins in The First Domain (a), Second Domain (b), and Third Domain (c).

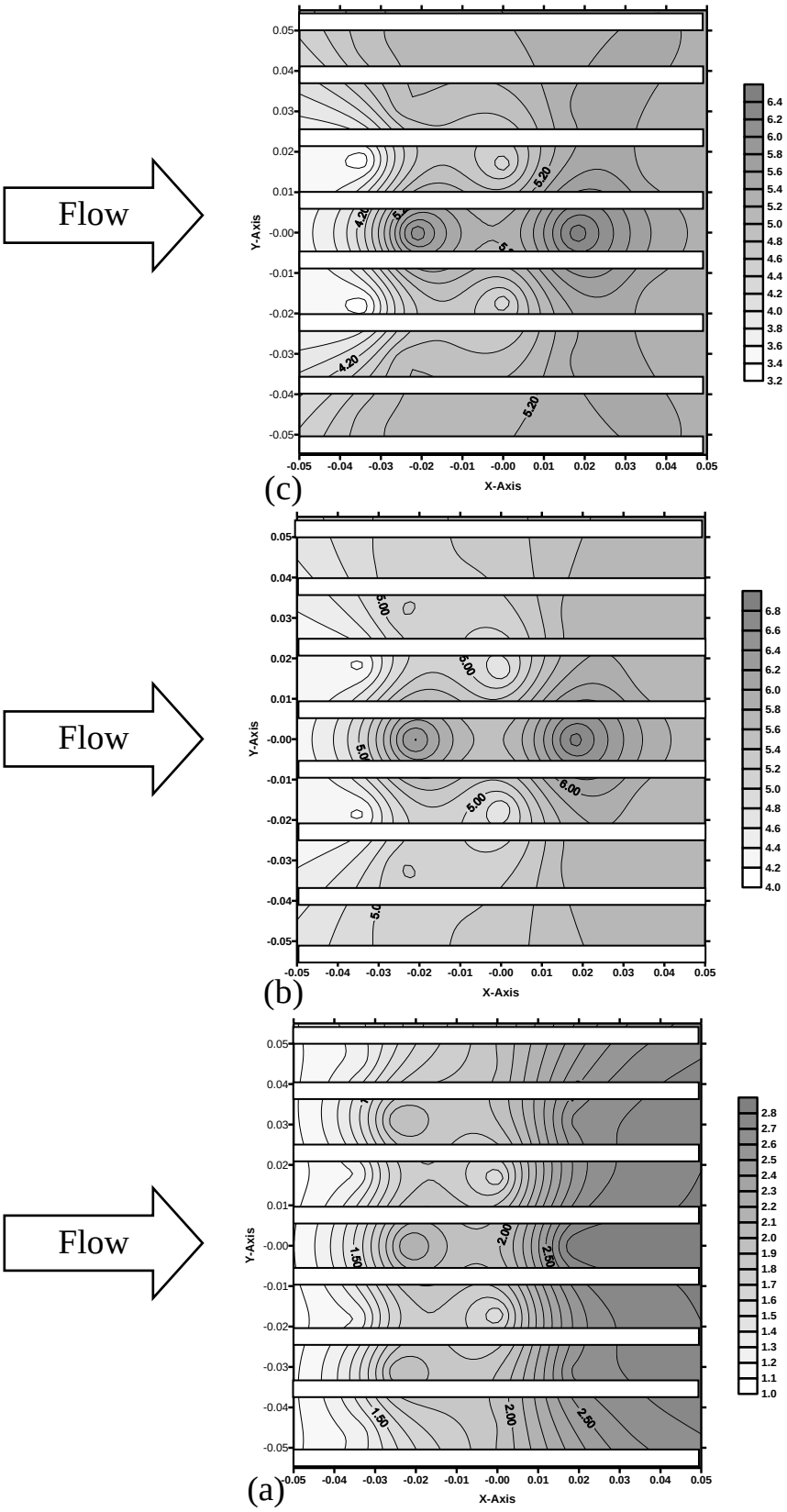

Fig. (٥-٢٧) Velocity Contour Map for Longitudinal Fins in The First Domain (a), Second Domain (b), and Third Domain (c).

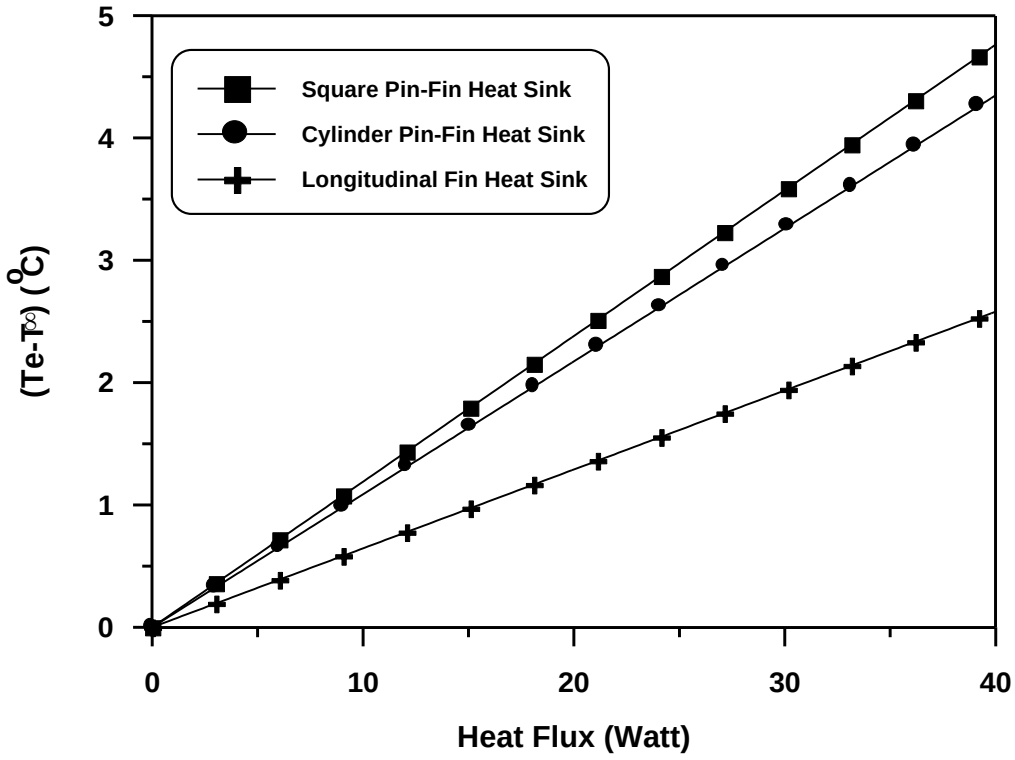

Fig. (٥-٢٨) Temperature Increase vs. Heat Flux for Air Velocity (٢) m/s.

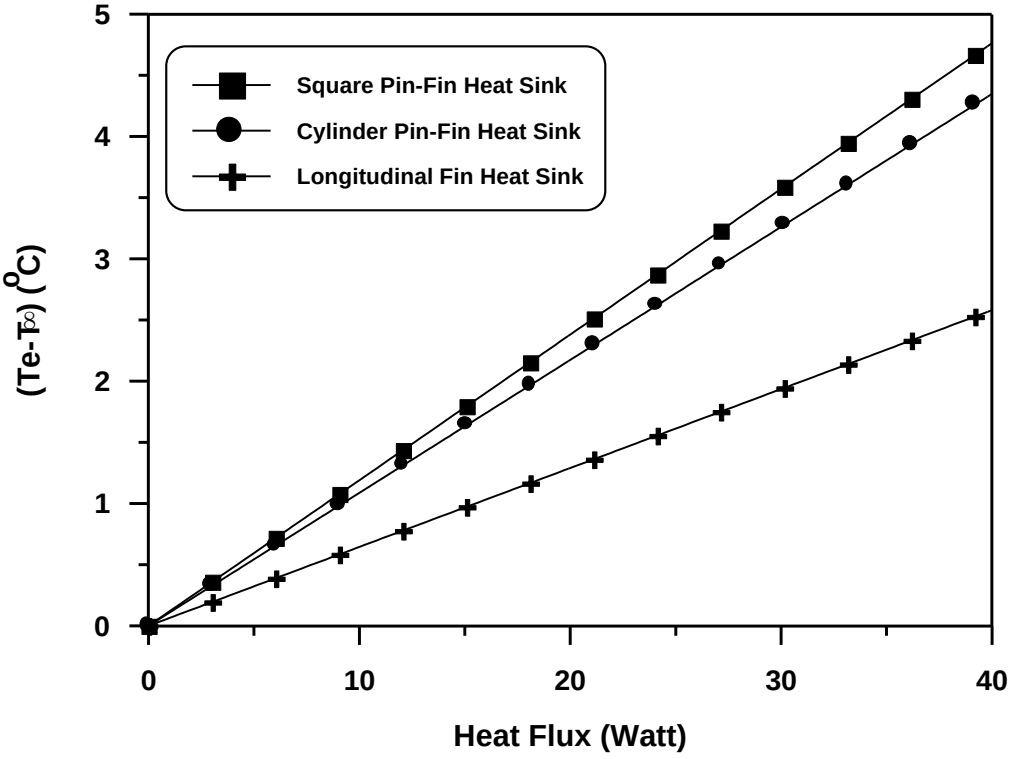

Fig. (٥-٢٩) Temperature Increase vs. Heat Flux for Air Velocity (٣) m/s.

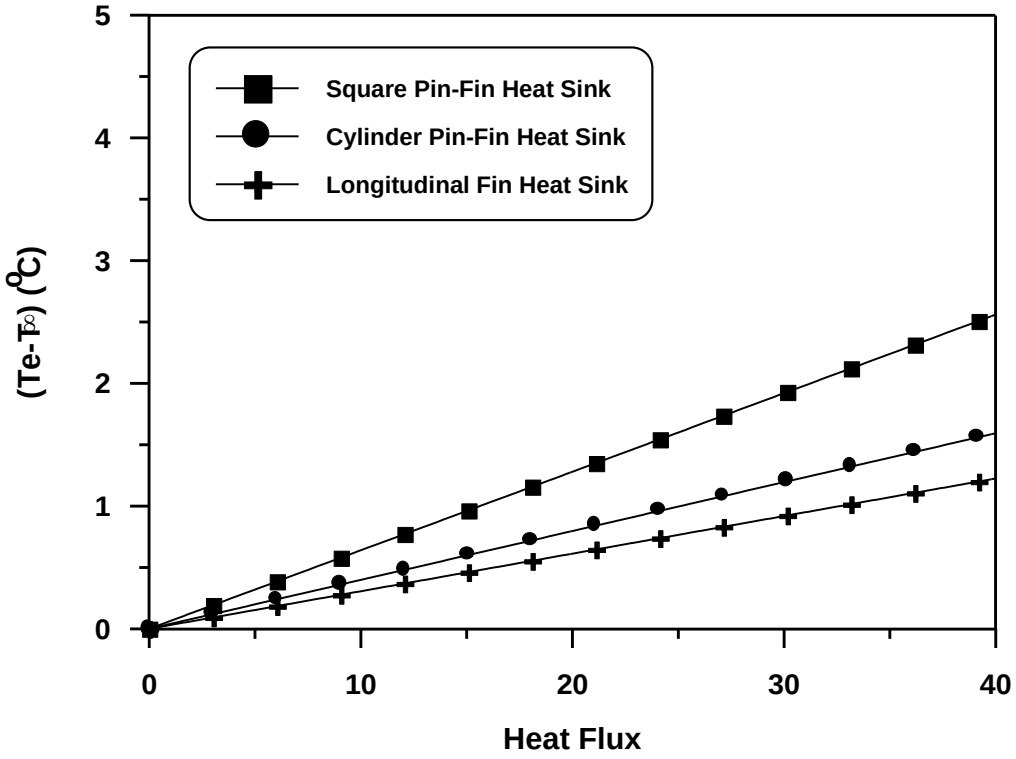

Fig. (٥-٣٠) Temperature Increase vs. Heat Flux for Air Velocity (٤) m/s.

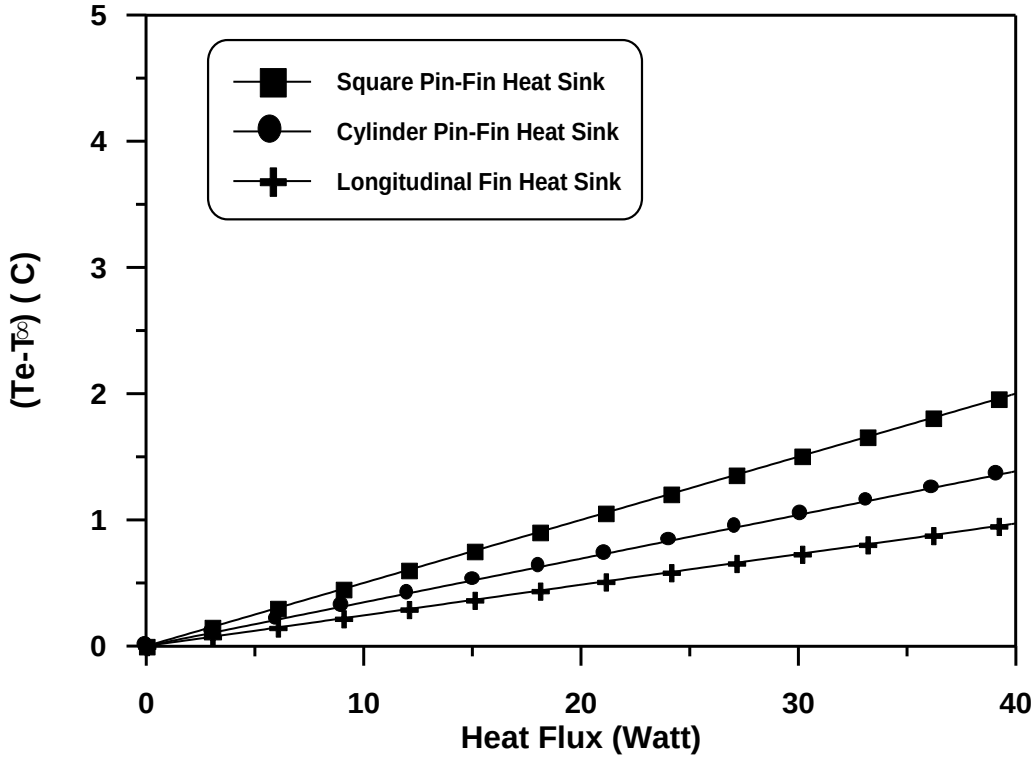

Fig. (٥-٣١) Temperature Increase vs. Heat Flux for Air Velocity (٦) m/s.

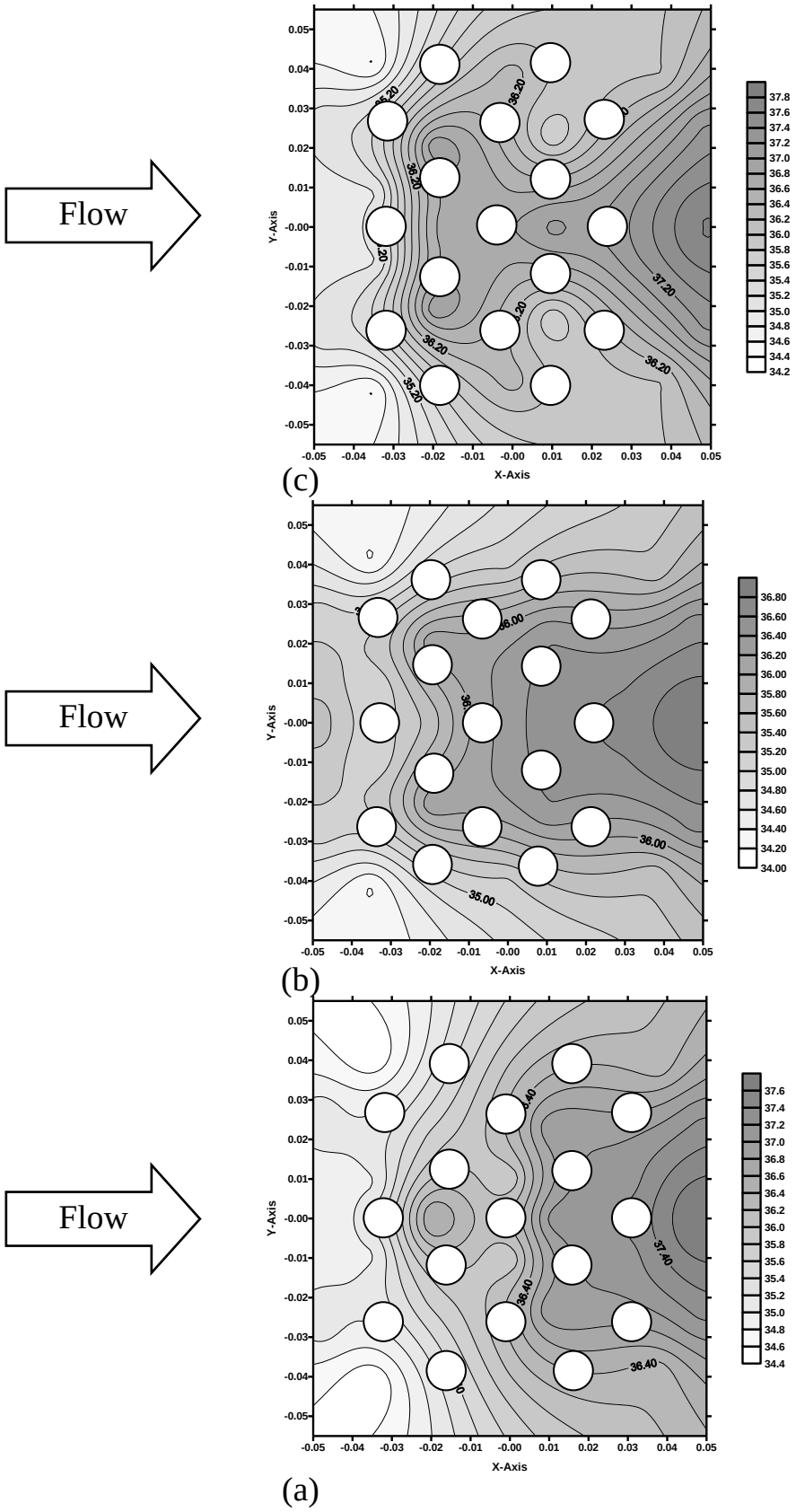

Fig. (٥-٣٢) Isothermal Contour Map for Cylindrical Pin-Fin in The First Domain (a), Second Domain (b), and Third Domain (c).

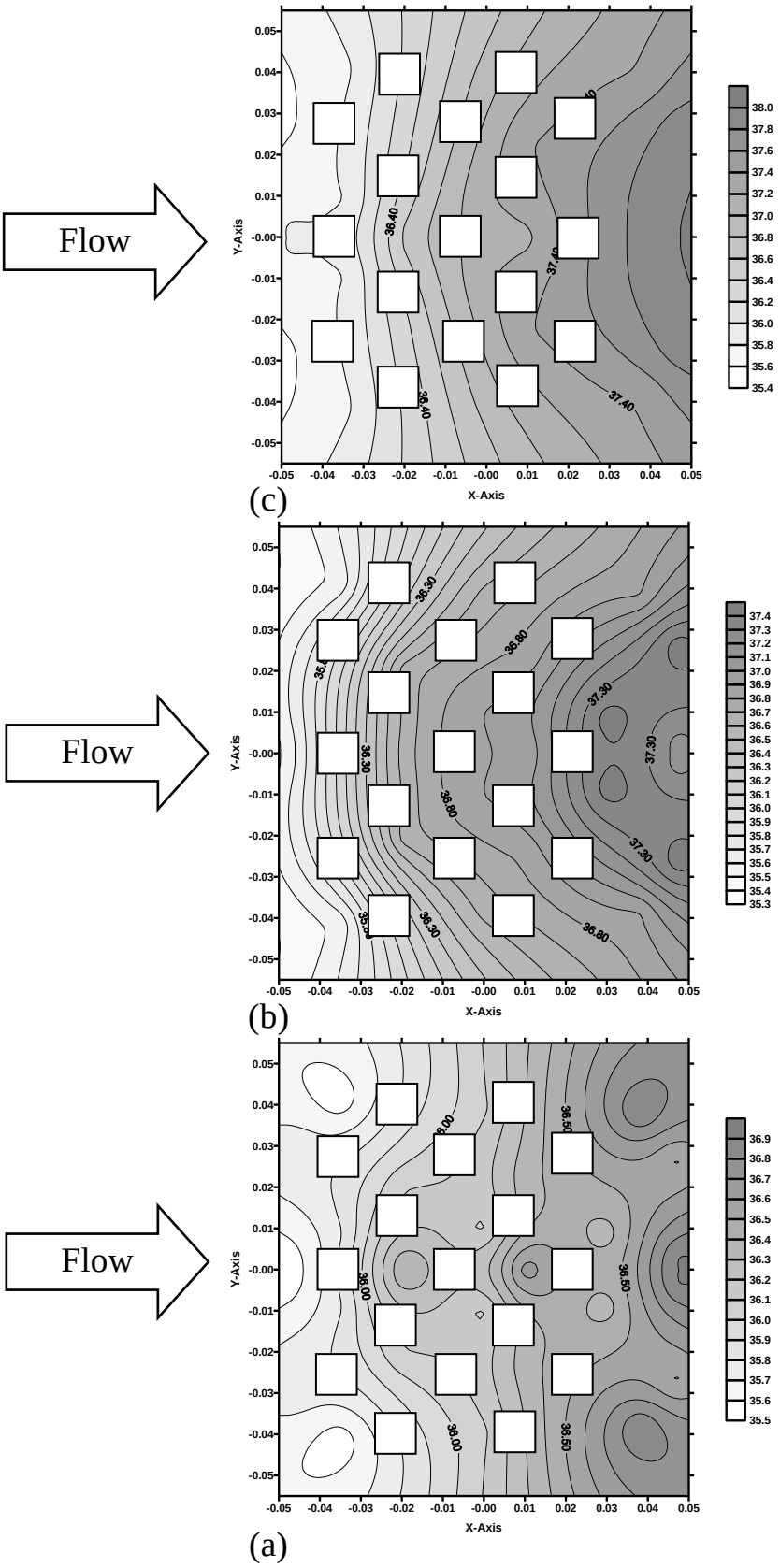

Fig. (٥-٣٣) Isothermal Contour Map for Square Pin-Fin in The First Domain (a), Second Domain (b), and Third Domain (c).

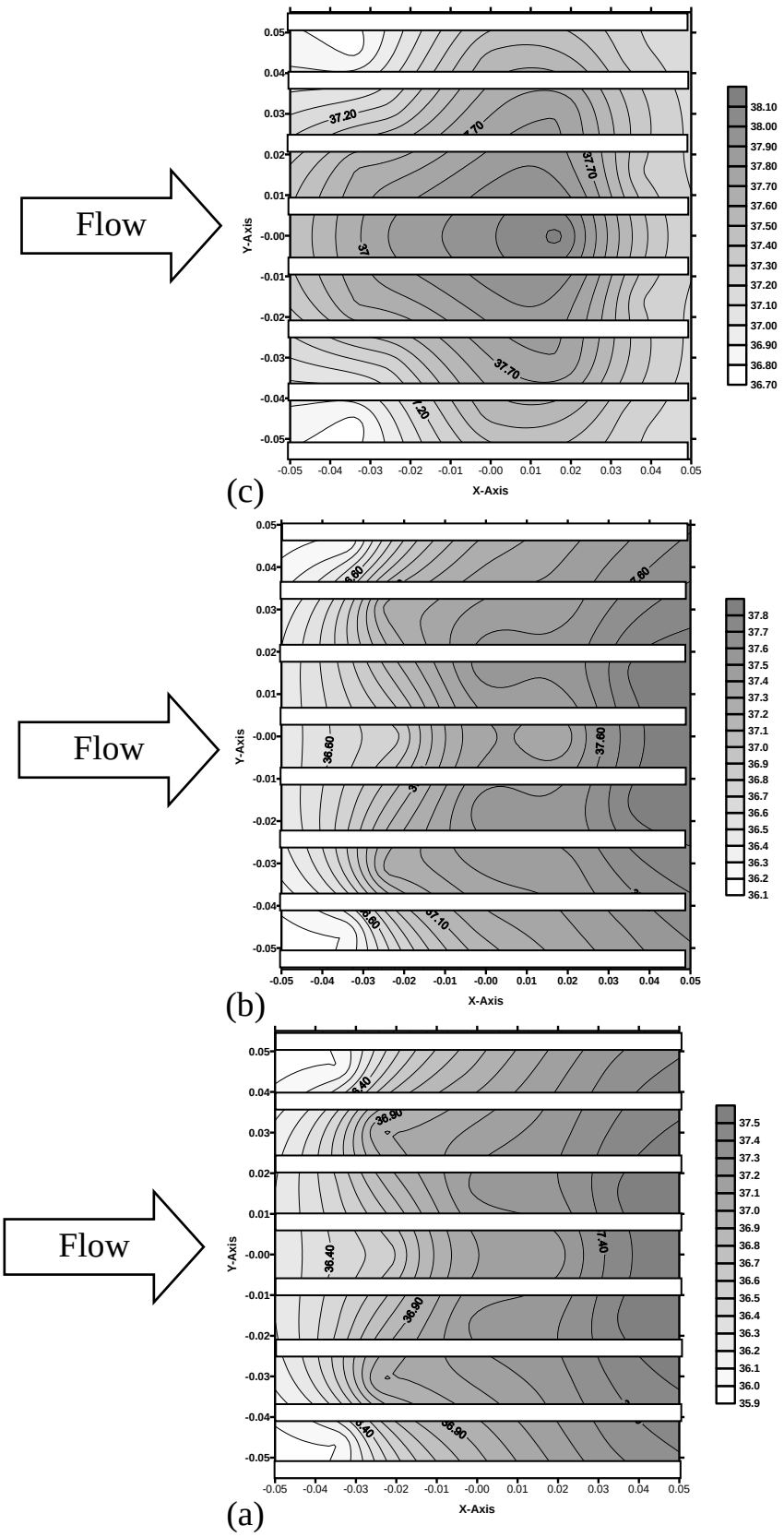

Fig. (٥-٣٤) Isothermal Contour Map for Longitudinal Fin in The First Domain (a), Second Domain (b), and Third Domain (c).

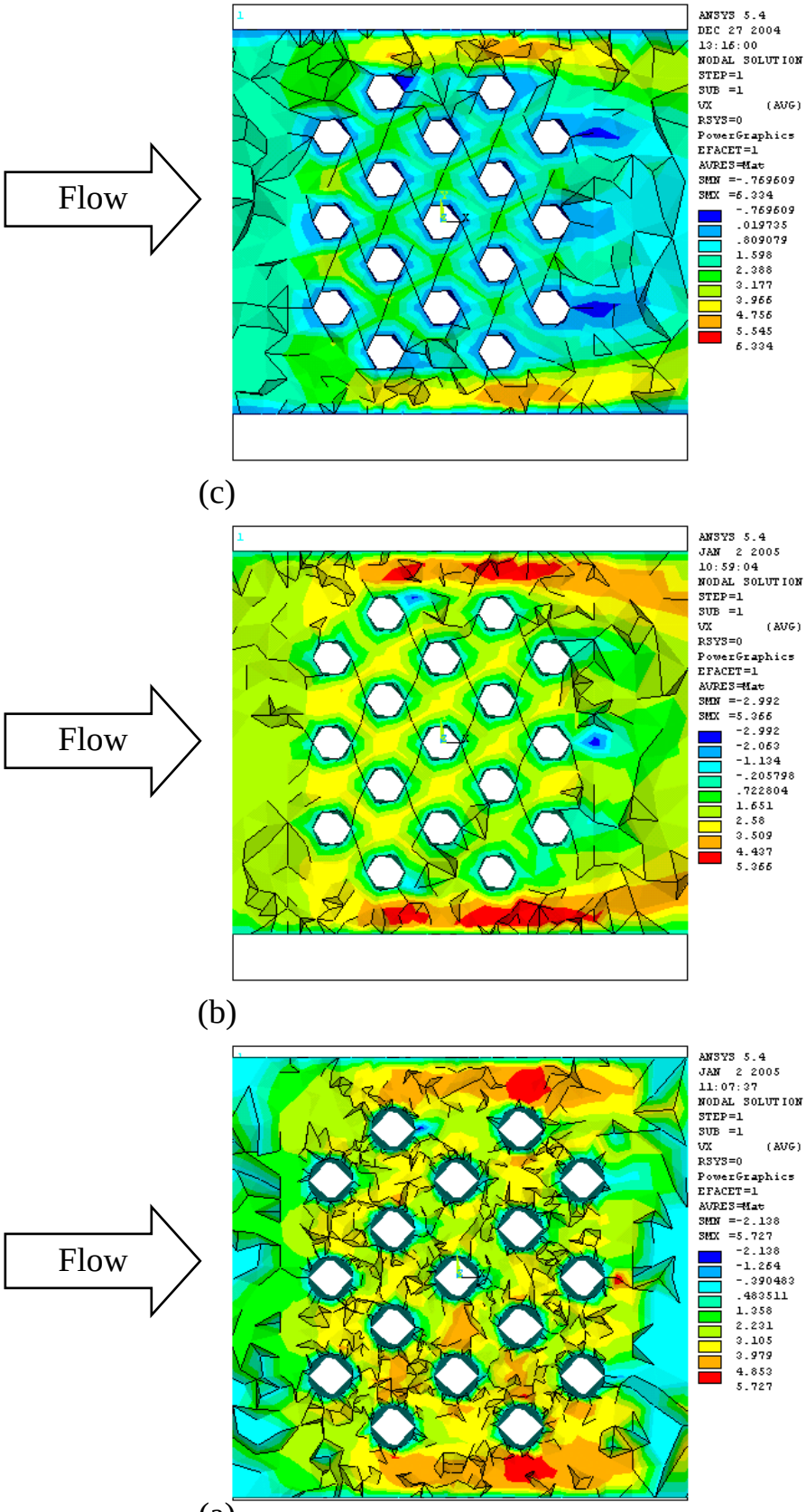

Fig. (٥-٣٥) Velocity Contour Map for Cylindrical Pin-Fin in the First Domain (a), Second Domain (b), Third Domain (c).

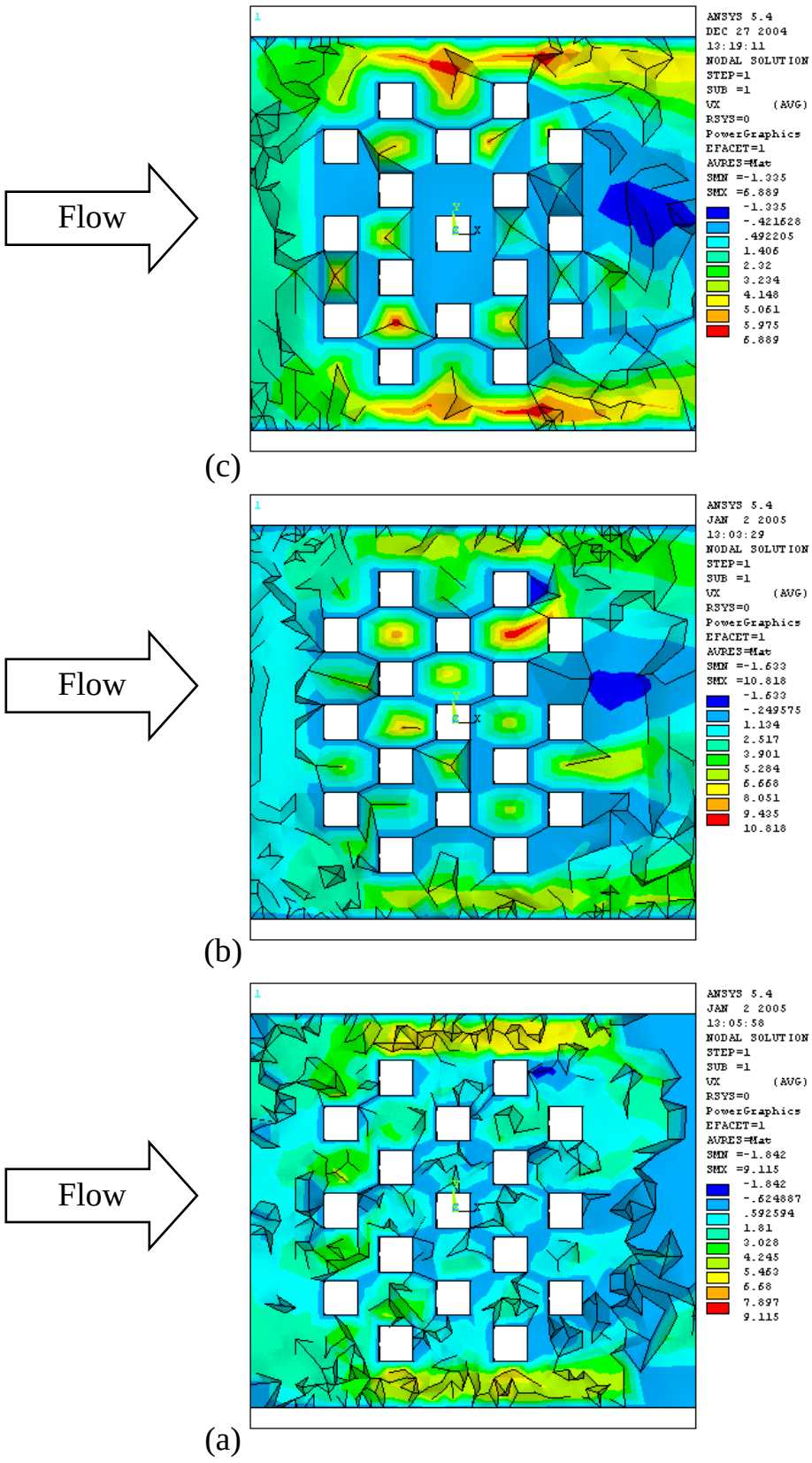

Fig. (٥-٣٦) Velocity Contour Map for Square Pin-Fin in the First Domain (a), Second Domain (b), Third Domain (c).

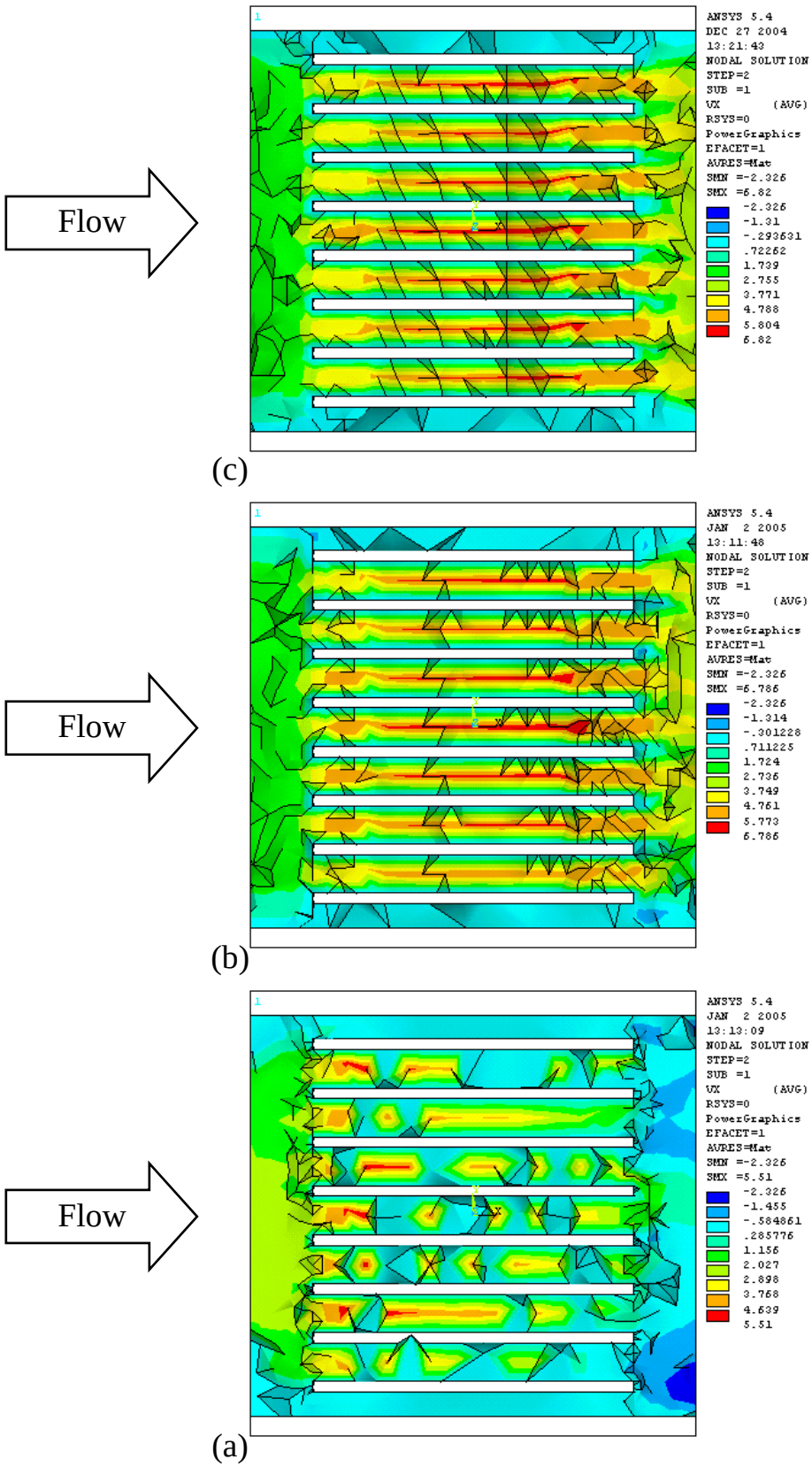

Fig. (٥-٣٧) Velocity Contour Map for Longitudinal Fins in the First Domain (a), Second domain (b), Third Domain (c).

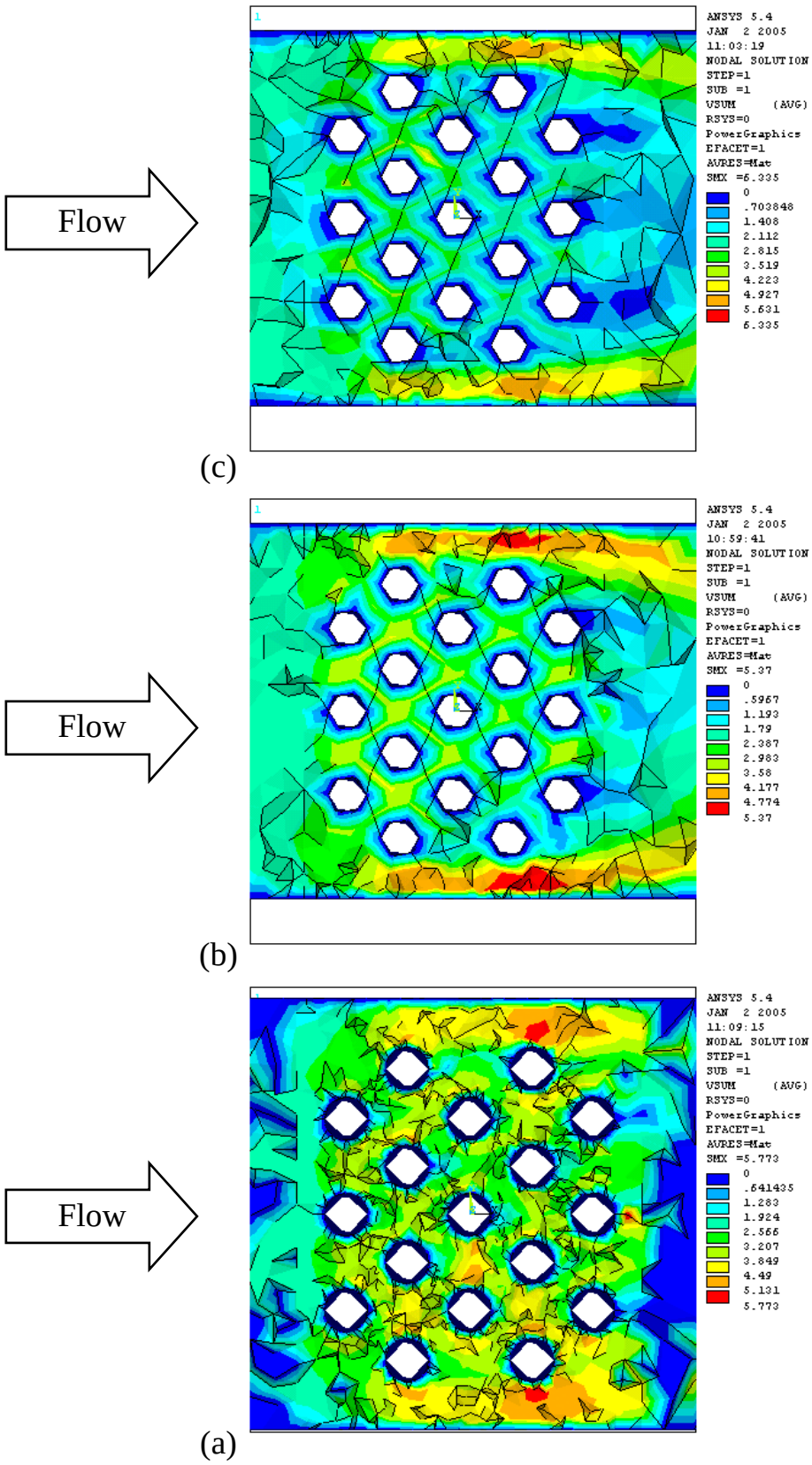

Fig. (٥-٣٨) Velocity Resultant Contour Map for Cylindrical Pin-Fin in The First Domain (a), Second Domain (b), Third Domain (c).

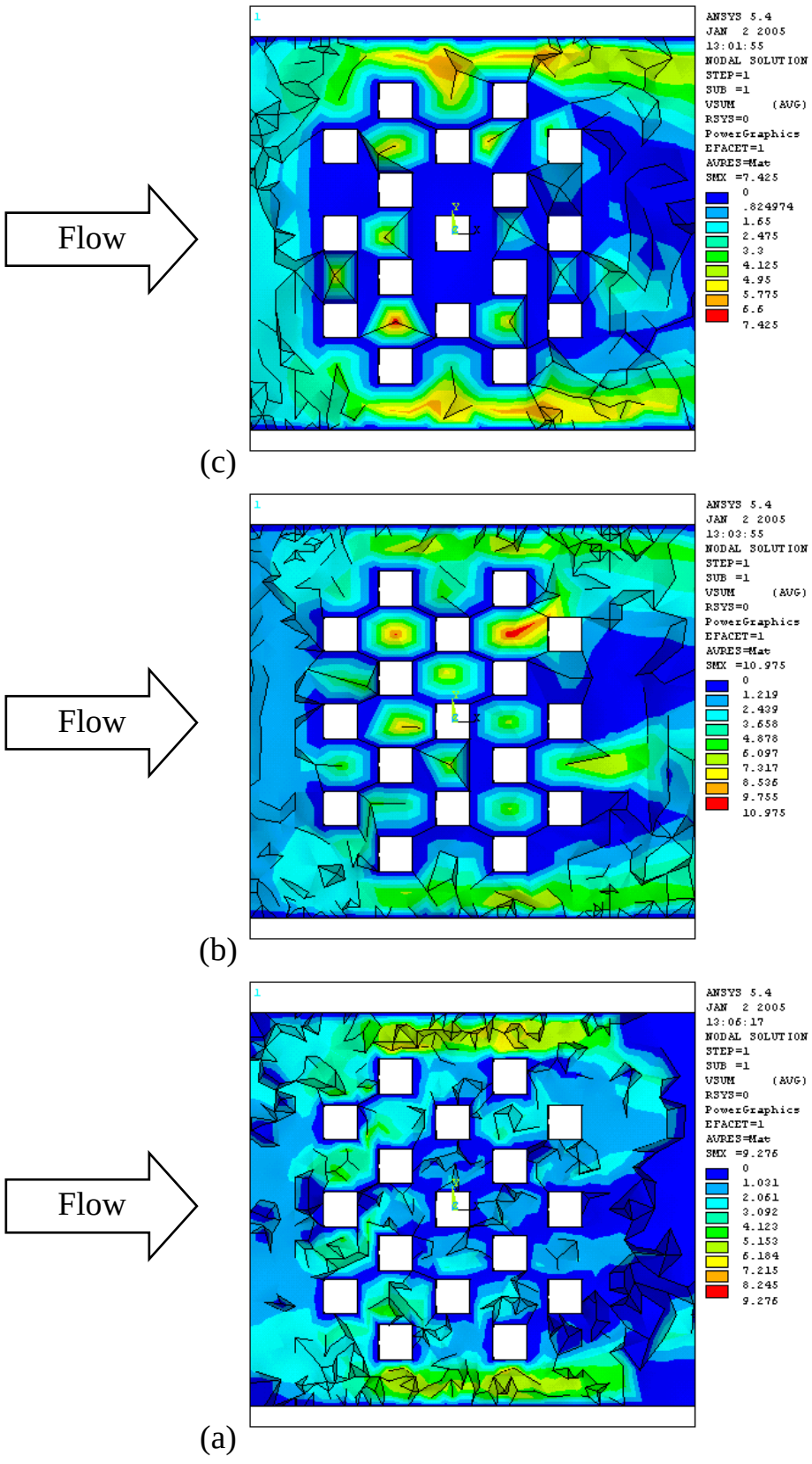

Fig. (٥-٣٩) Velocity Resultant Contour Map for Square Pin-Fin in The First Domain (a), Second Domain (b), Third Domain (c).

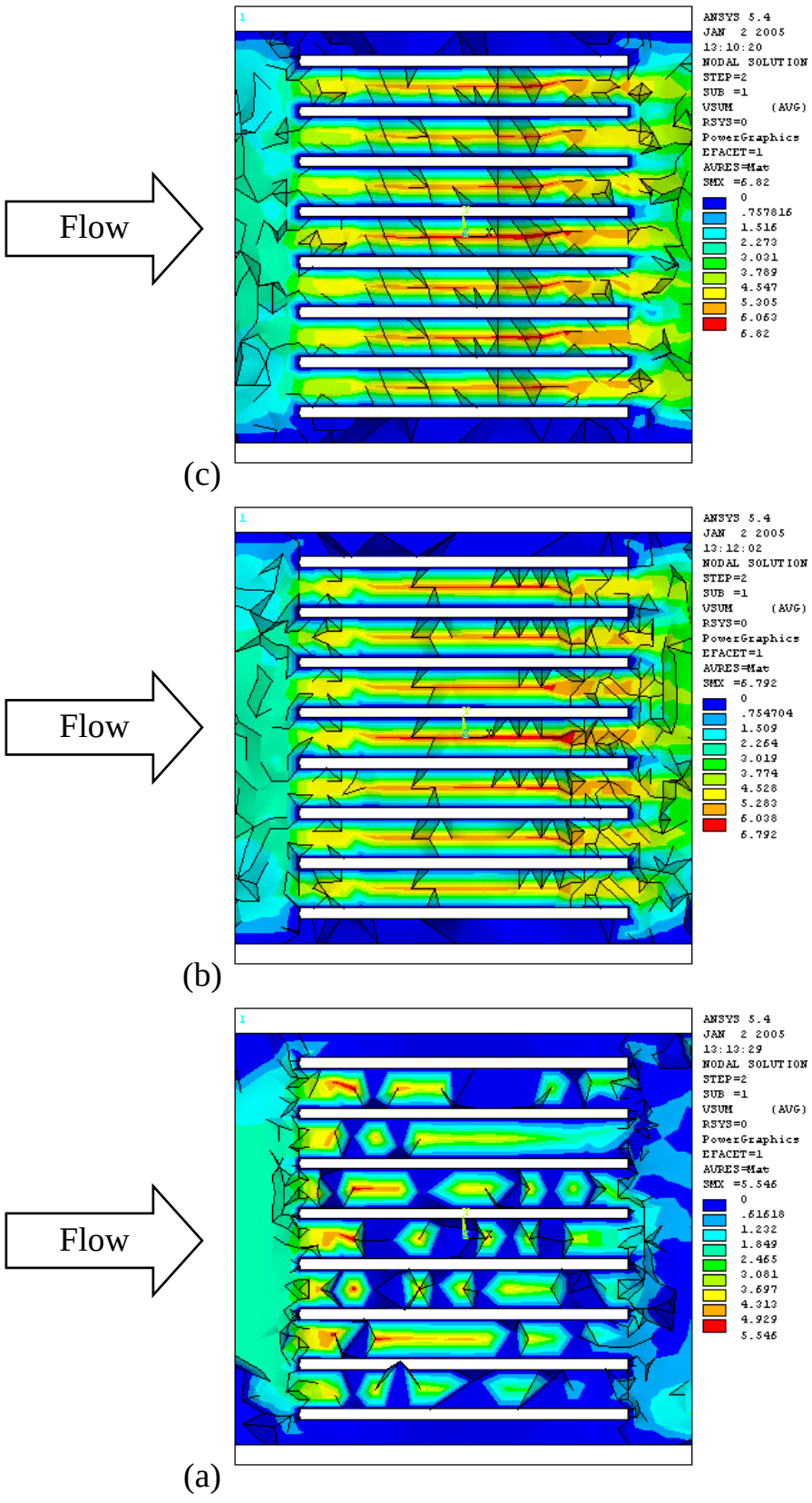

Fig. (٥-٤٠) Velocity Resultant Contour Map for Longitudinal Fins in the First Domain (a), Second Domain (b), Third Domain (c).

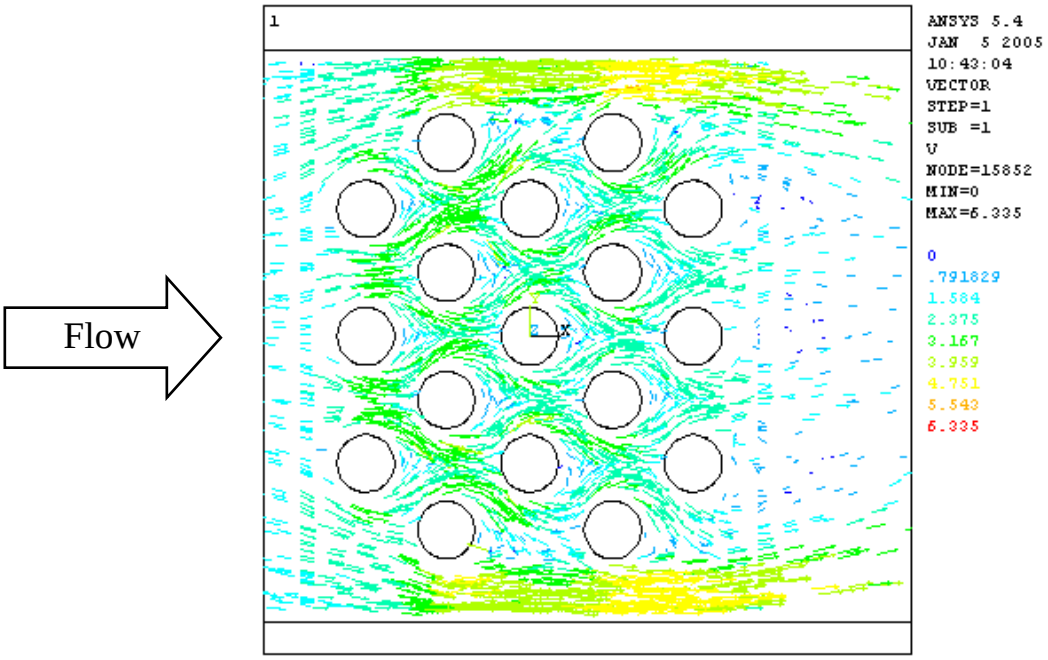

Fig. (٥-٤١) Velocity Vectors Field for Cylindrical Pin-Fin Heat Sink.

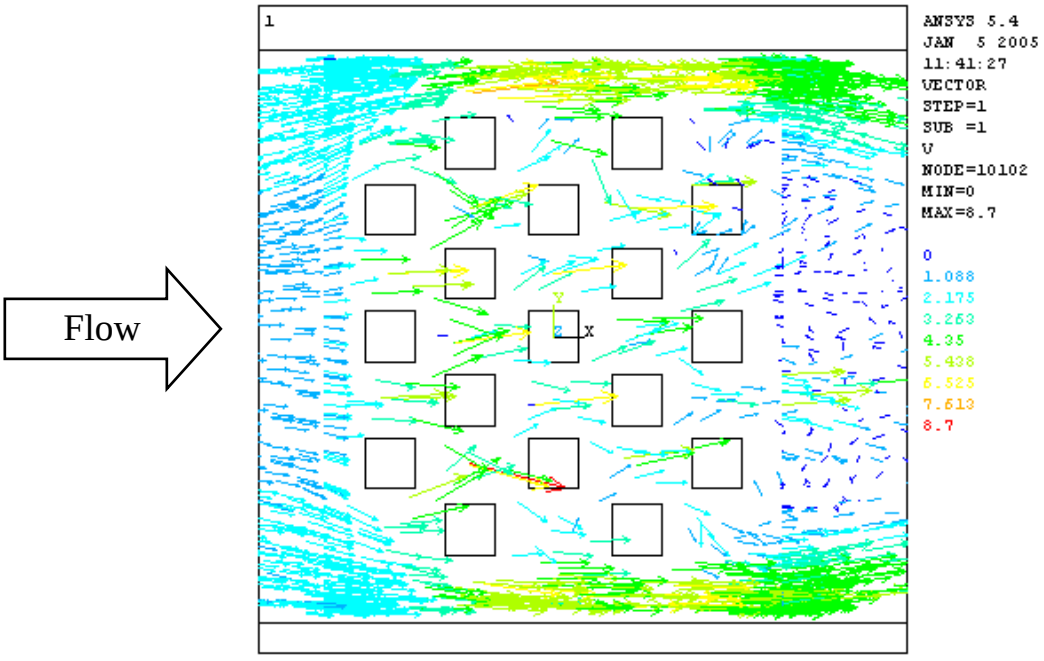

Fig. (٥-٤٢) Velocity Vectors Field for Square Pin-Fin Heat Sink.

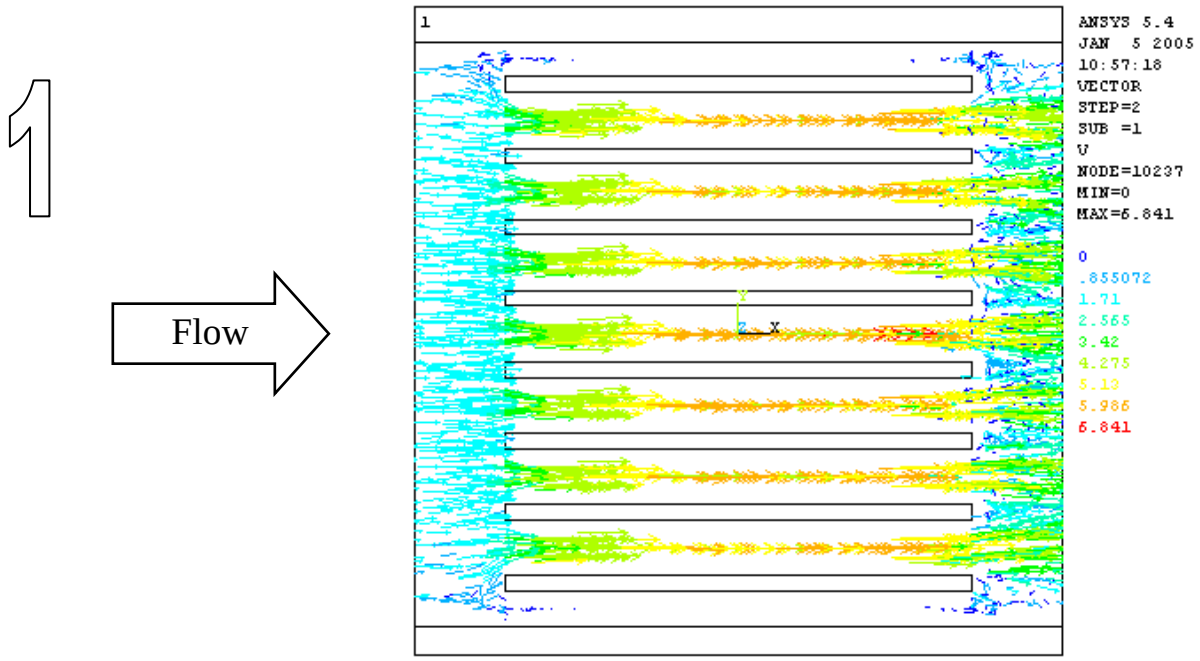

Fig. (٥-٤٣) Velocity Vectors Field for Longitudinal Fin Heat Sink.

Chapter 6

Conclusions and Suggestions

The following are conclusions drawn from the present investigation and suggestions for the future work are given.

٦.١ Conclusions

In the present study, a comparison of various heat sink geometries has been attempted in the heat transfer characteristics of heat sinks have been determined.

١- The result show that longitudinal fin heat sink geometry perform better that cylindrical and square pin-fin heat sink geometries when its have the same area of conduction because that the longitudinal fin gives high expose area (large area of convection).

٢- The cylindrical pin-fin heat sink have highest relative thermal resistance than that longitudinal and square pin-fin, this means that cylindrical pin-fin have higher performance for the same area of convection.

٣- In fully ducted environment which minimizes by-pass, the flow will be early constant in the *z*-direction, distributed only at the base and end of the fins.

٤- The manufacturing process for longitudinal fin heat sink is easier and lower in cost than the manufacturing of staggered cylinder and square pin-fin. This is due to the fact that the manufacturing process occurs on the one part of material by making grooves on it with dimensions that we need. But for staggered cylinder and square pin-fin the manufacturing process occurs on higher than one part of materials. The base of heat sink is manufactured alone and

each pin is also manufactured alone. This increases the cost and time of processing also it increases the thermal resistance.

٥- The shape and arrangement of longitudinal fin heat sink gives more surface area than cylinder and square pin-fin heat sink for the same base plate dimensions.

٦- The result show that with increasing Reynolds Number the flow thermal saturation decreases. The air flow leaves the heat sink at lower exit temperature, still capable of heat removal.

٧- There are very high different for the air behavior between longitudinal fin and staggered pins. For longitudinal fin heat sink, maximum velocity occurs at the core center of heat sink while for staggered pins the maximum velocity occurs at the tow sides of the heat sink.

٨- The longitudinal fin heat sink offers ease of production assembly where misalignment of the heat sink with respect to the direction of air flow will not result in failure.

٩- Variation in overall thermal resistance in total area, therefore there are important difference between the heat transfer coefficients for longitudinal fin and pins.

١٠- The performed calculations also verify that the developed numerical yields like ANSYS Program sufficiently accurate results to be applicable.

٦-٢ Suggestions For Future Work

As related to the present work, the following suggestions for future developments:

١- Treating the problem as three dimensional problem, natural convection, however the gravity of air and mixed convection is significant and should be taken into account.

٢- Considering the time effect, the inclusion of the unsteady-state term in the governing equation should be considered.

٣- Study the same problem experimental and numerically for the condition of impingement of flow.

٤- Studying the difference between staggered and in-line pin-fin heat sinks.

٥- Study the optimization of fin spacing and gaps between heat sinks to maximize heat transfer from an array of heat sinks.

EXAMINING COMMITTEES CERTIFICATE

We certify, as an examining committee that we have read this thesis **,EXPERIMENTAL AND NUMERICAL STUDY OF FIN HEAT SINKS SYSTEMS,** and examined the candidate in its content and that in our opinion it meets the standard of a thesis for the degree of Master of science in Mechanical Engineering.

Signature:
Name: Asst. Prof.
Dr. Haroun. A. K. Shahad AL-Janabi
(Supervisor)
Date: / /٢٠٠٥

Signature:
Name: Asst. Prof.
Dr. Tahseen. A. AL-Hattab
(Supervisor)
Date: / /٢٠٠٥

Signature:
Name: Asst. Prof.
Dr. Majid. H. Mejid
(Member)
Date: / /٢٠٠٥

Signature:
Name: Asst. Prof.
Dr. Emad. S. Ali
(Member)
Date: / /٢٠٠٥

Signature:
Name: Asst. Prof.
Dr. Adil. A. AL-Moosway
(Chairman)
Date: / /٢٠٠٥

Signature:
Dr. Ala'a. M. H. Muhsin
Asst. Prof., Head of the Mechanical Engineering Department.
Date: / /٢٠٠٥

Signature:
Dr. Haroun. A. K. Shahad AL-Janabi
Asst. Prof., Dean of the College of Engineering.

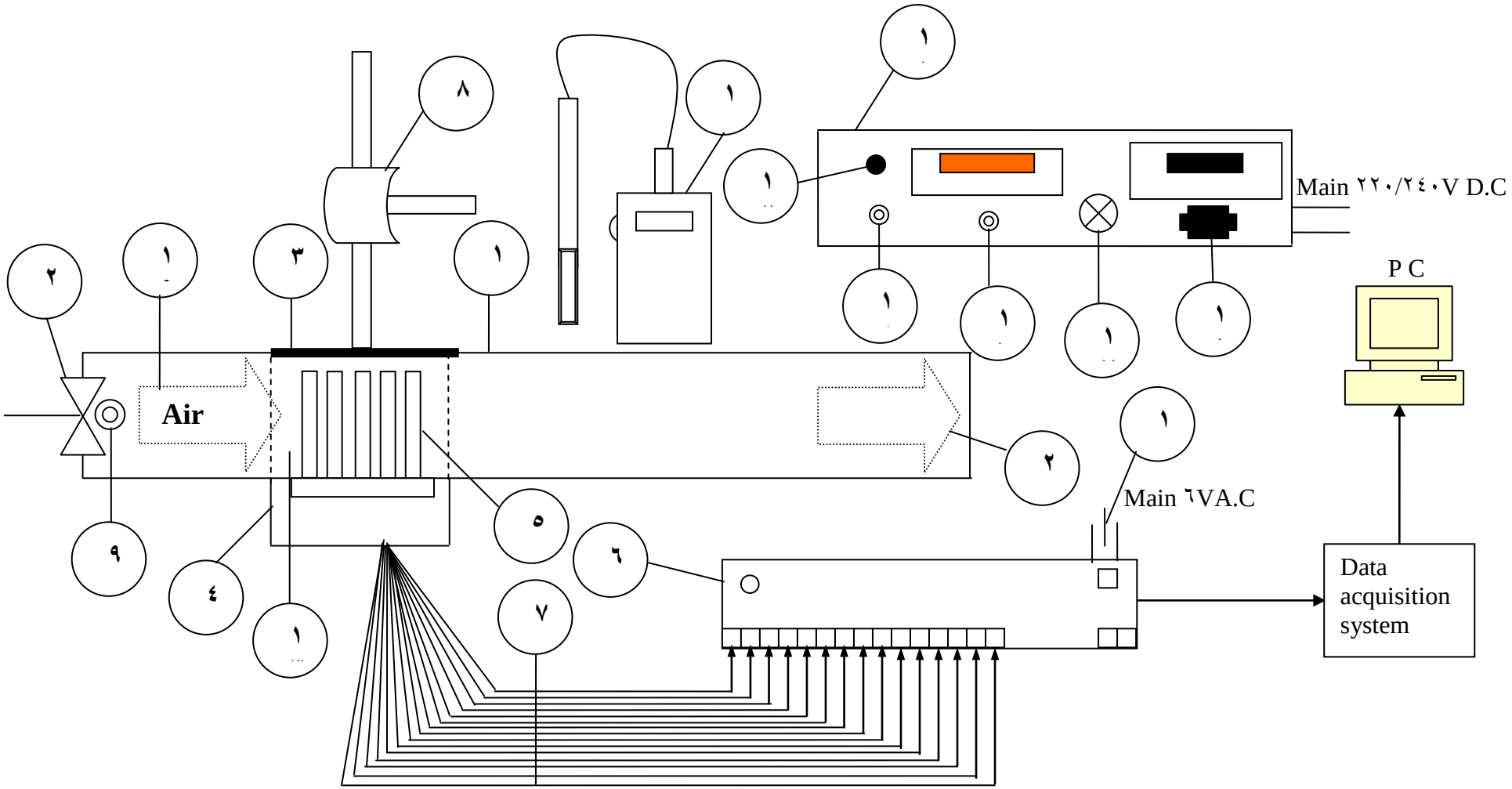

١-Aliminum duct	٦-Interface	١١-Power supply	١٦-Base temp. sensor
٢-Fan	٧-Thermocouple wire	١٢-Fan speed control	١٧-Heater power
٣-Perspex window	٨-Traversing mechanism	١٣-Test section	١٨-Supply lead
٤-Heater	٩-Inlet measurement	١٤- Electric console	١٩-Inlet flow region
٥-pinfin heat sink	١٠-Porable anemometer	١٥-Interface power	٢٠-Exit flow region

Fig. (٤-١) Schematic arrangement of experimental rig.

References

[١] Yunus, A.C., **"Heat Transfer: A practical Approach"** McGraw-Hill, New York, (١٩٩٧).

[٢] Kily, R.F, and Soul, C.A**,"Engneering Heat Sink",** Powertechnics Magazine, July, (١٩٩٠), Cited in Ref (٣٦).

[٣] Soul, C.A., **"Air and Liquid Cooled Techniques for High Power Density Components",** Power Conservation and Intelligent Motion, Vol.١٩, No.١١, (١٩٩٣), Cited in Ref(٣٦).

[٤] Sparrow, E.M., and Ramsey, J.W., **"Heat Transfer and Pressure Drop For a Staggered Wall-Attach Array of Cylinders with Tip Clearance".** Int. J. Heat and Mass Transfer,٢١, pp. ١٣٦٩-١٣٧٧, (١٩٧٨).

[٥] Sparrow, E.M., Ramsey, J. W., and Altemani, C.A.C., "**Experimental on In-Line Pin-Fin Array and Performance: Comparisons with Staggered Array"**, Asme J. Heat Transfer,١٠٢, pp.٤٤-٥٠, (١٩٨٠).

[٦] Sparrow, E.M., and Hajiloo, A**.," Measurements of Heat Transfer and Pressure Drop for an Array of Staggered Plates Aligned Parallel to an Air Flow"**, Asme J. Heat Transfer,١٠٢, pp.٤٢٦-٤٣٢, (١٩٨٠).

[٧] Tuckerman, D.B., and Pease, R.F.W., **"High Performance Heat Sinking for VLSI",** IEEE Electron Dev. Letters, Vol. EDL-٢,No.٥, pp.١٢٦-١٢٩, (١٩٨١),Cited in Ref(٣٦).

[٨] Sparrow, E.M., and Larson, E.D., **"Heat Transfer from Pin-Fins Situated in an Longitudinal Flow which Turns to Cross Flow",** International Journal of heat Mass Transfer, Vol.٢٥, No.٥, pp.٦٠٣-٦١٤, (١٩٨٢).

[٩] Sparrow, E.M., Niethammer, J.E., and Chaboki, A.," **Heat Transfer and Pressure Drop Characteristics of Arrays of Rectangular Modules Encountered in Electronic Equipment".** Int. J. Heat Mass Transfer,٢٥, No.,٧,pp.٩٦١-٩٧٣, (١٩٨٢).

[١٠] Metzger, D.E., Fan, C.S., and Pennington, J.W., **"Heat Transfer and Flow Friction Characteristics of Very Rough Transverse Ribbed Surfaces without Pin-Fin".,** Proceedings of the Asme-Jsme Thermal Engineering Joint Conference, Vol.١, pp.٤٢٩-٤٣٦, (١٩٨٣), Cited in Ref(٣٦).

[١١] Steuber, G.D., and Metzger, D.E., **"Heat Transfer and Pressure Loss Performance for Families of Partial Length Pin-Fin Arrays In High Aspect Ratio Rectangular Ducts",** Proceedings of the Eighth International Heat Transfer Conference,pp.٢٩١٥-٢٩٢٠, (١٩٨٦), Cited in Ref(٣٦).

[١٢] Goldberg, N., **"Narrow Channel Forced Air Heat Sink",** IEEE Transactions on Components, Hybrids and Manufacturing Technology, Vol. CHMT-٧,No.١,Mar. (١٩٨٤), Cited in Ref(٣٦).

[١٣] Sparrow, E.M., and Kadle, D.S., **"Effect of Tip-to-Shroud Clearance on Turbulent Heat Transfer from a Shrouded, Longitudinal Fin Array",** Asme J. Heat Transfer, Vol.١٠٨, pp.٥١٩. (١٩٨٦).

[١٤] Mahalingam, M., and Andrews, J**., "High Performance Air Cooling for Microelectronics",** Cooling Technology for Electronic Equipment, W., Aung, ed., Hemisphere, Washington, DC. (١٩٨٨), Cited in Ref(٣٦).

[١٥] Minakami, K., Mochizuki, S., Murata, A., and Yagi, Y., **"High Performance Air-Cooling for LSIs Utilizing a Pin-Fin Heat Sink",** Paper No.٩٢-WA/EEP-٥, Asme Winter Annual Meeting, Anaheim, CA.(١٩٩٢), Cited in Ref(٣٦).

[١٦] Hollworth, B.R., and Durbin, M., **"Impingement Cooling of Electronics"** ASME Journal of Heat Transfer, Vol.١١٤, AUGUST, pp.٦٠٧-٦١٣, (١٩٩٢).

[١٧] Wirtz, R.A., Chen, W., and Zhou, R., **"Effect of Flow By-Pass on the Performance of Longitudinal Fin Heat Sinks",** Asme J. Electronic Packaging, Vol.١١٦, pp.٢٠٦-٢١١, (١٩٩٤), Cited in Ref (٣٦).

[١٨] Azar, K., and Mandrone, C,A., "**Effect of Pin-Fin Density of the Thermal**

Performance of un Shrouded Pin-Fin Heat Sink", Asme J. Electronic Packaging, Vol.١١٦, pp.٣٠٦-٣٠٩, (١٩٩٤), Cited in Ref(٣٥).

[١٩] Tahat, M.A., Babushaq, R.F., and Probert, S.D., **"Forced Steady State Convection from Pin-Fin Array",** Applied Energy, Vol.٤٨, No.٤, pp.٣٣٥-٣٥١ (١٩٩٤).

[٢٠] Shaukatullah, H., Storr, W.R., Hanse, B.J., and Gaynes, M.A., **"Design and optimization of Pin-Fin Heat Sinks for Low Velocity Application",** ١٢th IEEE Semi-Therm Symposium Proceedings, pp.١٥١-١٦٣. (١٩٩٦), Cited in Ref (٣٦).

[٢١] Marlin, R.V**., "Thermal Performance of Air-cooled Hybrid heat Sinks for a Low Velocity environment"** ١٠th IEEE Semi-Therm Symposium. pp.١٧-٢٢, (١٩٩٤), {inter}.

[٢٢] Wirtz, R.A., Sohal, R., and Wang, H., **"Thermal Performance of Pin-Fin Fan-Sink Assemblies",** Journal of Electronic Packaging, Vol.١١٩ pp.٢٦-٣١, (١٩٩٧), Cited in Ref (٣٥).

[٢٣] Mario, U., Baris, M.D., and Alfonso O**., "Experimental and Modeling of the Heat Transfer of In-Line Square Pin-Fin Heat Sinks with Top By-Pass Flow"** Asme Int. Mechanical Engineering Congress and Exposition, November ١٧-٢٢,New Orleans, Louisiana, (٢٠٠٢), {inter}.

[٢٤] Sparrow, E.M., Baliga, B.R., and Patanker, S.V., **"Forced Convection Heat Transfer from a Shrouded Fin Array without Tip Clearance"** Transaction of the Asme, Vol.١٠٠, November, pp.٥٧٢-٥٧٩, (١٩٧٨).

[٢٥] Webb, B.W., and Ramadhyani, S., **"Conjugate Heat Transfer in a Channel with Staggered Ribs"** Int. J. Heat and Mass Transfer, Vol.٢٠, No.٩, pp.١٦٧٩-١٦٨٧, (١٩٨٥).

[٢٦] Constans, E.M., Belegunda, A.D., and Kulkarni, A.K., **"Optimization of a Pin-Fin Heat Sink: a Design Tool"** CAE/CAD Application to Electronic Packaging, Asme EEP-Vol.٩, pp.٢٥-٣٢, (١٩٩٤), Cited in Ref(٣٦).

[٢٧] Dereje, A., and Arnold F**., "Conjugate Model of Pin-Fin Heat Sink Using**

a Hybrid Conductance and CFD Model within an Integrated Mcae Tool" Eurothrem Seminar No.٤٥, (١٩٩٥), {inter}.

[٢٨] Paul, G., **"A Design Approach to Thermal Characterization of Forced Convection System using Superposition in CFD",** Flomerics Inc. (٢٠٠١). {Inter}.

[٢٩] Kadel, D.S., and Sparrow, E.M., **"Numerical and Experimental Study of Turbulent Heat Transfer and Fluid Flow in Longitudinal Fin Arrays",** Transaction of the ASME, Vol.١٠٨, February, (١٩٨٦).

[٣٠] You, H.I., **"Experimental Determination of Heat Transfer Coefficient between a Microstructure and Fluid",** Int. Comm. Heat Mass Transfer, Vol.١٦, pp. ٥٣٧-٥٤٦, (١٩٨٩).

[٣١] Vivek, M., and Karl, H., **"Thermal Analysis of a Pin Grid Array Package",** Flomerics Limited. (١٩٩١). {Inter.}.

[٣٢] Knight, R.W., Goodling, J.S., and Gross, B.E., **"Optimal Thermal Design of Air-Cooled Forced Convection Heat Sink- Experimental Verification",** IEEE Intersociety Conference on Thermal Phenomena, Piscata Way, NJ, pp.٢٠٦-٢١٢, (١٩٩١), Cited in Ref.(٣٦).

[٣٣] Mohaney, H.V., and Vader, D.T., **"Predicted and Measured Performance an Advanced Laminated Heat Sink for Multi-Chip Modules",** Enhanced Cooling Techniques for Electronics Applications, ASME. NEY YORK, pp.٤٩-٥٧. (١٩٩٣).

[٣٤] Christopher, L.C., and Seri, L,. **"Thermal Performance of an Elliptical Pin-Fin Heat Sink",** Tenth IEEE SEMI-THERM™, (١٩٩٤). {Inter}.

[٣٥] Arnold, F.J., Richard, R., and Jeffery, L., **"Recent Advances in Thermal/Flow Simulation: Integrating Thermal Analysis in to the Mechanical Design Process",** Eleventh IEEE SEMI-THERM™, February. (١٩٩٥). {Inter}.

[٣٦] Sath, S., and Sammakia, B., **"A Review of Recent Developments in Some Practical Aspects of Air-Cooled Electronic Package",** Transaction of

the ASME Vol. ١٢٠, November, pp, ٨٣٠-٨٣٩, (١٩٩٨).

[٣٧] Adam, V., and Izundu, F.O., **"Characterization of Longitudinal Fin Heat Sink Thermal Performance and Flow By-Pass Effects Through CFD Methods",** Maya Heat Transfer Technologies, LTD. (٢٠٠٠).{Inter}.

[٣٨] Baris, D.M., Alfonso, O., and Mario, U., **"Experimental and Modelling of the Hydraulic Resistance of In-Line Square Pin-Fin Heat Sinks with Top By-Pass Flow",** Department of Aerospace and Mechanical Engineering and the Centre for Electronic Packaging Research. (٢٠٠١). {Inter}.

[٣٩] Launder, B. E., Spalding, D. B. **"The Numerical Computation of Turbulent Flows",** Computer Methods In Applied Mechanics and Engineering, Vol. ٣, pp ٢٦٩-٢٨٩, (١٩٧٤).

[٤٠] Viollet, P. L., "The Modeling of Turbulent Recalculating Flow for the Purpose of Reactor Thermal-Hydraulic Analysis", Nuclear Engineering and Design, Vol. ٩٩, pp ١٤٥-١٨٧. (١٩٨٧).

[٤١] Omega, **"The Temperature Hand Book"**, Omega Engineering Inc., Stamford, CT, ٠٦٩٠٧, Pg.z-١٨, (١٩٩٨). {Inter}.

[٤٢] Ali, H. S., "Flow Around Bus", M. Sc. Thesis, University of Babylon, Iraq, (١٩٩٩).

[٤٣] Holman, J. P., "Heat Transfer" McGraw-Hill, New York, (١٩٨٦).